Factors influencing tumour uptake and retention of benzonaphthyridine derivatives in mice

A thesis submitted to The University of Auckland in fulfilment of the requirements for the degree of Doctor of Philosophy in Pharmacology

by

Bhanu Pradeep Lukka, BPharm, MSc (hons)

Pharmacology & Clinical Pharmacology

Auckland Cancer Society Research Centre

Faculty of Medical and Health Sciences

The University of Auckland

August 2013

Abstract

The DNA-binding benzonaphthyridine derivatives have demonstrated to have high and even curative activity against the Colon-38 murine adenocarcinoma. A homologous series of derivatives with, hydrogen, methyl, ethyl, propyl and butyl groups attached to the 2-position of the chromophore, was used to investigate the role of physicochemical properties on the tissue pharmacokinetics and its contribution to anti-tumour activity. The methyl derivative, SN 28049, N-[2-(dimethylamino)ethyl]-2,6-dimethyl-1-oxo-1,2-dihydrobenzo[b]-1,6-naphthyridine-4-carboxamide, was the most active of the series.

A rapid and sensitive LC-MS/MS method with a run time of 7 min for the simultaneous measurement of the five analogues in a pooled sample was developed. The method was validated in mouse plasma and tissues and had a limit of quantitation of 0.001 µM and was linear over the range, 0.001 – 0.3 µM in all matrices with acceptable intra- and inter-assay precision and accuracy. Plasma protein binding and metabolic stability was assessed by equilibrium dialysis. Plasma and tissue pharmacokinetics were assessed in mice after administration of each analogue (25 µmol/kg) to healthy, as well as mice with Colon-38, Lewis Lung and melanoma tumours. Antiproliferative activity (IC_{50}) was assessed cultures by ^{3}H-thymidine incorporation method. Intracellular concentrations were determined following exposures *in vitro*. Susceptibility to multi-drug resistance was performed in leukaemia cultures over-expressing P-gp and MRP1.

Plasma pharmacokinetics conformed to a model where increasing lipophilicity was associated with a decreasing area under the concentration-time curve (AUC) and an increasing clearance and volume of distribution. In contrast, tumour tissue pharmacokinetics showed a very different relationship where the AUC of the methyl derivative (2334 µM.h) was 89-fold higher than the hydrogen derivative (26.3 µM.h) with other homologues having intermediate values. The tumour AUC correlated with the *in vivo* anti-tumour activity of the series. The methyl derivative had a 24 min *in vitro* microsomal half-life, while other analogues ranged from 1.6 - 12.2 min. The plasma free fraction decreased (17 - 5 %) significantly with lipophilicity. SN 28049's pharmacokinetics were evaluated in mice with LLTC, NZM4, NZM10 and NZM52 tumours. The tumour AUCs were 2.7 to 36-fold greater than the plasma, but higher AUCs were observed in the kidney. Overall, the tumour exposures were significantly lower than the Colon-38 tumour.

Cellular uptake and retention varied widely with different cell lines and in general showed a parabolic dependence on lipophilicity, but not clearly related to antiproliferative activity. The analogues were only marginally susceptible to MRP1, 2.3-fold (methyl, ethyl and propyl) and P-gp (2-fold, hydrogen).

The plasma pharmacokinetics of this series are related to changes in lipophilicity. However, the tumour pharmacokinetics reveal a strong dependence on the nitrogen substituent on the benzonaphthyridine chromophore, with the methyl group providing by far the best retention in tumour.

Acknowledgements

It may be impossible to name each and everyone involved, I will nonetheless try.

The first are my supervisors, A/Prof James Paxton and Prof Bruce Baguley whose support, in all forms was unparalleled. James, Bruce – I cannot thank you both enough. Dr Philip Kestell, my advisor for this project was instrumental in daily teaching in the laboratory whether it is, developing new methodologies, learning a new technology, or troubleshooting the mass spectrometer, he was the one-stop shop for advice. Phil, thank you.

On the list of advisors in an unofficial capacity, support on many occasions was sought from a few people in the ACSRC. Whether it is synthesis of a new compound or clarification with basic concepts in Cancer Biology or setting up a high-throughput methodology, Drs Graham Atwell, Graeme Finlay and Jagdish Jaiswal were of great help.

Thanks are due to the funding bodies, Auckland Division of the Cancer Society of New Zealand, Auckland Uniservices Ltd whose support made this work possible. Additionally, thanks are due to The Maurice & Phyllis Paykel Trust, The University of Auckland, Postgraduate students association (FMHS-PGSA) for conference travel grants.

Collaboration and technical support was sought on several occasions. Thanks to Mr Sarath Liyanage, Mr Sisira Kumara, Dr Sandy Chen, Ms Emma Richardson and Ms Angela Ding.

My friends are instrumental in making me realise from time to time that I have a social life. Thanks are due to Smitha, Sunali, Paresh, Shiv, Foram and Shevan for the hangouts. All my colleagues and friends in the student offices, Kashyap, Yongchuan, Kaveshree, Diana, Rana and Melissa. Thank you – I had a good time chit chatting.

In a less direct way my parents, brother and sister have supported me in their own personal way. Thanks for your unconditional support.

Table of contents

List of tables

List of figures

Abbreviations

ACSRC	Auckland Cancer Society Research centre
ADME	Absorption, distribution, metabolism and excretion
AUC	Area under the concentration-time curve extrapolated to infinity
a.u.	Atomic units
BBB	Blood brain barrier
CCRF-CEM	Cell line derived from lymphoblastic leukaemia
CL	Total clearance
CL/F	Clearance uncorrected for bioavailability
CL_H	Hepatic clearance
CL_{int}	Intrinsic clearance
C_{max}	Maximal concentration
CV	Coefficient of variation
CYP	Cytochrome P-450 enzyme system
DAD	Diode Array detector
DMPK	Drug metabolism and pharmacokinetics
DMSO	Dimethyl sulfoxide
F	Bioavailability
g	Gravity
g	gram
h	hour
HCl	Hydrochloric acid
HCOOH	Formic acid
HPLC	High performance liquid chromatography
i.p.	Intraperitoneal
i.v.	Intravenous

IS	Internal standard
kg	kilogram
LC-MS/MS	Liquid chromatography mass spectrometry
LLTC	Lewis lung tissue culture
LLOQ	Lower limit of quantitation
Log D	Distribution / partition coefficient at pH 7.4
m/z	mass to charge ratio
MDR	Multi-drug resistance
MeCN	Acetonitrile
MeOH	Methanol
µg	microgram
µM	micromolar
mg	milligram
$MgCl_2.6H_2O$	Magnesium chloride
min	minute
ml	millilitre
mm	millimetre
mM	millimolar
MRM	Multiple reaction monitoring
MRP	Multi-drug resistance protein
MRT	Mean residence time
MTD	Maximum tolerated dose
MW	Molecular weight
NCA	Non-compartmental analysis
nM	nanomolar
NZM	New Zealand melanoma
PBS	Phosphate buffered saline
PD	Pharmacodynamics

p.o	oral
P-gp	P-glycoprotein
pH	Hydrogen ion concentration
PK	Pharmacokinetics
QC	Quality control
rpm	Revolutions per minute
RSD	Relative standard deviation
RT	Retention time
s.d.	Standard deviation
s.e.	Standard error
S/N	Signal to noise ratio
$T_{½}$	Terminal half-life
T_{max}	Time to reach maximal concentration
USFDA	United States Food and Drug Administration
V_{SS}	Volume of distribution at steady state
V_{SS}/F	Volume of distribution at steady state uncorrected for bioavailability
^	transition in tandem mass spectrometry

List of publications

Publications from this thesis

Refereed Journal

1. ***Lukka PB, Paxton JW, Kestell P, Baguley BC (2012). Comparison of a homologous series of benzonaphthyridine anti-cancer agents in mice: divergence between tumour and plasma pharmacokinetics. Cancer Chemother Pharmacol. 70:151-160.***

2. ***Lukka PB, Paxton JW, Atwell GJ, Kestell P, Baguley BC (2012). A rapid LC–MS/MS method for the quantitation of a series of benzonaphthyridine derivatives: Application to in vivo pharmacokinetic and lipophilicity studies in drug development. J Pharm Biomed Anal. 63:9-16.***

Refereed Conference Abstracts

1. ***Lukka PB, Paxton JW, Chen YY, Kestell P, Baguley BC (2011). Pharmacokinetic and Pharmacodynamic evaluation of a series of benzonaphthyridine anti-cancer agents in mice. American Association of Pharmaceutical Scientists (AAPS) Annual Meeting, Washington DC, USA.***

2. ***Lukka PB, Paxton JW, Kestell P, Baguley BC (2010). The effect of lipophilicity on the pharmacokinetics and tumor exposure of a series of 5 benzonaphthyridine anti-cancer agents in mice. Pharmaceutical Sciences World Congress (PSWC), New Orleans, LA, USA.***

3. ***Lukka PB, Paxton, JW, Kestell P, Baguley BC (2009). Pharmacokinetics of benzonaphthyridine anti-cancer agents in mice – Effects of lipophilicity. American Association of Pharmaceutical Scientists (AAPS) Annual Meeting. Los Angeles, CA, USA.***

4. ***Lukka PB, Kestell P, Paxton JW, Baguley BC (2008). Tumor pharmacokinetics of SN 28049 in mice. 15th North American Regional ISSX Meeting, San Diego, CA, USA.***

Chapter 1

Introduction

1.1 Cancer

Cancer is a multifaceted disease sharing a common characteristic of poorly controlled cell proliferation and is one of the leading causes of death [1] and is continuing to increase each year [2]. According to the latest consensus figures available, cancer is a leading cause of death in New Zealand, accounting for 29.4 % of deaths [3]. This mortality rate is a compelling reason for the continued research to develop more effective treatments to combat cancer. The majority of cancers are solid tumours that can be treated by surgery, radiation and/or a combination including chemotherapy, but metastatic and inoperable cases of cancer require the systemic use of chemotherapy [4, 5].

1.2 Cancer chemotherapy

The modern era of chemotherapy is believed to have started in 1865 with the use of potassium arsenite to treat chronic myelogenous leukaemia by Lissauer [6]. The first major advance in chemotherapeutic treatment was the discovery of the potential therapeutic applications of the chemical warfare agent, mustard gas, developed during World War I [7, 8]. Mustard gas produced profound lymphoid hypoplasia and myelosuppression, which consequently led to the discovery of its anti-tumour effects [9]. In 1942, the first patients were treated with a nitrogen mustard, an analogue of sulphur mustard gas (1,5-dichloro-3-thiapentane), with encouraging results [10]. Introduction of nitrogen mustard [11], was followed by methotrexate, chlorambucil and thioguanine leading eventually to more advanced agents such as cisplatin, gemcitabine, docetaxel, topotecan and irinotecan as some of the most commonly used cytotoxic drugs [12, 13].

1.3 The solid tumour environment

Solid tumours are complex heterogeneous organ-like structures, comprising cancer cells and stromal cells (such as fibroblasts and inflammatory cells) embedded in an extracellular matrix and nourished by a vascular network of varying quality within the tumour. As compared to normal tissues, the tumour stroma is associated with an altered extracellular matrix and increased number of fibroblasts that synthesize growth factors, chemokines and adhesion molecules, with varying compositions between tumours [14, 15]. The tumour stroma can influence malignant transformation and plays a vital role in the ability of tumours to invade and metastasize [16-18]. The composition and structure of the stromal components in tumours also contribute to an increase in interstitial fluid pressure, which hinders the penetration of macromolecules through tissue [19, 20].

1.4 Drug distribution in tumour

Drugs must leave the tumour blood vessels efficiently and then penetrate tumour tissues to reach all of the cancer cells [21, 22]. Both processes depend on convection and/or diffusion. Convection depends on: the gradients of pressure (both hydrostatic and osmotic) between the vascular space and the interstitial space; vessel permeability; the surface area for exchange; and the volume composition and structure of the extracellular matrix. Drug diffusion is determined by its concentration gradient in the tumour tissue and by various physicochemical properties, including its molecular size, shape and its solubility in water and lipids [21, 22]. Sequestration of drugs in tumour cells and/or their binding to components of the extracellular matrix or at the target site may inhibit drug penetration to deeper regions of the tumour [23]. Impaired drug penetration due to binding in tissue may apply in particular to basic drugs (e.g., doxorubicin and mitoxantrone) that are sequestered in acidic organelles such as the perinuclear endosomes [24, 25] and to drugs that bind avidly to DNA [26, 27]. Sequestration in acidic organelles and avid binding to DNA has been implicated in the poor tissue penetration of doxorubicin, epirubicin and mitoxantrone [25, 27].

1.4.1 Acidic environment of tumour

The environmental acidity has a significant influence on oncogenesis, malignant transformation, metastasis and angiogenesis. The heterogeneity of the tumour vascular network causes insufficient oxygen supply to parts of tumours, leading to hypoxia. The resultant hypoxia forces glucose metabolism through the glycolytic pathway instead of respiration, thereby resulting in the formation of lactic acid [28-31]. Additionally, tumour cells convert glucose and other substrates preferentially to lactic acid and other acidic metabolites even under aerobic conditions, leading to acidification of the intra-tumour environment [30]. While the interstitial or extracellular pH (pHe) in tumours is acidic, the intracellular pH (pHi) in tumours has been found to be neutral, similar to the pHi of normal tissues [28-30, 32, 33]. Several studies have reported that the pHe of human tumours was lower than that in normal tissues [34-38]. This pH difference indicates the existence of powerful mechanisms to prevent acidification of the intracellular environment [39-42]. Such a significant gradient between pHe and pHi has been attributed to the existence of short-term and long-term mechanisms for pHi control [39]. The short-term mechanisms include: physicochemical buffering of the acids; metabolic consumption of non-volatile acids; and the transfer of acids from the cytosol to the organelles. However, their capacity to maintain the intracellular environment at neutral pH for a prolonged period is limited. Most mammalian cells possess powerful systems to regulate pHi using long-term mechanisms, such as the exchange of Na+ ions for H+ ions using the Na+/H+ antiport, an ion exchanger in the plasma membrane [41, 43]. Additionally, bicarbonate-linked mechanisms such as: (a) Na^+ dependent $Cl^-/HCO3^-$ exchange, (b) Na^+ independent Cl^-/HCO_3^- exchange; and (c) Na^+/HCO_3^- symport, play a role in regulating the pHi [39, 42-44].

It is well known that the influx of many drugs into tumour cells by passive diffusion may be influenced by the pKa value of the drug. In the acidic extracellular environment in the tumour weakly basic drugs will tend to be more ionized, thereby hindering their passive diffusion into cells; whereas weakly acidic drugs are less ionized [45, 46]. For example, the acidic pH environment increases the cellular uptake of 5-fluorouracil, a weak acid, where it is converted to the active moiety [47]. In contrast, doxorubicin is a primary amine with a basic pKa and thus, its cellular uptake may be reduced in an acidic medium. For example, the uptake of doxorubicin at pH 6.6 is only half that at pH 7.4 [45, 46]. Furthermore, doxorubicin is trapped and sequestrated in acidic vesicles within the cytoplasm, reducing the interaction with its target, DNA. A number of agents have been used to enhance the cytotoxicity of doxorubicin by inhibiting the formation of acidic vesicles, thereby releasing the doxorubicin into the cytoplasm [45, 46].

1.5 Cellular uptake and efflux

Several mechanisms exist by which substances may be translocated across the cell membrane. The two most common mechanisms for the absorption of drugs are passive transfer by diffusion across the lipid membranes (transcellular absorption) and passive diffusion through the aqueous pores at the tight junctions between cells (paracellular absorption). Additionally, the similarity in membrane structure between species tends to result in similar transcellular absorption across animal species and humans [48-52].

One mechanism of multi-drug resistance is characterized by reduced cellular accumulation of the anti-cancer agents, which are actively effluxed out of the cells by plasma membrane transporters, such as P-glycoprotein (P-gp), or multi-drug resistance transporter (MRP) [53]. One approach to overcome this problem is to develop drugs that inhibit P-gp mediated drug efflux (MDR modulators), while another was the identification of anti-cancer drugs devoid of cross-resistance with the original compounds [54]. Such drugs, which do not display cross-resistance to the classical anthracyclines, were mostly developed to circumvent multi-drug resistance [55]. Anthracyclines are considered to diffuse passively through the plasma membrane as unionized forms and are effluxed out of resistant cells by active transporters such as P-gp [56]. In theory, the new lipophilic anthracyclines could overcome multi-drug resistance either due to their high influx rate overwhelming P-gp's efflux efficiency or because these drugs cannot be recognized and transported by P-gp, resulting in higher steady-state accumulation within the cell [57].

1.6 Lipophilicity and pharmacokinetics

The body can be visualized as an infinite series of aqueous compartments bounded by lipid membranes. Membranes control the disposition of compounds and are therefore, involved in all the vital processes that determine the pharmacokinetics of a drug. The ability of a drug molecule to cross the membranes of the gastrointestinal tract controls the absorption. Tissue membranes control drug distribution and may determine the exposure of the drug to the target site. This same process also affects the accessibility of the drug to most of the drug metabolizing enzymes, the actual binding sites of which rely in part on hydrophobic forces. Finally, the ability of a molecule to cross the renal tubular membrane governs the urinary excretion of a compound. Following glomerular filtration or active secretion, molecules that cannot be reabsorbed across the tubular membrane will be excreted in the urine and thus irreversibly lost from the systemic circulation. The ability of molecules to partition into biological membranes is mainly governed by lipophilicity. Hence, lipophilicity is a major factor in determining a drug's disposition processes, such as absorption, cell membrane permeation, membrane and protein binding and subsequently metabolism and clearance [58, 59]. The effects of altered lipophilicity on drug disposition and action have been known for over a century [60] and several reviews have summarised the effects of increased lipophilicity with various classes of drugs [58, 61-63]. Lipophilicity is determined as Log P (partition coefficient between n-octanol and water) or Log D (partition coefficient between n-octanol and phosphate buffered saline at pH 7.4) [64]. Several methods are available for determining these experimentally, such as shake-flask method, potentiometric titrations and high throughput alternatives, such as reverse-phase high performance liquid chromatography (RP)-HPLC, electrophoretic methods such as microemulsion electrokinetic chromatography (MEEKC) and immobilized artificial membrane (IAM) HPLC-columns. These methods are reviewed elsewhere in detail and are not repeated here in the interest of brevity [65-67].

1.6.1 Absorption and permeability

It is well recognised that the molecular size and lipophilicity are two important properties for membrane uptake of drugs [68]. Dissolution is a prerequisite for absorption as only the compound in solution is available for permeation across the gastrointestinal barrier. This is dependent of the aqueous solubility of the compound and was recognized as a limiting factor in the absorption process [69]. High lipophilicity is the major reason for poor solubility leading to poor absorption. Studies by Gleeson showed that the chances of achieving high solubility are increased significantly for a Log P < 3 with a set of 44,584 Glaxo SmithKline compounds [70]. Various strategies are available to improve the aqueous solubility of a compound including the incorporation of an ionisable centre, such as an amine or similar group. Dissolution testing has been used as a prognostic tool for oral drug absorption [71]. A biopharmaceutics classification scheme (BCS) has been proposed under which drugs can be categorized into four groups according to their solubility and permeability properties [72] and has been adopted as a regulatory guidance for bioequivalence studies. The relationship between permeability and lipophilicity has been reported to be linear [73], hyperbolic [74-76], sigmoidal [77, 78], parabolic [69] and bilinear [73, 79]. These relationships have indicated a moderate permeability at the lower end of the lipophilicity scale; while at the upper end (Log D > 3) these fluctuating relationships are likely due to their increased affinity for the phospholipid phase. However, this is likely to occur at very high Log D values and other issues with high lipophilicity are likely to impact on a molecule's pharmacokinetic profile before this is observed.

1.6.2 Distribution

Lipophilicity is a key determinant in the distribution of compounds within the body and has profound effects on pharmacokinetic parameters such as clearance [80] and volume of distribution [81]. Since lipophilicity is likely to govern the extent of tissue and plasma protein binding, the balance between them may be the key determinant of the extent of partitioning. Another group of drugs which require a special consideration of their lipophilicity are those acting on the central nervous system (CNS). An additional obstacle is the presence of the blood-brain barrier [82]. A study of 50 marketed CNS drugs revealed that 75 % of these compounds have Log P values > 2 and their *in situ* rat brain permeability is related to Log P in a non-linear manner, reaching a maximum between Log P values of 2 and 3 [83]. Consistent with this, a summary of two studies has indicated that for compounds to cross the blood-brain barrier, they should optimally have a Log D between 1 and 3, similar to that for oral drug absorption in general [82].

1.6.2.1 Protein binding

Lipophilicity is well established to be a major determinant in the degree of plasma protein binding. Valko et al have shown a linear correlation between Log P and the Log K value for binding to human serum albumin for 135 diverse drugs and simpler organic compounds [84]. However, acidic compounds in particular tend to bind with greater affinity than would be expected from their Log D values. Additionally, when considering the distribution of various compounds within the body, (e.g., such as volume of distribution) and partitioning into specific effect compartments, protein binding may be a major determining factor.

1.6.3 Lipophilicity and anti-cancer drug development

There have been very few reports on the influence of lipophilicity on drug distribution into tumours. Early attempts were made to correlate increases in lipophilicity with anti-tumour activity for doxorubicin analogues [85, 86] and lipophilic analogues of anti-cancer agents were used to overcome multi-drug resistance [87]. Lipophilic formulations and analogues of several anti-cancer agents, such as chlorambucil [88], boronated DNA intercalating compounds [89], gimatecan, a camptothecin analogue [90] and platinum derivatives [91] have also been investigated with the aim of improving efficacy.

1.7 Topoisomerase inhibitors and poisons

Topoisomerases catalyze DNA relaxation/supercoiling, catenation/decatenation and knotting and unknotting reactions. The mechanism by which topoisomerases resolve DNA topology problems, involves breaking the phosphodiester backbone of the DNA. Two broad types of topoisomerases are defined based on the differences in their mechanism of this reaction [92-95]. The drugs targeting topoisomerase I that are now currently in clinical use are derivatives of camptothecin [96]. Camptothecin induced DNA breaks are probably converted into double strand DNA breaks only when they occur on the leading strand during DNA replication [97].

Anti-cancer drugs targeting topoisomerase II include doxorubicin, etoposide, mitoxantrone, amsacrine and others [98-102]. A transient double strand DNA break is characteristic of the topoisomerase II enzymatic reaction. Topoisomerase II poisons increase the steady state levels of this transient intermediate. They do this either by increasing the rate of DNA cleavage (ellipticine, genistein) or by inhibiting the rate of DNA religation (etoposide, amsacrine, teniposide). In either case, these drugs convert the enzyme into a DNA damaging agent. This is a stoichiometric relationship because there is the potential for one DNA double strand break for every drug stabilized topoisomerase II enzyme. Thus sensitivity to the topoisomerase II poisons is dependent on high levels of enzyme; the more enzyme, the more DNA damage [103]. Topoisomerase poisons are reviewed in detail elsewhere [104-109].

1.8 Evolution of SN 28049

The topoisomerase poisons have been the focus of a drug development programme at the Auckland Cancer Society Research Centre (ACSRC). Amsacrine was the first topoisomerase II poison developed in the 1970s, but had limited activity against solid tumours [110]. This stimulated the start of a synthesis programme to identify analogues with improved solid tumour activity. This led to the discovery of asulacrine [111], N-[2-(dimethylamino)ethyl]acridine-4-carboxamide (DACA) [112] and a series of benzonaphthyridine derivatives, of which N-[2-(dimethylamino)ethyl]-2,6-dimethyl-1-oxo-1,2-dihydrobenzo[b]-1,6-naphthyridine-4-carboxamide (SN 28049) was chosen as the lead compound for further development [113].

1.8.1 Amsacrine derivatives

Amsacrine is a 9-aminoacridine derivative developed in the ACSRC [110] and is a DNA-binding anti-cancer agent. It is active against a number of experimental tumours in mice, including L1210, P388 leukaemia and B16 melanoma [114]. Marginal activity was also found in Lewis Lung carcinoma [115]. However, a severe limitation of amsacrine was the lack of activity in solid tumours. Thus, the goal was to identify analogues of amsacrine that possess enhanced activity against solid tumours.

1.8.1.1 4,5-disubstituted amsacrine derivatives

Several analogues of amsacrine were synthesised with a goal of identifying analogues with activity against solid tumours implanted in mice subcutaneously and intracerbrally [116]. Analogues with substitutions at 4 and 5 position of the ring structure (Figure 1.1) with functional groups such a methyl (CH_3) or methoxy (OCH_3) or carbamoyl ($CONH_2$) were tested for *in vitro* cytotoxicity, *in vivo* anti-tumour activity [(increased life span, (ILS %)] and DNA binding affinity. Another objective was to assess the activity of these analogues when administered orally (p.o.). Published data from selected analogues of this series are presented in Table 1-1.

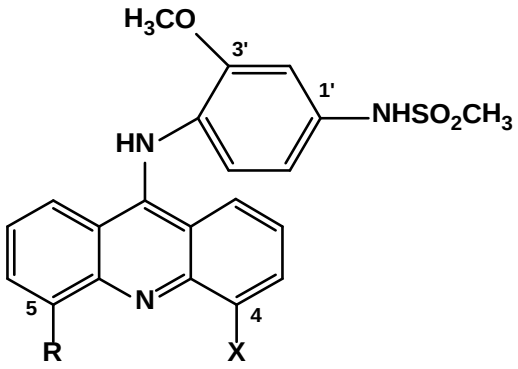

Figure 1.1 Chemical structure of 4,5-disubstituted amsacrine derivatives.

Table 1-1 Substituents of amsacrine, DNA binding constants(Log K), *in vitro* IC_{50} (L1210) and *in vivo* (mice with P388 tumours) anti-tumour activity data [116].

X	R	Log K#		L1210 IC_{50} (nM)	Optimal dose (mg/kg)*	ILS %
		AT	GC			
H	**H**	5.57	5.65	35	13.3	78
CH_3	**H**	6.03	5.96	30	20	143
OCH_3	**H**	5.94	6.00	40	30	139
CH_3	**CH_3**	6.91	6.14	110	45	135
OCH_3	**OCH_3**	6.90	6.32	65	45	99
CH_3	**$CONH_2$**	6.62	6.92	47	20	113

Drugs administered i.p. on days 1, 5 and 9; #Log K values for the binding of drugs to poly [d(A-T)] and poly[d(G-C)] were determined by the fluorometric method [117].

These structural modifications led to analogues with greater DNA binding properties than amsacrine. *In vitro* cytotoxicity in L1210 cultures revealed that none of the analogues were more potent than amsacrine. However, these analogues appeared less toxic *in vivo* allowing administration at higher doses (20 – 45 mg/kg) resulting in an increase in survival times (99 – 143 %) in mice with P388 tumours. However, p.o. activity was observed only with the 4-methyl-5-carbamoyl derivative and none of these progressed with their development as anti-cancer drugs [116].

1.8.2 N-[2-(dimethylamino)ethyl]acridine-4-carboxamide

N-[2-(dimethylamino)ethyl]acridine-4-carboxamide (DACA), (Figure 1.2) is a DNA binding topoisomerase poison developed in the ACSRC with an aim of treating solid tumours as its predecessors, amsacrine and asulacrine, which progressed to clinical trials were marginally active [112]. DACA was identified as the most active analogue in the class of acridine-4-carboxamides against subcutaneously implanted Lewis Lung tumours [112], in addition to its potent *in vitro* cytotoxic activity in L1210 leukaemia, human colon tumour (HCT-8) cultures [112] and Colon-38 tumours [118].

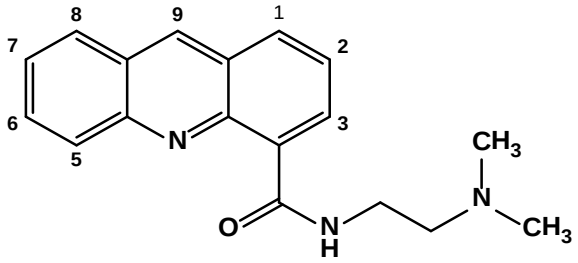

Figure 1.2 Chemical structure of N-[2-(dimethylamino)ethyl]acridine-4-carboxamide.

The pharmacokinetics and tissue distribution of DACA were studied after i.v. administration (121 µmol/kg) to mice [119]. The concentration-time profiles in mouse plasma after i.v. administration exhibited biphasic kinetics. DACA was rapidly taken up by the tissues with the maximal concentrations in kidney, followed by brain, which was at least 10-fold higher than plasma concentrations [119]. Tumour distribution was studied in mice with s.c. LLTC tumours. Peak tumour concentrations were 3-fold greater than plasma and the area under the concentration-time curve (AUC) was 20-fold higher than plasma AUC and a longer half-life ($T_{½}$), (16.3 h) than plasma and other tissues [120].

The favourable activity and pharmacokinetic profile led this drug to a *Phase* I clinical trial with a starting dose of 9 mg/m^2 given daily on 3 successive days. An early phase II study of DACA was conducted to evaluate the anti-cancer activity and safety profile when given as second-line chemotherapy in patients with ovarian cancer who had relapsed within 1-year after first-line chemotherapy with taxanes and platinum for advanced disease [121]. The complete lack of any objective response did not justify further evaluation of DACA in patients with advanced ovarian cancer using this dose and schedule, although the therapy was generally well tolerated.

DACA was also evaluated in patients with advanced non-small cell lung cancer (NSCLC) at the dose of 3010 mg/m^2 (i.v. infusion over 120 h) [122]. The toxicities observed were granulocytopaenia, thrombocytopaenia, deep venous thrombosis, fatigue, epileptic seizures which led to death in 2 patients. With only 4 out of 12 patients reaching stable disease when using this dose and regimen, further evaluation of DACA in advanced NSCLC was not justified [122].

1.8.2.1 Acridine-4-carboxamide analogues

Following on from DACA, several derivatives were synthesised by varying substituents on the acridine ring [123]. The intent was to identify potent and active analogues which can be used effectively to treat solid tumours. Small structural modifications were made on the acridine ring as shown in Figure 1.3, with substituents indicated in Table 1-2.

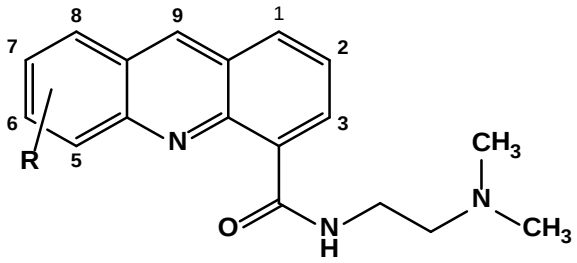

Figure 1.3 Chemical structure of DACA analogues. R indicates the position and substituent [123].

Table 1-2 *In vitro* and *in vivo* activity of DACA analogues. Data from Spicer et al [123].

R	IC_{50} (nM) in LLTC culture	Optimal dose (mg/kg)	Growth delay in Colon-38 tumours (days)
H	189	200	11
5-Me	6.4	20	11
5-Et	18	ND*	ND*
5-Pr	650	ND*	ND*
7-Bu	4590	ND*	ND*
6-Br	160	200	Inactive
6-NMe_2	260	90	4
7-Cl	250	200	4

Not determined

Substitution at 5 position by a methyl group resulted in analogues more potent than the parent DACA *in vitro. The in vivo* activity in Colon-38 tumours was similar to DACA only with this analogue. Increase in chain length at this position only decreased the cytotoxic potency (5-Et, 5-Pr, 7-tBu). Other small substituents such as Cl, Br had lesser activity

than DACA *in vivo*. This resulted in the synthesis of bis-acridines and bis-phenazines which are discussed in the following sections.

1.8.3 Bis(acridine-4-carboxamide) derivatives

Bis(acridine-4-carboxamides) (Figure 1.4) were developed as a continuation of the programme for developing better DNA-binding drugs with activity in solid tumours [124]. Several analogues were synthesised and screened in a panel of cell lines *in vitro* and the *in vivo* activity of the selected analogues were tested for tumour growth delays in mice with Colon-38 tumours. These analogues were structurally related to DACA but were more lipophilic. Several analogues with substituents at various positions on the ring structure were tried. A few of the analogues relevant to this topic are presented in Table 1-3.

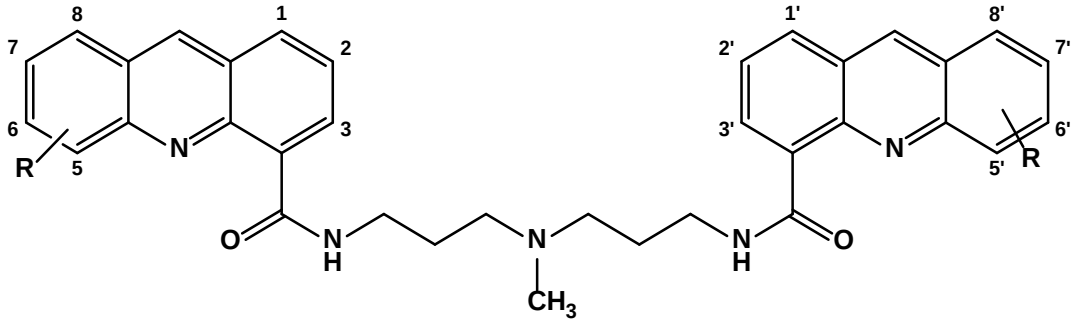

Figure 1.4 Chemical structure of Bis(acridine-4-carboxamide) derivatives.

Table 1-3 Antiproliferative activity and *in vivo* growth delay data for substituted Bis(acridine-4-carboxamide) derivatives [124].

R	*In vitro* Lewis Lung IC_{50} (nM)	*In vivo* growth delay Colon-38 tumours (days)*
5,5'-Me	1.8	6
5,5'-Et	27	ND#
5,5'-Pr	1050	ND#
5,5'-Br	6	5
6,6'-Cl	13	2

Drugs were administered i.p. (90 mg/kg), single dose, #ND – not determined.

These analogues were more potent compared to DACA *in vitro* and a single dose (90 mg/kg) with the most potent 5-methyl analogue was able to achieve growth delay of 6 days in mice with s.c. Colon-38 tumours. The more lipophilic analogues in this series, 5,5'-Et and 5,5'-Pr were far less potent with IC_{50} values of 27 and 1050 nM respectively, compared to the 5,5'-Me analogue. No *in vivo* activity data in this tumour model was available to confirm the effects of increasing the chain length. However, no further data was available on this series.

1.8.4 Bis(phenazine-1-carboxamide) derivatives

Bis(phenazine-1-carboxamide) derivatives (Figure 1.5) were synthesised in an attempt to discover improved and potent analogues to DACA [125]. These were structurally similar to the Bis(acridines-4carboxamides) (discussed previously), where the dimeric acridine ring was replaced by phenazine. Several analogues were synthesised and a few of them were found to be potent *in vitro* and had significant growth delays in mice with Colon-38 tumours (Table 1-4).

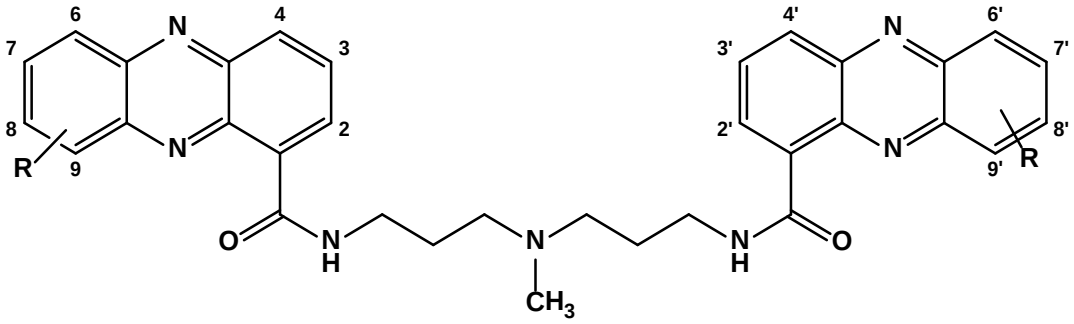

Figure 1.5 Chemical structure of Bis(phenazine-1-carboxamide) derivatives.

Table 1-4 Antiproliferative activity and *in vivo* growth delay data for substituted Bis(phenazine-4-carboxamide) derivatives [125].

R	*In vitro* Lewis Lung IC_{50} (nM)	*In vivo* growth delay Colon-38 tumours (days)*
8,8'-OMe	24	8
9,9'-Me	1.6	12
9,9'-Cl	8.8	7

Analogues were administered i.p. as single dose for 8,8'-OMe and 9,9'-Cl derivatives. 9,9'-Me was administered every 4 days x 3 (30 mg/kg).

Analogues with small, lipophilic substituents (e.g., Me, Cl) at the 9-position were the most potent inhibitors in the Lewis Lung culture *in vitro* and were superior to the corresponding dimeric bis(acridine-4-carboxamides) [124]. Several analogues produced significant growth delays in the relatively refractory subcutaneous Colon-38 tumour model *in vivo*. In particular, the 9,9'-Me analogue was more potent in this tumour model than the clinical dual topo I/II poison DACA (total dose: 90 versus 400 mg/kg) with comparable activity [118].

1.8.5 XR11576

XR11576 (Figure 1.6) is an angular tetracyclic phenazine-1-carboxamide developed by Xenova which progressed to a Phase I clinical trial. This was an orally active dual topoisomerase poison [126].

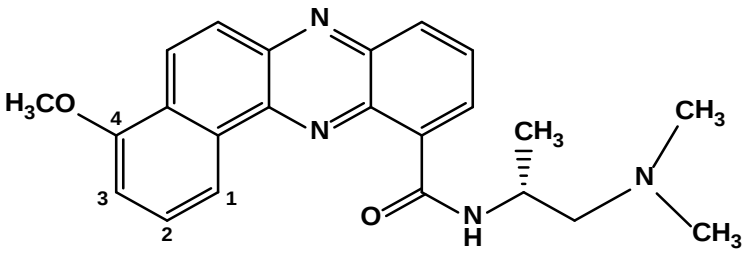

Figure 1.6 Chemical structutre of XR11576.

In vitro cytotoxicity evaluation was performed in COR-L23/P, non-small cell lung carcinoma (NSCLC) and H69/P small cell lung carcinoma (SCLC) cell lines and their respective drug-resistant sublines H69/LX4 and L23/R, Jurkat cell lines, P388 and Lewis lung (LLTC) and MC26 mouse colon carcinoma cultures [127]. XR11576 was found to be cytotoxic in these cultures in nanomolar concentrations [5.6 (LLTC) to 23 (H69/P) nM] [127]. Susceptibility to multi-drug resistance was minimal with P-gp and MRP resistance factors of 1.2 as tested in H69/LX4 and L23/R sublines.

In vivo anti-tumour activity was tested in mice with H69/P and the MDR H69/LX4 SCLC xenograft tumours. Significant growth delays were observed in mice with H69 tumours after i.v. (q7d x 3) and p.o. (q7d x 3) administration of XR11576 [i.v. - (30 mg/kg), T/C – 58 %; p.o. – 50 and 65 mg/kg, T/C – 63 and 64%] (T/C: The percentage ratio of the mean relative tumour volume (RTVm) of treated mice (T) and the RTVm of the controls (C), calculated (T/C%) [127].

In vivo pharmacokinetic studies were performed in BALB/c healthy mice and CD1 nude mice with H69 SCLC tumours. In healthy mice, XR11576 was administered i.v. and p.o.

(50 mg/kg), (p.o. bioavailability of 72 %). After i.v. administration normal tissue levels also displayed biphasic kinetics with an elimination $T_{½}$ (2.6 – 3.6 h) similar to that in plasma. Tumour XR11576 levels decreased at a much slower rate than in other tissues, with AUCs in tumours after i.v. (20 mg/kg) and p.o. (50 mg/kg) administration (150 and 100 mg µg.h/ml) were higher than in the liver (60 and 82 µg.h/ml) or heart (47 and 27 µg.h/ml), respectively [127].

Phase I clinical trial of XR11576 was undertaken in 22 patients with malignant solid tumours. XR11576 was formulated as gelatin capsules comprising 5, 20, 60 and 120 mg of active drug and administered on days 1 – 5 of a 3-weekly cycle with escalating doses of 30 – 80 mg/day. Maximum plasma concentrations occurred at 3.7 h post dose and declined with a mean terminal $T_{½}$ of up to 70 h. Severe nausea and vomiting were the major dose limiting toxicities and this was considered a major drawback, leading to the cessation of further development of this drug [126].

1.8.6 SN 28049

SN 28049 (Figure 1.7) was developed in collaboration with Professor Les Deady at La-Trobe University, Melbourne, VIC, Australia with all biological evaluation being carried out at the ACSRC [113, 128]. SN 28049 is thought to bind to DNA by intercalation, preventing the ligation step of topoisomerase II, as well as interfering with the action of topoisomerase I [129].

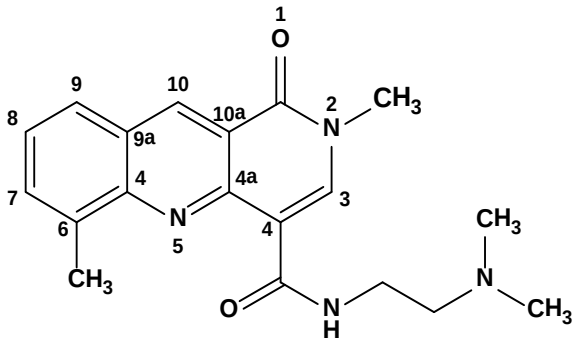

Figure 1.7 Chemical structure of SN 28049. (N-[2-(dimethylamino)ethyl]-2,6-dimethyl-1-oxo-1,2-dihydrobenzo[b]-1,6-naphthyridine-4-carboxamide).

1.8.6.1 Activity of SN 28049

SN 28049 is a dose potent analogue compared to other topoisomerase poisons. A comparison of the *in vitro* activity of SN 28049 with several other anti-cancer drugs shows it to be highly potent (Table 1-5) (B. Baguley, unpublished data).

Table 1-5 IC_{50} values (nM) of topoisomerase II poisons. (B. Baguley, unpublished data).

Cell line	SN 28049	Etoposide	Amsacrine	DACA	Doxorubicin
P388	2.1	25	20	98	15
LLTC	1.7	180	12	190	22
HCT116p53$^+$	8.4	210	25	360	10.5
HCT116p53$^-$	16	390	52	510	21
Jurkat	6.7	160	37	580	9.6
JL_A	38	2080	3100	1100	42
JL_D	53	14400	2700	2500	270

P388 is a murine leukaemia; LLTC is a murine lung carcinoma line; HCT116 is a human carcinoma line that has either wild-type p53 function (p53+) or lacks p53 function (p53-); Jurkat is a human leukaemia line and JL_A and JL_D are multi-drug resistant derivatives of the Jurkat line with lowered topoisomerase I.

In vivo growth delay studies were performed in C57 Bl/6 female mice implanted with Colon-38 tumours. A single intraperitoneal (i.p.) dose of SN 28049 at 3.9 mg/kg induced a growth delay of 8 days and 8.9 mg/kg resulted in complete regressions of the tumour for a period of at least 20 days [113]. A comparison of tumour growth delays of SN 28049, etoposide and doxorubicin is shown in Figure 1.6. Doxorubicin (4 mg/kg) and etoposide (45 mg/kg) had to be administered once every three days to achieve partial remission. Additionally, SN 28049 was found to be orally active, with a single p.o. dose (8.9 mg/kg) inducing complete regression of Colon-38 tumours (Figure 1.8).

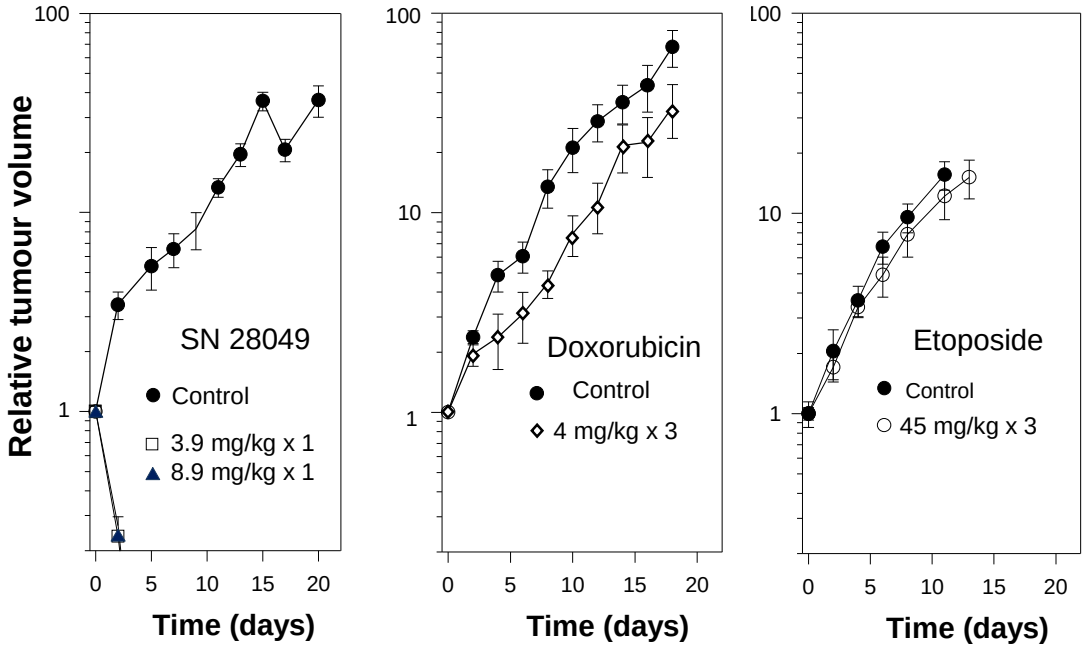

Figure 1.8 Growth delay curves of SN 28049, Doxorubicin and Etoposide in murine Colon-38 tumours after i.p. administration. (B. Baguley, unpublished data).

1.8.6.2 *In vivo* pharmacokinetics of SN 28049 in mice

SN 28049 was rapidly absorbed upon administration and had a high i.p. plasma bioavailability (86 %) and a moderate (55 %) p.o. bioavailability in mice. The biphasic concentration-time elimination profile observed in plasma after an i.v. bolus dose indicated that a two-compartment model was the most appropriate model to describe its pharmacokinetics. SN 28049 had a relatively high volume of distribution (V_{SS}), 35 l/kg and a moderate clearance (CL) (12 l/h/kg). Distribution to tissues (brain, heart, liver, lung and kidney) was rapid and tissue concentrations were 12 to 120-fold higher than those in plasma but tended to follow the plasma profile [130]. However, the tumour profile was very different. The maximal concentrations were achieved more slowly (6 – 12 h) and tumour exposure was 658-fold greater than plasma. The elimination $T_{½}$ and the mean residence

time (MRT) were also significantly longer ($P < 1 \times 10^{-3}$) compared to plasma and other tissues with SN 28049 measurable in tumour for up to 72 h following a single i.p. dose. This slow uptake and longer retention in tumour tissue is thought partly to be the reason for the greater efficacy of SN 28049. Preliminary studies on the identification of metabolites in urine, plasma and liver indicate that relatively high concentrations are excreted unchanged via urine. Four additional metabolites were identified with SN 28049-N-oxide being the major metabolite in urine [131]. The potential enzymes involved are shown in Figure 1.9.

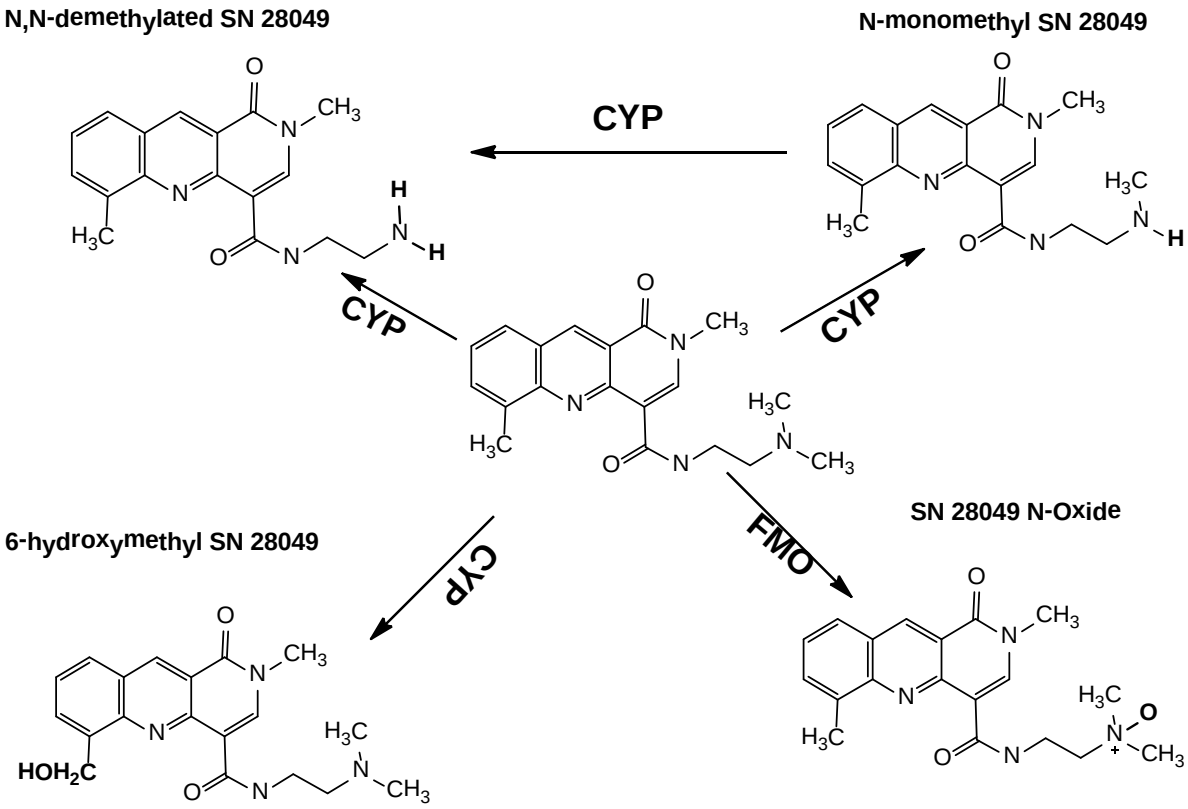

Figure 1.9 Metabolites of SN 28049 identified in mice with possible enzymes involved. The latter are based on similar reactions with DACA [131].

1.9 Aims

The benzonaphthyridine derivatives incorporate a DNA-binding chromophore with a sequence selective carboxamide side chain. The ring structure with various substitutions at the N-2 position were synthesised in ACSRC.

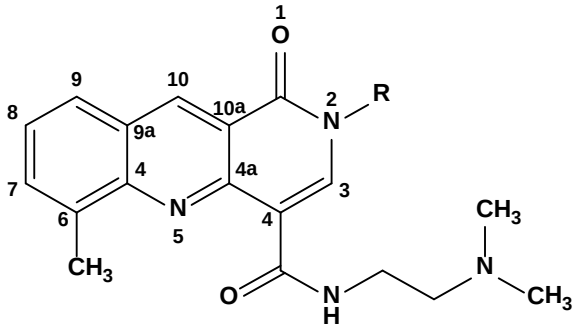

R = -H, Hydrogen; SN 28101
$-CH_3$, Methyl; SN 28049
$-C_2H_5$, Ethyl; SN 28668
$-C_3H_7$, Propyl; SN 32116
$-C_4H_9$, Butyl; SN 28048

Figure 1.10 Chemical structure of benzonaphthyridine with substitutions at N-2 position.

The aim was to identify the factors responsible for the exceptional tumour pharmacokinetics of SN 28049. In particular, whether the latter is related to its lipophilicity, protein binding affinity, or possibly active cellular uptake/efflux rates. To achieve this, a series of benzonaphthyridine derivatives with minor structural modifications at the N-2 position (Figure 1.10) were synthesised in the ACSRC. The chain length was increased by a methyl group to obtain a series (hydrogen – butyl) with increasing lipophilicity. Specific aims and approaches are listed in the chapters to follow.

Chapter 2

A rapid LC-MS/MS method for the quantitation of a series of benzonaphthyridine derivatives

2.1 Introduction

N-[2-(dimethylamino)ethyl]-2,6-dimethyl-1-oxo-1,2-dihydrobenzo[b]-1,6-naphthyridine-4-carboxamide (SN 28049) is a DNA intercalating topoisomerase II poison being tested for its anti-cancer activity. The latter (methyl analogue) along with hydrogen, ethyl, n-propyl and n-butyl substitutions at the N-2 position of the benzonaphthyridine ring structure were synthesised and utilised as a homologous series to study the effects of lipophilicity (as determined by their partition coefficient; Log D values) on their pharmacokinetics. SN 28049 exhibited curative anti-tumour activity in a Colon-38 murine tumour model and was greatly superior to the standard topoisomerase II poisons such as etoposide and doxorubicin as demonstrated by Deady et al [113]. A previous study by Lukka et al [130] suggested that pharmacokinetics may play a major role in its superior anti-tumour properties. We have previously reported an ion-trap liquid chromatography – mass spectroscopy (LC-MS/MS) method [132] for the quantitation of SN 28049 and its application to a pharmacokinetic study in mice. The limit of quantitation of the latter method (0.062 µM) was acceptable, but the sensitivity was in insufficient to measure the concentrations beyond 12 h post administration. In addition, no analytical method was available for the other four analogues to be investigated.

2.2 Aims and approach

The aims were:

1. To develop a selective and sensitive LC-MS/MS method to quantitate a series of benzonaphthyridine analogues simultaneously.

2. Validation of the method in a variety of biological matrices such as human plasma, mouse plasma and tissue homogenates such as brain, heart, kidney, liver, lung and tumour.

2.3 Materials and methods

The series of benzonaphthyridine analogues with substitutions at the N-2 position were used. SN 28101 (hydrogen) (free base, 99 % pure by LC; MW, 324); SN 28049 (methyl) (free base, 99 % pure by LC; MW, 338); SN 28668 (ethyl) (free base, 99 % pure by LC; MW, 352); SN 32116 (propyl) (free base, 99 % pure by LC; MW, 366); SN 28048 (butyl) (free base, 99 % pure by LC; MW, 380) and the deuterated internal standard (IS) SN 32444 (free base, 98% pure by LC; MW, 374) were synthesized in the Auckland Cancer Society Research Centre using previously published methods [113]. Unless stated, all other chemicals were commercially available and of analytical grade. Water used in all experiments was purified by filtering through ion exchange columns and a 0.22 µ filter (Milli Q purification system, Millipore Corporation, Bedford, MA, USA).

2.3.1 Mice

C57 Bl/6 female mice (20 – 25 g; 8 – 12 week old) were housed under constant temperature, humidity and lighting (12 h light per day). All experiments which included blood collection in mice from the ocular sinus under isofluorane anaesthesia were approved by The University of Auckland Animal Ethics Committee and conformed to the Guidelines for the Welfare of Animals in Experimental Neoplasia, as set out by the United Kingdom Co-ordinating Committee on Cancer Research.

2.3.2 Subcutaneous Colon-38 tumour transplantation

The murine Colon-38 adenocarcinoma (obtained from the Mason Research Institute, Worcester, MA, USA) was maintained *in vivo* by serial passage in C57 Bl/6 mice. The tumour was surgically removed from the donor mice (after cervical dislocation) and transferred to a Petri dish (BD Falcon Labware, Franklin Lakes, NJ, USA) containing 10 ml phosphate buffered saline (PBS). Viable tumour fragments (1 mm^3) were isolated and transplanted subcutaneously into recipient mice previously anaesthetized by intraperitoneal (i.p.) administration (10 µl/g body weight) of a xylazine (10 mg/kg), ketamine (150 mg/kg) mixture. The incision was closed using a Michel wound clip (Aesculap, Tuttlingen, Germany). Experiments were carried out when tumours reached 8 – 10 mm in diameter, 15 – 20 days after transplantation.

2.3.3 Preparation of mouse plasma and tissue homogenates

Mouse plasma was prepared from the blood of anaesthetised C57 Bl/6 mice and stored at –80°C. To prevent coagulation, blood was collected in BD Vacutainer® (BD Biosciences, Franklin Lakes, NJ, USA) tubes coated with K_2 EDTA and plasma was separated by centrifugation at 6000 × *g* for 10 min. Tissues (brain, heart, kidney, liver, lung and tumour) were collected after cervical dislocation of the anaesthetized mice. Collected tissues were washed with 1 ml phosphate buffered saline (PBS) to remove blood contamination, briefly dried, transferred to 2 ml nunc CryoTubes® (Thermo Scientific, Rochester, NY, USA) and stored at –80°C. Frozen tissues were thawed at room temperature (25°C) and transferred in to glass tubes, weighed and homogenized in PBS (4-volumes) using a tissue homogenizer (S/N TH-71, Omni TH homogenizer, Gainesville, VA, USA) operated at 24000 rpm.

2.3.4 Liquid Chromatograph – Mass Spectrometer

The LC-MS/MS system was an Agilent 1200 Rapid Resolution liquid chromatograph (LC) and Agilent 6410 triple quadrupole mass spectrometer (QqQ) equipped with a multimode ionisation source (Agilent Technologies, Santa Clara, CA, USA). Chromatographic separation was achieved on an Agilent Zorbax SB-C18 (50 mm × 2.1 mm, 5 µm) column with a 0.2 µm in-line filter and was maintained at 35°C. The mobile phase consisted of 80 % acetonitrile with 0.01 % formic acid (mobile phase A) and water containing 0.01 % formic acid (mobile phase B) with a fast gradient elution at a flow rate of 0.5 ml/min and run time of 7 min. The following gradient was applied: 0 min, 90 % B; 1 min, 90 % B; 2.5 min, 10 % B; 5 min, 10 % B; 6 min, 90 % B; 7 min, 90 % B. The column was equilibrated for 1 min between injections. The eluent flow was led into the MS/MS starting 0.5 min after injection by switching the MS inlet valve. The sample volume injected was 25 µl and the autosampler was set at 4°C. The mass spectrometer was run in positive ion ESI-APCI combined mode using multiple reaction monitoring (MRM) to monitor the mass transitions. The retention times for the analogues were as follows: Hydrogen, 3.04 min; methyl, 3.60 min; ethyl, 3.81 min; propyl, 4.05 min; butyl, 4.36 min; d_7 IS, 4.05 min. The mass resolution was set at 0.7 u FWHM (unit mass resolution) for both quadrupoles. Other parameters of the mass spectrometer were: collision energy 15 V; fragmentor voltage 130 V; gas flow 5.5 l/min; gas temperature 350°C; vaporizer temperature 225°C; nebulizer 55 psi; capillary 3000 V, corona current positive 3 µA, charging voltage 1500 V. Data were acquired and analysed with Agilent MassHunter® software.

2.3.5 Stock solutions, calibrants and quality controls

Stock solutions (1 mM) of all 5 benzonaphthyridine analogues were prepared individually in acetonitrile. Subsequent dilutions of individual analogues using a pooled approach resulted in a final concentration range of 0.001, 0.005, 0.01, 0.025, 0.05, 0.1 and 0.3 µM for the calibration curve for all 5 analogues in plasma and tissue homogenates. Freshly prepared working solutions of all 5 analogues from an independently weighed 1 mM stock were used to prepare quality control (QC) samples. Appropriate volumes were then added to freshly thawed particle-free human plasma, mouse plasma and mouse tissue homogenates to give concentrations of 0.001, 0.025 and 0.3 µM (5 ml of each concentration). Aliquots (200 µl) of each QC samples were stored at −80°C immediately after the preparation. During each subsequent analytical run, one set (triplicate) of each QC concentration was included (scattered in between the calibrants and the unknown samples) and processed with the calibrants and *in vivo* study samples.

2.3.6 Sample preparation

Aliquots (25 µl) of plasma or tissue homogenates (either calibrants, quality controls) were precipitated with 3-volumes (75 µl) acetonitrile:methanol (3:1) mixture containing deuterated (d_7) internal standard (IS) (0.05 µM). For analysis of samples from the *in vivo* study, 25 µl samples of each analogue were pooled and precipitated with 3-volumes of the acetonitrile:methanol (3:1) mixture containing deuterated (d_7) internal standard (IS) (0.05 µM). Samples were vortexed for 30 sec, followed by centrifugation at 13,000 × *g* (5 min, 4°C). A 50 µl aliquot of each supernatant was then diluted in 50 µl of mobile phase B and injected in to the LC-MS/MS (25 µl injection volume). Blank samples were prepared from plasma (human and mouse) and tissue homogenates using the same extraction procedure.

2.3.7 Validation procedures

Analytical specificity was tested by inspection of chromatograms of extracted drug-free plasma and tissue homogenate samples for interfering peaks. Extraction recoveries were assessed by comparing peak areas of each analyte and IS from extracted plasma QC samples, to standards prepared in blank matrix extract. All recovery studies were performed at three different concentrations and in triplicate. To determine intra-day reproducibility 5 – 6 replicates of the QC samples were analysed, including the LOQ. Inter-day precision was calculated from QC samples analysed on three or more different

days. At each concentration, precision was calculated as the relative standard deviation (RSD) and accuracy as the percentage of the true value. Acceptable precision was defined by a RSD within 15 % and accuracy within 85 – 115 % of the true value. The LOQ was defined to be the lowest concentration that could be measured with the minimum acceptable accuracy (within 80 – 120 % of the true value) and precision (RSD within 20 %). Matrix effects on each analyte were assessed in triplicate by spiking the analytes in different batches of extracted (with 3 volumes of acetonitrile:methanol (3:1)) plasma (mouse and human) and mouse tissue homogenates. Each analytical run consisted of a single calibration curve, triplicate QC samples at three concentrations, one reagent blank, one plasma/tissue blank and one zero-level (blank matrix sample with d_7 IS) standard. The stability of all 5 analogues was measured in duplicate at room temperature over 24 h in plasma and tissue homogenates. At each time point, plasma/tissue samples containing all 5 analogues were removed and then extracted as described above. In addition, the stability of all 5 analogues in plasma and tissue homogenates was assessed at three different concentrations in triplicate when left on ice or on the benchtop for 0 – 24 h. Similarly, stability during storage in the autosampler was determined at three different concentrations in triplicate over 24 h at 4°C. Three freeze-thaw cycles at −80°C were used to test the stability all 5 analogues in plasma. Long-term plasma stability was assessed at −80°C over 1 year. For short–term/bench-top, long-term and freeze-thaw stability, mean concentrations of triplicate samples were compared to the initial values.

2.4 Results and discussion

2.4.1 Specificity

The product ion fragments of all the 5 analogues and the IS were monitored using MRM following extraction from the matrices. No interference was observed from the endogenous components of the matrices. A blank chromatogram (Figure 2.1) and extracted MRM traces for all mass transitions at the LOQ are shown in Figure 2.2. Additionally, precursor ions arising from possible metabolites (N-demethylation, hydroxymethylation and N-mono demethylation) were verified for each analogue and no interference from transitions was observed.

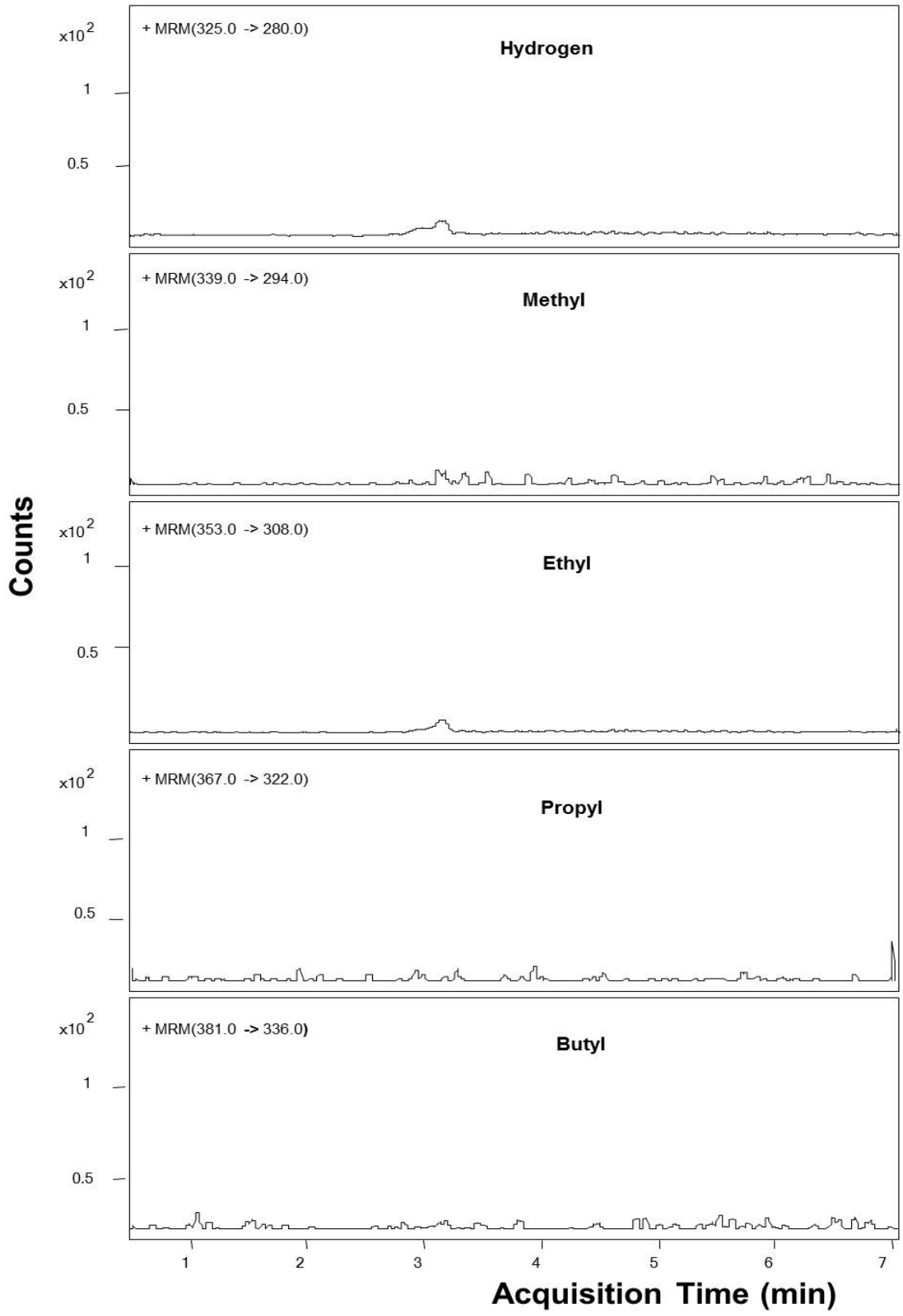

Figure 2.1 Blank traces of 5 benzonaphthyridine analogues (hydrogen – butyl).

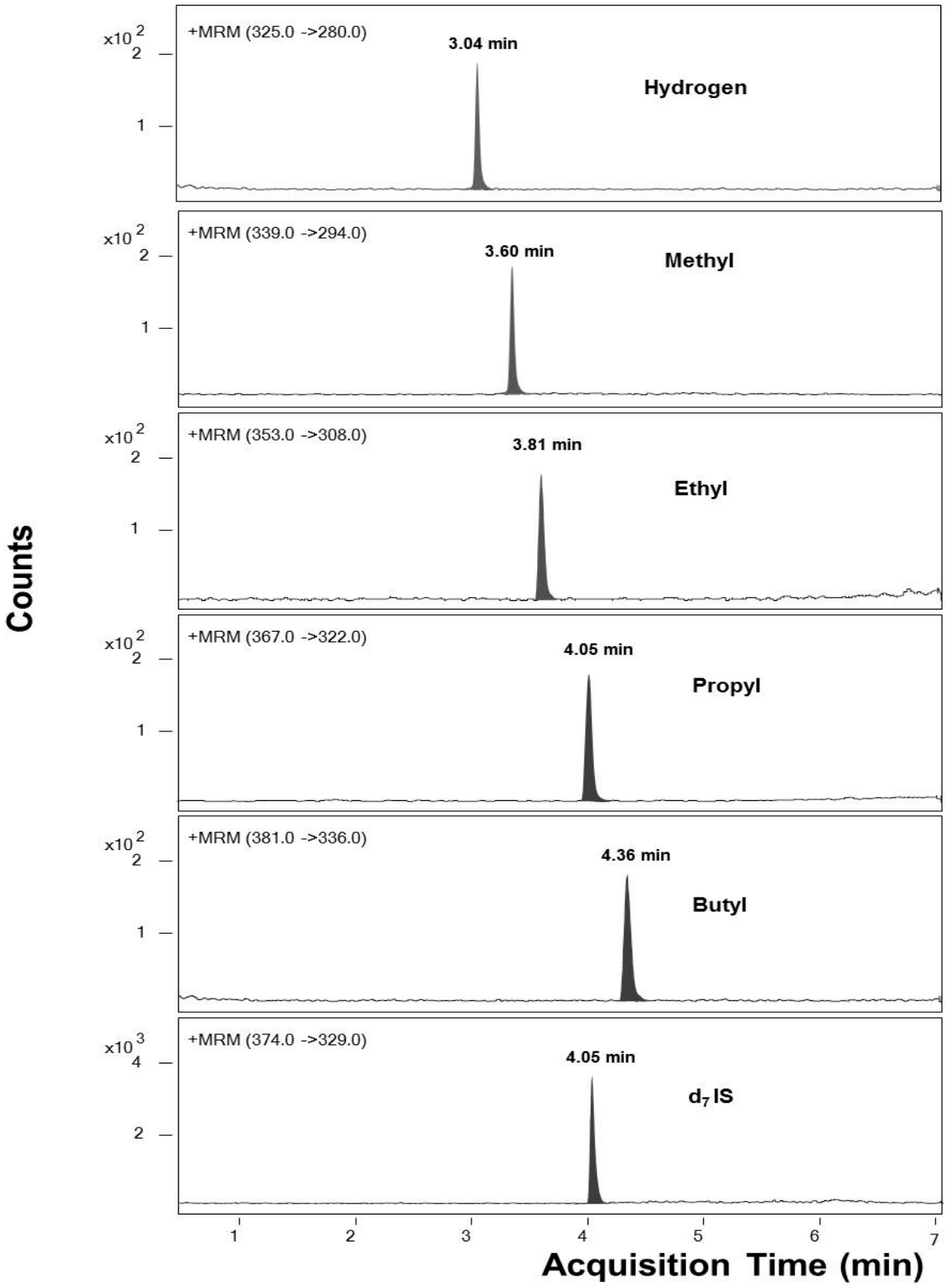

Figure 2.2 MRM traces of 5 benzonaphthyridine analogues (hydrogen – butyl) at the LOQ. The d_7 internal standard is co-eluted with the propyl analogue and had a retention time on 4.05 min.

2.4.2 Linearity

The calibration curve was assessed based on a plot of the ratio of peak areas for each analogue/IS. A linear fit model with no weighting best described the concentration-response relationship. A representative calibration curve is shown in Figure 2.3. The assay was found to be linear for all the analogues over the concentration range 0.001 – 0.3 µM in all the matrices tested (r^2 > 0.99). Plasma and tissue samples with concentrations > 0.3 µM were diluted accordingly. Accuracy and precision data obtained from the calibration curves of plasma and tissues matrices prepared on six different occasions over the concentration range were within the acceptable range (Precision, < 7.0 % and Accuracy, 93.8 – 106.2 % of nominal values) as shown in Table 2-1.

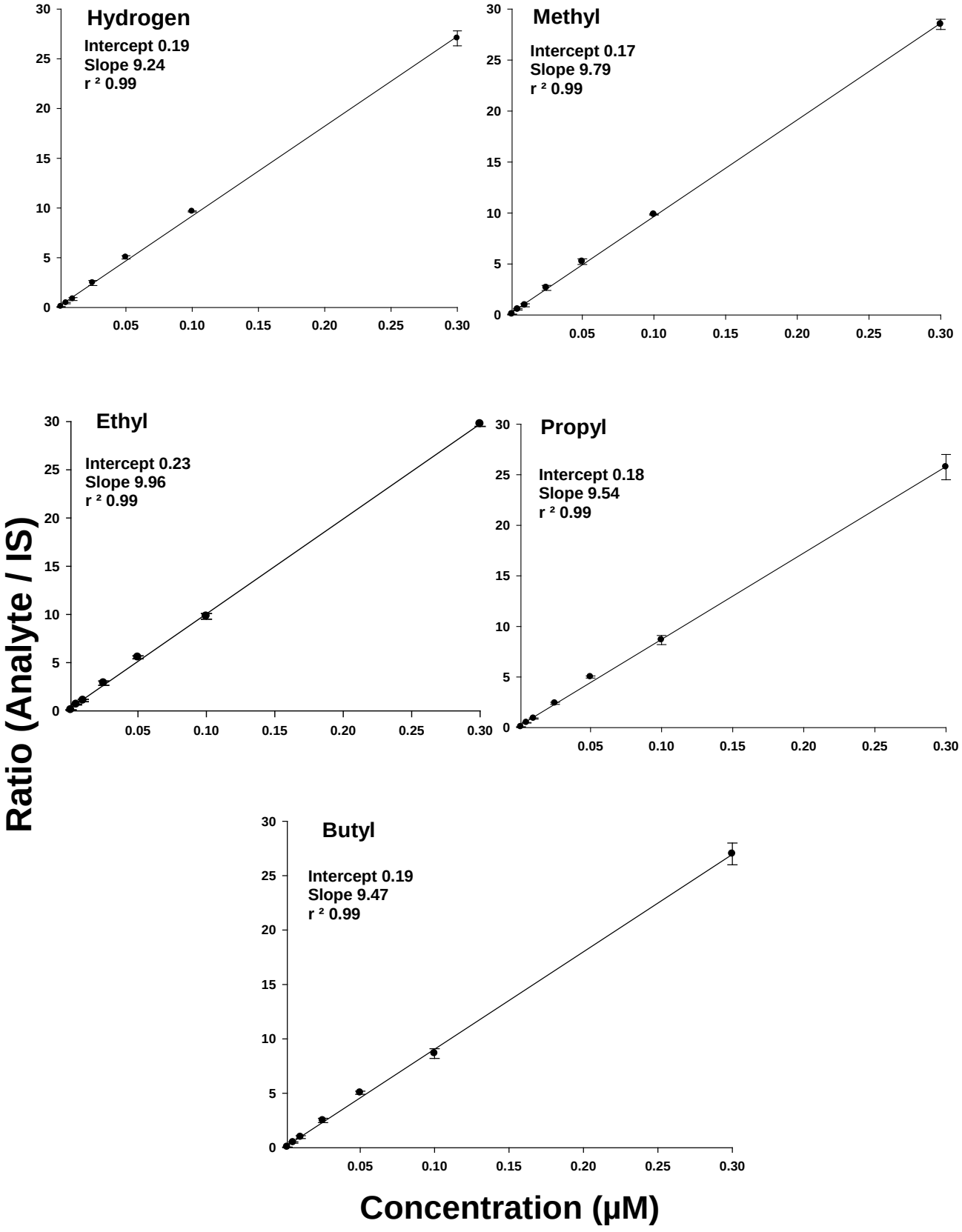

Figure 2.3 A representative standard curve of each analogue (hydrogen – butyl) over the linear range of 0.001 – 0.3 µM. Each point is mean ± s.e (n = 3).

Table 2-1 Linearity, Accuracy and Precision of the calibrants (0.001 – 0.3 µM) of the benzonaphthyridine analogues. Results are mean ± s.e (n = 10).

	Hydrogen			Methyl			Ethyl		
Matrix	**Linearity (r^2)**	**Precision (RSD %)**	**Accuracy (%)**	**Linearity (r^2)**	**Precision (RSD %)**	**Accuracy (%)**	**Linearity (r^2)**	**Precision (RSD%)**	**Accuracy (%)**
Human Plasma	>0.99	<3.5	96.1 ± 4.1	>0.99	<6.2	95.2 ± 5.6	>0.99	<2.5	94.7 ± 2.4
Mouse Plasma	>0.99	<4.1	98.2 ± 2.5	>0.99	<3.5	94.1 ± 4.1	>0.99	<1.6	100.4 ± 4.3
Brain	>0.99	<5.6	97.3 ± 3.5	>0.99	<4.1	97.3 ± 2.3	>0.99	<4.6	105.2 ± 3.4
Heart	>0.99	<6.1	94.6 ± 2.9	>0.99	<5.3	96.2 ± 1.8	>0.99	<5.1	94.8 ± 6.2
Kidney	>0.99	<2.8	100.2 ±5.7	>0.99	<2.3	97.1 ± 4.2	>0.99	<2.6	95.7 ± 3.2
Liver	>0.99	<3.9	98.6 ± 5.1	>0.99	<3.8	98.1 ± 3.5	>0.99	<6.1	98.1 ± 6.4
Lung	>0.99	<4.6	97.2 ± 4.3	>0.99	<7.0	95.2 ± 6.1	>0.99	<5.6	94.3 ± 5.6
Tumour	>0.99	<3.1	95.4 ± 4.6	>0.99	<5.6	99.3 ± 4.2	>0.99	<4.8	93.7 ± 4.2

	Propyl			Butyl		
Matrix	**Linearity (r^2)**	**Precision (RSD %)**	**Accuracy (%)**	**Linearity (r^2)**	**Precision (RSD %)**	**Accuracy (%)**
Human Plasma	>0.99	<4.1	94.5 ± 5.1	>0.99	<6.2	97.1 ± 2.3
Mouse Plasma	>0.99	<3.5	94.1 ± 6.2	>0.99	<1.5	94.3 ± 1.7
Brain	>0.99	<2.6	99.4 ± 3.4	>0.99	<2.6	93.4 ± 3.5
Heart	>0.99	<5.1	97.2 ± 4.6	>0.99	<4.2	92.4 ± 4.6
Kidney	>0.99	<3.4	96.4 ± 5.2	>0.99	<3.8	106.2 ± 3.8
Liver	>0.99	<6.1	95.4 ± 3.5	>0.99	<2.6	96.2 ± 2.9
Lung	>0.99	<4.5	96.1 ± 4.3	>0.99	<4.6	95.1 ± 3.2
Tumour	>0.99	<3.8	97.1 ± 1.8	>0.99	<5.6	97.4 ± 5.4

2.4.3 Fragmentation patterns

SN 28101 (hydrogen) ionizes in the positive ionization mode, gaining a proton and entering the metastable state of $[M+H]^+$ and can be seen in the spectrum as m/z 325. The latter can then be fragmented and characterized in MS2 mode ($[M+H]^+ – C_2H_7N$) to give a MS2 ion at m/z 280. The other analogues in this series (methyl, ethyl, propyl and butyl) and the d_7 also fragment in the similar fashion producing product ions as follows: methyl, 339^294; ethyl, 353^308; propyl, 367^322; butyl, 381^366; d_7 IS, 374^329. The structure of these fragments were simulated and established with the help of ACD/MS fragmenter (ver. 12, ACD Labs, Toronto, Ontario, Canada). The fragmentation pattern and the mass spectra are shown in Figure 2.4.

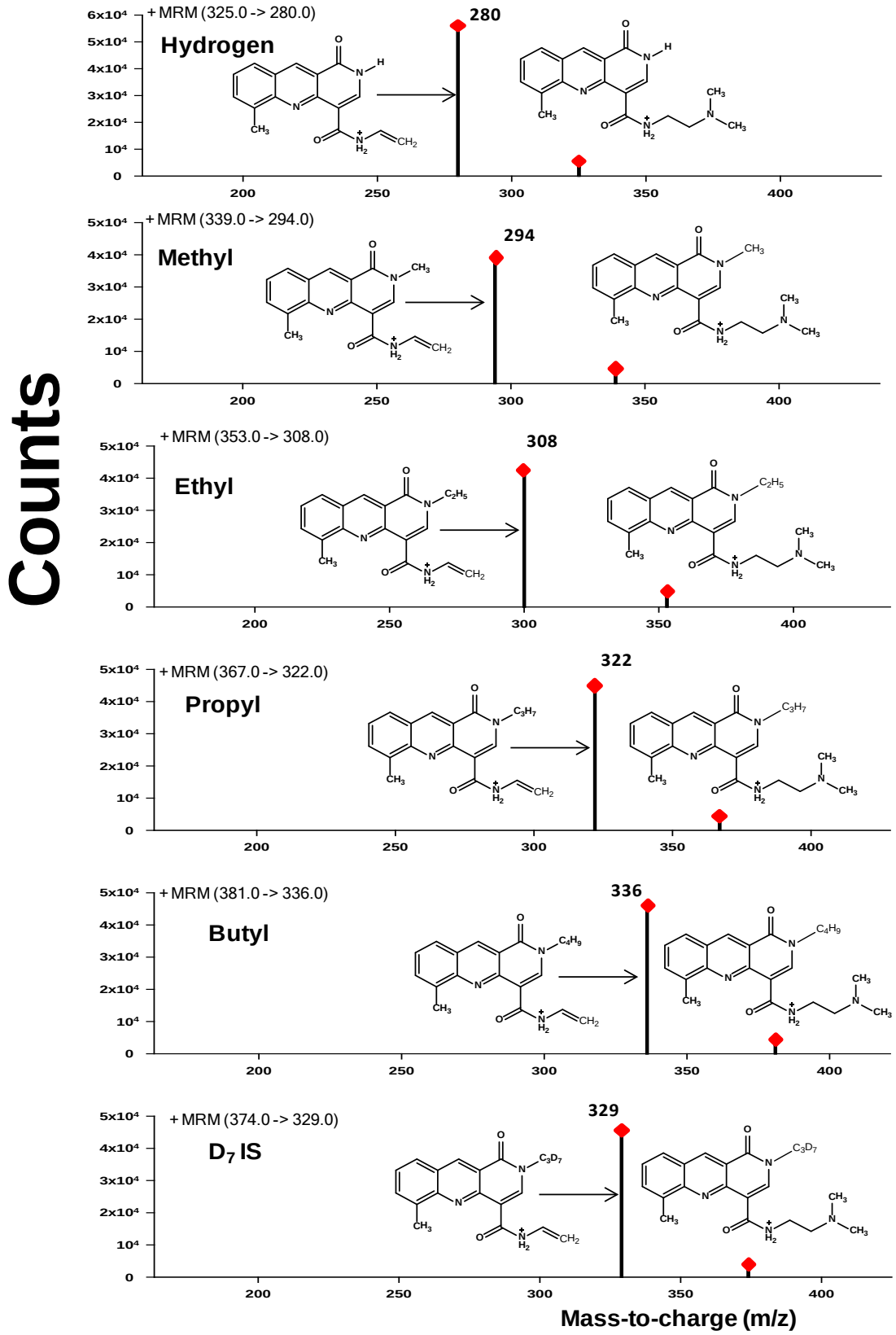

Figure 2.4 Fragmentation spectra and simulated structures of the fragments of the benzonaphthyridine analogues (hydrogen – butyl) and the d_7 internal standard.

2.4.4 Recovery and matrix effects

The extraction recovery was determined by comparing peak areas of standards prepared in Milli Q water containing 0.01 % formic acid to those extracted from spiked plasma and tissue homogenates. Authentic standards, spiked plasma and tissue homogenates were prepared in triplicate in the same manner over three concentrations 0.001, 0.025 and 0.3 µM. The absolute recoveries for all analogues (0.001 – 0.3 µM) were > 82.0 ± 1.5 % and the IS (0.05 µM) > 87.1 ± 2.5 %, respectively. Matrix effects tested by spiking the analytes in extracted plasma and tissue homogenates and comparing them standards prepared in Milli Q water containing 0.01 % formic acid indicated a lack of ion suppression by matrix components.

2.4.5 Limit of quantitation

The lower limit of quantitation (LOQ) in plasma and tissue matrices analysed by LC-MS/MS was found to be 0.001 µM. Concentrations below the LOQ were detected with unacceptable accuracy and precision (i.e., RSD > 20%, accuracy < 80 % and > 120% of the nominal values).

2.4.6 Precision and accuracy

The intra-assay precision was determined by calculating the RSD of 8 repeat measurements at three different concentrations (0.001, 0.025 and 0.3 µM) of all analogues in plasma and tissue homogenates on 1 day and was found to be < 7.1% for all concentrations. The intra-assay accuracy was determined by comparing the means of the measured concentrations to their true concentrations on the same day. The intra-assay accuracy was also acceptable over the three concentrations, varying between 92.1 ± 5.5 % and 102.1 ± 3.8 % of the true values as shown in Table 2-2.

The inter-assay precision was determined by replicate measurements performed on ten different occasions over 1-year for three concentrations in plasma and tissue homogenates. The inter-assay precision was less than 6.5 %. The inter-assay accuracy was calculated over 10 different occasions and was between 92.1 ± 5.5 % and 102.1 ± 5.5 % of the nominal values as shown in Table 2-3.

Table 2-2 Intra-assay precision and accuracy data for benzonaphthyridine analogues (hydrogen – butyl) over three concentrations (0.001, 0.025 and 0.3 μM) for plasma and tissue homogenates. Results are mean ± s.e (n = 8).

	Hydrogen						Methyl						Ethyl					
Concentration (μM)	0.001	0.025	0.3	0.001	0.025	0.3	0.001	0.025	0.3	0.001	0.025	0.3	0.001	0.025	0.3	0.001	0.025	0.3
Matrix	**Precision (RSD %)**			**Accuracy (%)**			**Precision (RSD %)**			**Accuracy (%)**			**Precision (RSD %)**			**Accuracy (%)**		
Human Plasma	<6.5	<2.5	<4.1	96.1 ± 7.2	95.1 ± 5.2	98.1 ± 5.2	<6.5	<2.8	<5.9	98.1 ± 6.4	97.1 ± 6.4	95.1 ± 5.4	<6.0	<2.3	<5.4	103.1 ± 7.7	93.1 ± 7.2	93.1 ± 7.7
Mouse Plasma	<5.8	<3.8	<3.6	94.1 ± 6.3	94.4 ± 3.3	94.4 ± 3.8	<5.4	<4.9	<2.9	97.3 ± 7.6	98.3 ± 4.6	101.3 ± 1.6	<5.5	<7.3	<5.3	95.1 ± 4.9	96.1 ± 4.9	102.1 ± 4.9
Brain	<7.1	<5.4	<5.3	98.1 ± 6.4	97.1 ± 6.4	95.1 ± 5.4	<4.6	<4.8	<2.5	96.1 ± 7.2	95.1 ± 5.2	98.1 ± 5.2	<5.7	<6.3	<5.1	94.1 ± 6.3	101.4 ± 3.3	101.4 ± 3.8
Heart	<6.5	<4.9	<4.6	96.1 ± 5.5	96.1 ± 5.5	97.1 ± 2.5	<5.9	<3.8	<5.4	96.1 ± 5.5	96.1 ± 5.5	97.1 ± 2.5	<5.6	<4.5	<5.0	96.3 ± 3.8	102.1 ± 3.8	102.1 ± 3.2
Kidney	< 6.4	< 4.8	<5.9	97.3 ± 7.6	98.3 ± 4.6	101.3 ± 1.6	<2.9	<4.6	<4.6	96.1 ± 3.8	102.1 ± 3.8	102.1 ± 3.2	<3.5	<1.8	<4.9	92.1 ± 5.5	96.1 ± 5.5	97.1 ± 2.5
Liver	<5.8	<3.8	<2.9	101.1 ± 7.7	93.1 ± 7.7	93.1 ± 7.7	<2.5	<5.9	<4.9	94.1 ± 6.3	94.4 ± 3.3	94.4 ± 3.8	<5.4	<3.6	<4.7	94.1 ± 7.2	99.1 ± 5.2	102.1 ± 5.2
Lung	<4.5	<5.1	<2.7	96.1 ± 3.8	102.1 ± 3.8	102.1 ± 3.2	<6.1	<2.9	<4.8	94.1 ± 4.9	96.1 ± 4.9	102.1 ± 4.9	<4.2	<2.5	<4.6	97.3 ± 7.6	96.3 ± 4.6	101.3 ± 1.6
Tumour	<5.8	<2.9	<6.1	94.1 ± 4.9	96.1 ± 4.9	102.1 ± 4.9	<5.8	<4.1	<5.4	101.1 ± 7.7	93.1 ± 7.7	93.1 ± 7.7	<5.1	<3.4	<4.5	99.1 ± 6.4	97.1 ± 6.1	95.1 ± 5.4

Table 2-2 continued.

	Propyl						Butyl					
Concentration (μM)	0.001	0.025	0.3	0.001	0.025	0.3	0.001	0.025	0.3	0.001	0.025	0.3
Matrix	**Precision (RSD %)**			**Accuracy (%)**			**Precision (RSD %)**			**Accuracy (%)**		
Human Plasma	<3.5	<1.8	<4.9	96.3 ± 3.8	92.1 ± 5.5	94.1 ± 7.2	<5.1	<3.4	<4.5	96.1 ± 4.9	94.3 ± 3.8	93.1 ± 7.2
Mouse Plasma	<5.4	<3.6	<4.8	102.1 ± 3.8	96.1 ± 5.5	99.1 ± 5.2	<5.6	<4.5	<5.0	102.1 ± 4.9	96.1 ± 3.8	95.1 ± 7.7
Brain	<4.2	<2.5	<4.6	102.1 ± 3.2	97.1 ± 2.5	102.1 ± 5.2	<3.5	<1.8	<4.9	96.3 ± 4.6	102.1 ± 3.2	101.3 ± 1.6
Heart	<5.1	<3.4	<4.5	103.1 ± 7.7	95.1 ± 4.9	94.1 ± 6.3	<5.4	<3.6	<4.8	101.3 ± 1.6	93.1 ± 7.7	92.1 ± 5.5
Kidney	<5.6	<4.5	<5.0	93.1 ± 7.2	96.1 ± 4.9	101.4 ± 3.3	<4.2	<2.5	<4.6	92.1 ± 5.5	93.1 ± 7.2	96.1 ± 5.5
Liver	<3.5	<1.8	<4.9	93.1 ± 7.7	102.1 ± 4.9	101.4 ± 3.8	<3.5	<1.8	<4.9	96.1 ± 5.5	95.1 ± 7.7	97.1 ± 2.5
Lung	<5.4	<3.6	<4.8	99.1 ± 5.2	96.3 ± 4.6	97.1 ± 6.1	<5.4	<3.6	<4.8	97.1 ± 2.5	99.1 ± 5.2	102.1 ± 4.9
Tumour	<4.2	<2.5	<4.6	102.1 ± 5.2	101.3 ± 1.6	95.1 ± 5.4	<4.2	<2.5	<4.6	101.4 ± 3.8	102.1 ± 5.2	96.3 ± 4.6

Table 2-3 Inter-assay precision and accuracy data for benzonaphthyridine analogues (hydrogen – butyl) over three concentrations (0.001, 0.025 and 0.3 μM) for plasma and tissue homogenates. Results are mean ± s.e (n = 10).

	Hydrogen						Methyl											
Concentration (μM)	0.001	0.025	0.3	0.001	0.025	0.3	0.001	0.025	0.3	0.001	0.025	0.3	0.001	0.025	0.3	0.001	0.025	0.3
Matrix	**Precision (RSD %)**			**Accuracy (%)**			**Precision (RSD %)**			**Accuracy (%)**			**Precision (RSD %)**			**Accuracy (%)**		
Human Plasma	<3.2	<4.5	<4.5	96.3 ± 3.8	102.1 ± 3.8	102.1 ± 3.2	<6.4	<4.8	<5.9	96.1 ± 5.5	96.1 ± 5.5	97.1 ± 2.5	<3.4	<4.6	<5.0	98.1 ± 3.8	96.1 ± 5.5	99.1 ± 5.2
Mouse Plasma	<3.4	<4.6	<5.0	92.1 ± 5.5	96.1 ± 5.5	97.1 ± 2.5	<5.8	<3.8	<2.9	97.3 ± 7.6	98.3 ± 4.6	101.3 ± 1.6	<4.5	<4.8	<4.8	101.1 ± 3.2	97.1 ± 2.5	102.1 ± 5.2
Brain	<4.5	<4.8	<4.9	94.1 ± 7.2	99.1 ± 5.2	102.1 ± 5.2	<4.5	<5.1	<2.7	94.1 ± 6.3	94.4 ± 3.3	94.4 ± 3.8	<1.8	<4.9	<6.5	103.1 ± 7.7	95.1 ± 4.9	94.1 ± 6.3
Heart	<1.8	<4.9	<6.5	96.1 ± 3.8	102.1 ± 3.8	102.1 ± 3.2	<5.7	<6.3	<5.1	98.1 ± 6.4	97.1 ± 6.4	95.1 ± 5.4	<5.4	<3.6	<4.8	93.1 ± 7.2	96.1 ± 4.9	101.4 ± 3.3
Kidney	<3.6	<5.0	<6.4	94.1 ± 6.3	94.4 ± 3.3	94.4 ± 3.8	<5.6	<4.5	<5.0	94.1 ± 7.2	99.1 ± 5.2	102.1 ± 5.2	<5.6	<4.5	<5.0	93.1 ± 7.7	102.1 ± 4.9	101.4 ± 3.8
Liver	<4.9	<5.1	<5.8	94.1 ± 4.9	96.1 ± 4.9	102.1 ± 4.9	<3.5	<1.8	<4.9	97.3 ± 7.6	96.3 ± 4.6	101.3 ± 1.6	<4.5	<5.1	<2.7	92.1 ± 5.5	93.1 ± 7.2	96.1 ± 5.5
Lung	<4.8	<5.3	<1.8	98.1 ± 6.4	97.1 ± 6.4	95.1 ± 5.4	<5.4	<3.6	<4.8	101.3 ± 1.6	93.1 ± 7.7	92.1 ± 5.5	<5.7	<6.3	<5.1	96.1 ± 5.5	95.1 ± 7.7	97.1 ± 2.5
Tumour	<4.6	<5.4	<3.6	96.1 ± 5.5	96.1 ± 5.5	97.1 ± 2.5	<5.6	<4.5	<5.0	92.1 ± 5.5	93.1 ± 7.2	96.1 ± 5.5	<5.6	<4.5	<5.0	97.1 ± 2.5	99.1 ± 5.2	102.1 ± 4.9

Table 2-3 continued.

	Propyl						Butyl					
Concentration (μM)	0.001	0.025	0.3	0.001	0.025	0.3	0.001	0.025	0.3	0.001	0.025	0.3
Matrix	**Precision (RSD %)**			**Accuracy (%)**			**Precision (RSD %)**			**Accuracy (%)**		
Human Plasma	<5.6	<4.5	<5.0	101.3 ± 1.6	93.1 ± 7.7	92.1 ± 5.5	<5.6	<4.5	<5.0	94.1 ± 6.3	94.4 ± 3.3	94.4 ± 3.8
Mouse Plasma	<3.5	<1.8	<4.9	92.1 ± 5.5	93.1 ± 7.2	96.1 ± 5.5	<4.5	<5.1	<2.7	98.1 ± 6.4	97.1 ± 6.4	95.1 ± 5.4
Brain	<5.4	<3.6	<4.8	96.1 ± 5.5	95.1 ± 7.7	97.1 ± 2.5	<5.7	<6.3	<5.1	94.1 ± 7.2	99.1 ± 5.2	102.1 ± 5.2
Heart	<5.6	<4.5	<5.0	95.1 ± 4.9	96.1 ± 4.9	102.1 ± 4.9	<1.8	<4.9	<6.5	97.3 ± 7.6	96.3 ± 4.6	101.3 ± 1.6
Kidney	<1.8	<4.9	<6.5	94.1 ± 6.3	101.4 ± 3.3	101.4 ± 3.8	<5.4	<3.6	<4.8	93.1 ± 7.2	96.1 ± 4.9	101.4 ± 3.3
Liver	<5.4	<3.6	<4.8	96.3 ± 3.8	102.1 ± 3.8	102.1 ± 3.2	<5.6	<4.5	<5.0	93.1 ± 7.7	102.1 ± 4.9	101.4 ± 3.8
Lung	<5.6	<4.5	<5.0	101.1 ± 7.7	93.1 ± 7.7	93.1 ± 7.7	<5.6	<4.5	<5.0	92.1 ± 5.5	93.1 ± 7.2	96.1 ± 5.5
Tumour	<4.5	<5.1	<2.7	96.1 ± 3.8	102.1 ± 3.8	102.1 ± 3.2	<3.5	<1.8	<4.9	101.1 ± 3.2	97.1 ± 2.5	102.1 ± 5.2

2.4.7 Stability

2.4.7.1 Freeze-thaw stability

All analogues in plasma and tissue homogenates were tested for stability by subjecting to multiple freeze-thaw cycles over 48 h. Three concentrations (0.001, 0.025 and 0.3 µM) were prepared in human plasma and tissue homogenates and frozen at −80ºC. These samples were then thawed and frozen three times at 24, 36 and 48 h after preparation. Samples were analysed in triplicate after the third freeze-thaw cycle and concentrations were determined from the calibration curve. The mean accuracies were in the range of 96.0 ± 0.3 % to 103.1 ± 4.1 % of the nominal values for all the analogues, indicating acceptable stability over 3 freeze-thaw cycles.

2.4.7.2 Long term storage stability

All analogues were stable in plasma and tissue homogenates over the 1-year validation period when stored at −80°C. QC samples prepared during the intra-assay analysis were stored for one year and subsequently analysed. The results showed an acceptable precision < 6.2 % and an accuracy of 102.1 ± 5.5 %.

2.4.7.3 Stock solution stability

Stock solutions were prepared in acetonitrile over a concentration range of 0.02 – 6.0 µM which were then diluted 20-fold in water containing 0.01 % formic acid leading to a concentration range of 0.001 – 0.3 µM. The stability of these solutions was then tested at room temperature as well as 4°C for 24 h. These solutions were found to be stable at room temperature (97.4 ± 0.2 % to 102.4 ± 0.4 %) as well at 4°C (95.1 ± 0.6 % to 104.4 ± 0.2 %).

2.4.7.4 Bench top stability

The analogue mix was spiked in to plasma and tissue homogenates at three concentrations (0.001, 0.025 and 0.3 µM) and left at room temperature. Triplicate aliquots of each concentration were analysed at 0, 12 and 24 h and found to be in the range of 94.5 ± 3.1 % to 103.2 ± 1.7 % and was acceptable.

2.4.7.5 Post preparative stability

Post preparative stability of the analogue mix was determined by processing the quality control samples in plasma and tissue homogenates (0.001, 0.025 and 0.3 µM) in triplicate and were held in the autosampler (4ºC) for 24 h. These samples were then analysed at 0, 12 and 24 h. All samples demonstrated accuracies in the range of 93.2 ± 0.7 % to 102.1 ± 1.3 %.

2.5 Conclusion

A relatively rapid and sensitive LC-MS/MS method was developed which allowed the simultaneous measurement of five benzonaphthyridine analogues down to a concentration of 0.001 µM in plasma and mouse tissues with acceptable precision and accuracy with a run time of 7 min. The method utilised the superior performance of the QqQ mass spectrometer in terms of selectivity and sensitivity to make sample pooling practicable. This feature is a more sophisticated development of our previously reported methodology for one of the analogues, SN 28049, using an ion-trap LC-MS [132].

Altogether, this sensitive validated method may further aid in more detailed mouse pharmacokinetic and tissue distribution studies required at the preclinical drug development stage.

Chapter 3

In vitro pharmacological assessment of a series of benzonaphthyridine derivatives

3.1 Introduction

Microsomal stability is most commonly used to identify compounds susceptible to oxidation, thus facilitating the process by which they are selected for further screening [133]. It is well established that most of the oxidative reactions are catalysed by enzyme systems in the endoplasmic reticulum of the hepatocytes which can be monitored *in vitro* using microsomal preparations [134, 135]. Determination of *in vitro* pharmacological properties such as microsomal stability, may aid in the prediction of *in vivo* pharmacokinetic properties of some drugs [136].

Plasma proteins are major contributors to drug binding in blood and it is generally accepted that the fraction of drug that is unbound by blood and tissue components is available for pharmacological interaction. The two methods generally used to determine the extent to which compounds bind to plasma proteins are ultrafiltration and equilibrium dialysis. While ultrafiltration offers an advantage of short experimental times, the major concern with this method is non-specific binding to the filtration matrix. Equilibrium dialysis using a Spectrum Dialyzer is considered a better alternative, despite requiring longer equilibration times and higher volumes of plasma (or other matrices). It is quite common when using this experimental technique for protein concentrations to be diluted during the dialysis, but this may be corrected by either measuring the protein concentrations before and after the dialysis using a bicinchoninic acid (BCA) assay [137], or using a mathematical correction as employed in the Boudinot equation [138]. Advances in this field have led to the development of a 96-well format high-throughput equilibrium dialysis apparatus [139] which was utilised in these studies to determine the binding of benzonaphthyridine analogues to plasma proteins, microsomes and tumour homogenates.

Partition coefficients are mostly determined by computational methods using software packages such as ACD/LogP (ACD Labs, Toronto, Ontario, Canada) and are calculated

using an atom-based approach [140]. The accuracy of such methods may be of concern as they usually require large training data sets. Experimental determination with n-octanol/PBS partition method may offer better precision and accuracy. A low volume shake-flask method was used to determine the Log D values of the compounds [141]. These *in vitro* assessment techniques can be utilised for high throughput screening of new chemical entities for their drug-like properties and the less favourable ones can be eliminated early from the development programmes.

The benzonaphthyridine derivatives are a potent series of DNA binding topoisomerase poisons (anti-cancer agents) [113] synthesised as a part of an on-going drug development programme in the Auckland Cancer Society Research Centre. Preliminary evaluation with the methyl (SN 28049) analogue in this series demonstrated favourable *in vivo* anti-tumour activity [113]. A series of analogues with minor structural modifications (hydrogen – butyl) at the N-2 position of the benzonaphthyridine ring were synthesised. These *in vitro* evaluation studies, such as lipophilicity, hepatic microsomal stability and plasma protein binding were considered fundamental to the prediction of the plasma clearance and distribution of these compounds *in vivo*.

3.2 Aims and approach

The aims were to:

1. Determine the partition coefficients (Log D) of this series of benzonaphthyridine analogues.

2. Assess their stability *in vitro* using mouse liver microsomes.

3. Utilising a low volume, high throughput equilibrium dialysis method, determine the free fraction of these analogues in mouse plasma, mouse liver microsomes and tumour tissue.

3.3 Materials and methods

3.3.1 Chemicals and reagents

Magnesium chloride ($MgCl_2.6H_2O$), β-nicotinamide adenine dinucleotide 2′-phosphate reduced tetrasodium salt (NADPH), propranolol hydrochloride and lidocaine were purchased from Sigma-Aldrich, St. Louis, MO, USA. Water used in all experiments was purified by filtering through an ion exchange column and a 0.22 µ filter (Milli Q purification system, Millipore Corporation, Bedford, MA, USA). Drug-free human plasma was obtained from the Regional Blood Transfusion Centre, Auckland Healthcare, NZ and was centrifuged (3000 × *g* for 10 min) prior to use to remove any fibrin clumps. Mouse plasma was prepared from the blood of anaesthetised C57 Bl/6 mice and stored at –80°C. To prevent coagulation, blood was collected in BD Vacutainer® (BD Biosciences, Franklin Lakes, NJ, USA) tubes coated with K_2 EDTA and plasma was separated by centrifugation at 3000 × g for 10 min.

3.3.2 Log D measurement

Partition coefficients (Log D) of this benzonaphthyridine series were determined by a low-volume octanol/PBS (pH 7.4) shake-flask method [141]. Saturated solutions of n-octanol and PBS were prepared by mixing equal volumes of n-octanol and PBS and leaving for four days. The octanol and PBS phases were then carefully separated and left to stand for a day. Stock solutions (25 µM) of each analogue were prepared in PBS saturated with octanol. Aliquots (500 µl) of the latter were then taken in triplicate and 500 µl of octanol saturated with PBS was added. The tubes were then wrapped in tin foil and rotated for 3 h at 1 rpm to equilibrate. After centrifugation at 13000 × *g* for 5 min, the octanol and the PBS phases were separated into different tubes, diluted 5-times with methanol and analysed by HLPC. The results were then expressed as the log ratio of peak areas obtained from the octanol and PBS phases.

3.3.3 Preparation of mouse liver microsomes

Mouse liver microsomes were prepared by differential centrifugation modified from a previously published method [142]. Livers from healthy C57 Bl/6 female mice weighing 20 – 23 g were collected, rinsed in phosphate buffer and homogenised in 3-volumes of ice cold 0.1 M sodium phosphate buffer with 0.67 M KCl at pH 7.4 (homogenisation medium). The resultant homogenates were transferred to centrifuge tubes and centrifuged at 9000 × *g* for 20 min at 4°C using a Beckman centrifuge (Beckman Coulter, Fullerton, CA). The supernatant (S9) was collected and centrifuged at 105000 × *g* for 1 h at 4°C using a L8-70 Beckman ultracentrifuge (Beckman Coulter, Fullerton, CA). The microsomal pellet was resuspended with homogenisation medium. Hepatic microsomal suspensions were aliquoted (0.5 ml) and stored at −80°C until used. Microsomal protein concentration was determined by the BCA assay [137].

3.3.4 *In vitro* microsomal stability assay

Microsomes (C57 Bl/6 mouse liver) were thawed on ice, diluted using 4 parts of 400 mM phosphate buffer, 1 part of Milli Q water with 1 part of microsomes, resulting in a protein concentration of 2.5 mg/ml in 300 mM phosphate buffer. NADPH (5 mM) was used as a co-factor. A 5 µM concentration of each of the analogues was prepared in Milli Q water. All the above solutions except NADPH were added to individual wells in triplicate (96-well) and were allowed to equilibrate for 5 min at 37°C. NAPDH was then added and 25 µl aliquots were drawn from the incubation mixture at 0, 5, 10, 15 and 20 min. Details of the concentrations and volumes of the reagents used is given in Table 3-1. These samples were processed and analysed by LC-MS/MS as previously described (see section 2.3.4). Propranolol was included as a positive control. Negative controls for each analogue were made and analysed at 0 and 20 min and were assessed with the addition of equal volume of water instead of NADPH to account for non-specific binding and any heat instability issues. In the determination of the $T_{½}$, the concentrations of the analytes were calculated and converted to remaining percentage drug. The slope of the natural log-linear regression was used to calculate the $T_{½}$ as shown in Equation 3-1. Intrinsic clearance (CL_{int}) from the microsomes was calculated using Equation 3-2. For the propyl and butyl analogues, the curves were fitted using a three parameter single-phase exponential decay equation with SigmaPlot®. The free fractions of the drug in microsomal preparations were used to estimate the unbound clearance using mathematical corrections.

$$T_{½} = \frac{0.693}{k}$$

k is the slope of the natural log-linear regression (– gradient)

Equation 3-1 Calculation of elimination half-life equation from liver microsomes.

$$CL_{int} = \frac{\text{volume of incubation (µl)} \times 0.693}{\text{protein in incubation (mg)} \times T_{½}\ \text{(min)}}$$

Equation 3-2 Intrinsic clearance (CL_{int}) equation in microsomes.

Table 3-1 Reagents for microsomal stability assay.

Initial concentration	Volume (µl)	Final concentration
Test compound (5 µM)	32	1 µM
NADPH (5 mM)	32	1 mM
Microsomes (2.5 mg/ml) in phosphate buffer (300 mM at pH 7.4)	64	1 mg/ml in 100 mM phosphate buffer
$MgCl_2.6H_2O$ (24 mM) – EDTA (5 mM) mixture	32	$MgCl_2.6H_2O$ (6 mM) – EDTA (1 mM)

3.3.5 High throughput equilibrium dialysis - plasma protein binding

Protein bound fractions of the benzonaphthyridine analogues in human and mouse (C57 Bl/6) plasma were determined using a high throughput 96-well equilibrium dialysis method with an HT Dialysis apparatus, model HTD96b (HTDialysis, LLC, Gales Ferry, CT) [139]. Mouse plasma was adjusted to pH 7.5 by adding 1 M phosphoric acid. Prior to use, each dry dialysis membrane [Molecular weight cut off (MWCO): 12 – 14 kDa] was hydrated by soaking in distilled water for 60 min, followed by 20 min in 20 % ethanol and rinsed twice in distilled water prior to loading. Drug solutions (1 µM) were spiked in the pH adjusted plasma and loaded in triplicate (a volume of 100 µl) to the sample side. A similar volume of phosphate buffer was loaded on the receiving side of the dialysis well. After the 96-well dialysis unit was loaded with sample and buffer, an easily removable adhesive/piercible cover was placed over the top of the wells to prevent evaporation and pH change during the incubation. The unit was then sealed in a plastic wrap and initially incubated in a water bath at 37°C with shaking at 80 rpm for 4, 6 and 24 h to determine the equilibration rate and then for 6 h for all subsequent experiments (n = 3). The stability of all five analogues in human and mouse plasma at 37°C was assessed (at 0, 6 and 24 h) and no degradation was observed over a 24 h time-course. Samples were collected from plasma and buffer sides and processed for analysis by LC-MS/MS. The Boudinot equation (Equation 3-3), which corrects for volume shifts during dialysis was used to calculate the fraction bound in plasma [138]. Lidocaine was used as a positive control.

$$\mathbf{fb} = \frac{\mathbf{Dte} - \mathbf{DF} * \frac{\mathbf{Vpe}}{\mathbf{Vpi}}}{\left[(\mathbf{Dte} - \mathbf{DF}) * \frac{\mathbf{Vpe}}{\mathbf{Vpi}}\right] + \mathbf{DF}}$$

fb – Bound fraction of drug

Dte – Total plasma concentration at equilibrium (sample side)

DF – Concentration on the buffer/dialysate side)

Vpi – Initial plasma volume

Vpe – Final plasma volume

Equation 3-3 Boudinot formula to calculate bound fraction of drug.

3.3.6 *In vitro* microsomal binding

C57 Bl/6 mouse liver microsomes were prepared as described previously (section 3.3.3). Microsomal binding was determined at 20 min using the dialysis apparatus and a similar procedure was followed as for plasma. Equilibration was carried up to 120 min and an optimal time of 20 min was chosen for further experiments. The experiments were repeated (n = 3) for precision. Drugs (1 µM) spiked in microsomal (1 mg/ml) mixture containing phosphate buffer, $MgCl_2$ – EDTA were loaded on the sample side. To the buffer side, 100 µl aliquot of phosphate buffer with $MgCl_2$ – EDTA was added and equilibrated at 37°C for 20 min. Samples from both microsomal and buffer sides were collected in triplicate and analysed by LC-MS/MS. Aliquots of drug-microsomal mix were added to empty wells (no dialysis membrane) to assess for the non-specific binding to the Teflon block.

3.3.7 Prediction of hepatic clearance by *in vitro – in vivo* extrapolation

Microsomal intrinsic clearance (CL_{int}) was calculated as shown in equation 3-2. These clearances were scaled to the whole liver CL_{int} using reported scaling factors for microsomal protein per gram of liver (MPPGL); 49 mg/g of liver [143], liver weight; 87.5 g/kg and hepatic blood flow for mouse; 90 ml/min/kg of mouse body weight [144]. *In vivo* hepatic clearance, CL_H, was predicted using the expression for well-stirred model [145] as shown in the Equation 3-4 below.

$$CL_H = \frac{Q_H * f_u * CL_{int}}{Q_H + (f_u * CL_{int})}$$

CL_H – Hepatic clearance

f_u – fraction unbound in plasma

CL_{int} – intrinsic microsomal clearance

Q_H – hepatic blood flow

Equation 3-4 Well-stirred model for prediction of *in vivo* hepatic clearance.

3.3.8 Tumour binding studies

Colon-38 tumours were implanted subcutaneously as described previously in section 2.3.2. Tumours were collected from these untreated mice and homogenised in 4-volumes of PBS (previously described in section 2.3.3). 1 µM concentration of each benzonaphthyridine analogue is spiked in to the homogenate individually and a 100 µl aliquot is loaded in triplicate in to each well of the dialysis apparatus. A similar volume of phosphate buffer was loaded on the receiving side of the dialysis well. After sealing the apparatus with an adhesive/piercible cover the unit was incubated at 37°C in a water bath for 12 h. To account for the nonspecific binding, 100 µl aliquots in triplicate were loaded to separate wells without the dialysis membrane. Samples from both the buffer and the homogenate side are collected at 0 and 12 h and analysed with LC-MS/MS.

3.3.9 Statistical analysis

The statistical differences between the groups were calculated using either One Way or Two Way ANOVA by SigmaPlot® 11 (Systat Software Inc., San Jose, CA, USA). In all analysis, a P value less than 5×10^{-2} was considered statistically significant. Correlation (represented by 'r') analysis was performed by Spearman's rank order method with P values less than 5×10^{-2} considered significant. Post hoc analysis were performed using Holm-Sidak multiple pairwise comparison method.

3.4 Results

3.4.1 Octanol – PBS partition coefficients

Partition coefficients (Log D) of this benzonaphthyridine series were determined by a low-volume octanol/PBS (pH 7.4) shake-flask method and were: 1.25 ± 0.003 (hydrogen); 1.82 ± 0.005 (methyl); 2.24 ± 0.08 (ethyl); 2.56 ± 0.03 (propyl); and 2.91 ± 0.03 (butyl).

3.4.2 Optimal plasma protein binding time

Solutions of each benzonaphthyridine analogue (1 µM) were prepared using human and mouse plasma and equilibrated for 24 h. Aliquots were taken in triplicate at 4, 6, 12 and 24 h from individual wells corresponding to each analogue and measured to establish the optimal equilibration time for binding to occur. The plots for human and mouse plasma are shown in Figure 3.1 and Figure 3.2. The optimal equilibration time was determined as 6 h for all analogues in both human and mouse plasma.

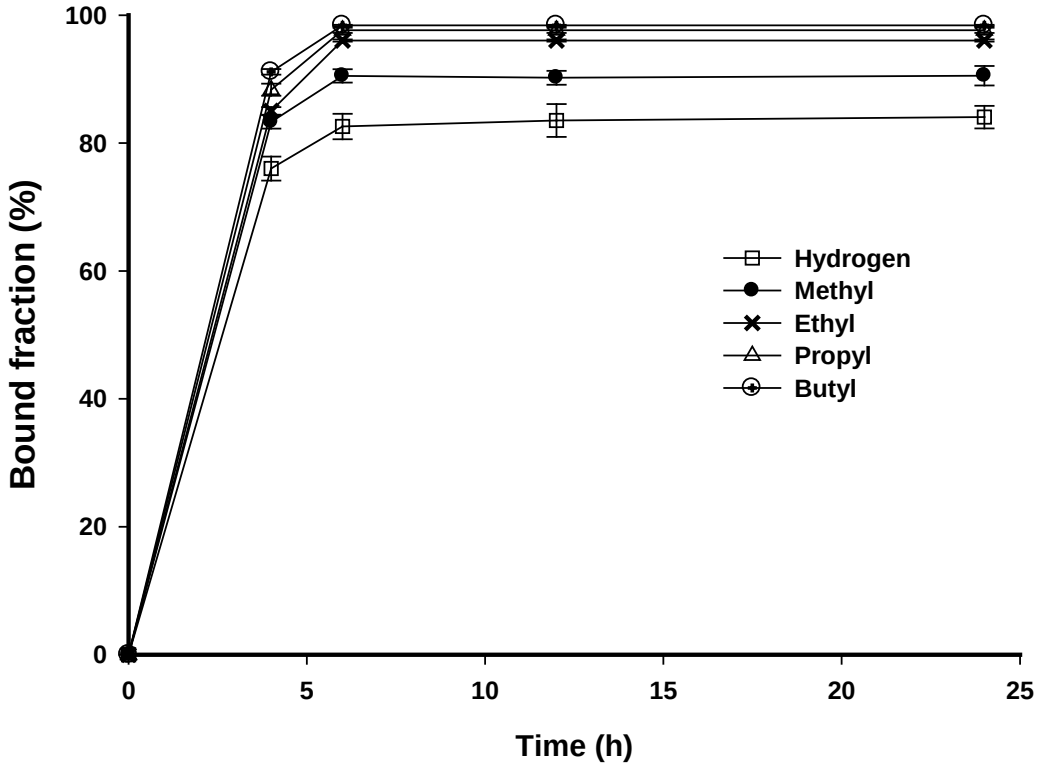

Figure 3.1 Bound fraction in human plasma. Each point is mean ± s.e. (n = 3).

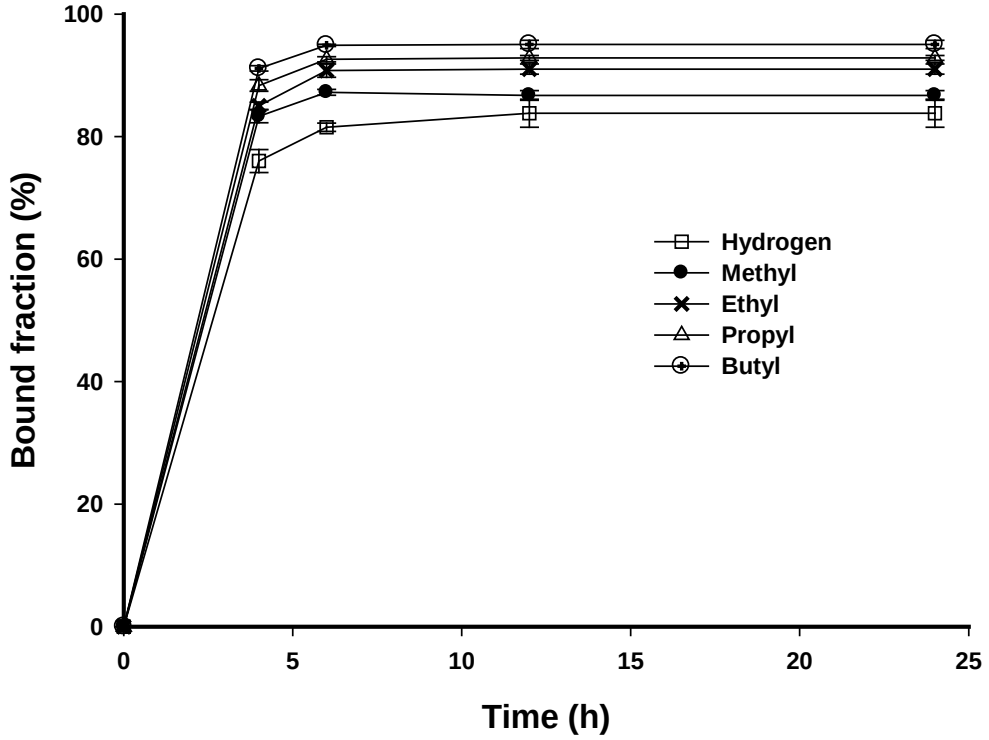

Figure 3.2 Bound fraction in mouse plasma. Each point is mean ± s.e. (n = 3).

3.4.3 Plasma protein binding

The fraction bound of each analogue in human and mouse plasma was calculated after equilibration for 6 h (see Figure 3.3 and Figure 3.4) and the results are shown in Table 3-2. There was a significant positive correlation between the % bound ($r = 0.96$, $P = 2 \times 10^{-7}$) in both human and mouse plasma and lipophilicity as represented by Log D (Figure 3.3 and Figure 3.4). Lidocaine was used as a positive control and gave a % plasma bound values of 68.1 ± 2.1 % (human) and 49.6 ± 1.4 % (mouse) which is in agreement with the reported literature values [139]. Small but significant differences ($P < 2 \times 10^{-2}$) were observed between the fraction bound of each analogue to the proteins found in human and mouse plasma except in the case of the hydrogen analogue ($P = 98 \times 10^{-1}$).

Table 3-2 Bound fraction (%) in human and mouse plasma of benzonaphthyridine analogues (hydrogen – butyl). Results are mean ± s.e (n = 3).

Analogue	Human plasma	Mouse plasma
Hydrogen	84.0 ± 1.1	83.4 ± 2.1
Methyl	91.0 ± 0.9	87.3 ± 0.4
Ethyl	96.1 ± 0.1	91.2 ± 0.7
Propyl	97.6 ± 0.3	93.0 ± 0.3
Butyl	98.4 ± 0.1	95.0 ± 0.1

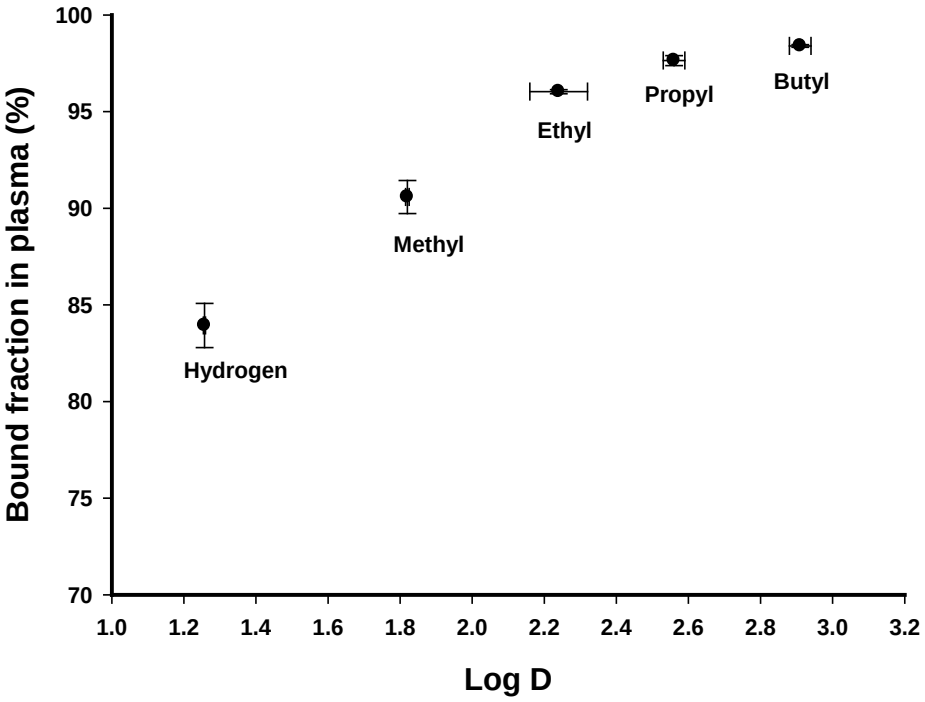

Figure 3.3 Bound fraction of benzonaphthyridine analogues (hydrogen – butyl) in human plasma *vs* their Log D. Results are mean ± s.e. (n = 3).

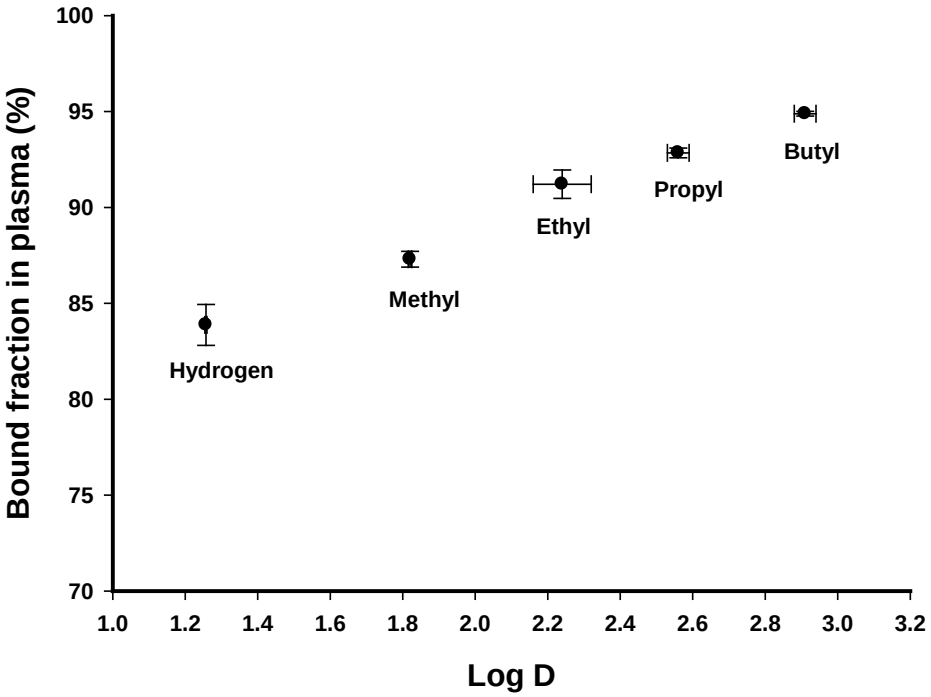

Figure 3.4 Bound fraction of benzonaphthyridine analogues (hydrogen – butyl) in mouse (C57 Bl/6) plasma *vs* their Log D. Results are mean ± s.e. (n = 3).

3.4.4 Murine hepatic microsomal stability *in vitro*

Half-lives of the benzonaphthyridine derivatives upon incubation with the C57 Bl/6 mouse liver microsomes were calculated from the log concentration-time plots shown in Figure 3.5. They were: 7.0 ± 0.2 (hydrogen); 24.3 ± 1.6 (methyl); 11.3 ± 0.5 (ethyl); 4.6 ± 0.01 (propyl); and 1.7 ± 0.001 min (butyl). The relationship between microsomal half-life and Log D is shown in Figure 3.6.

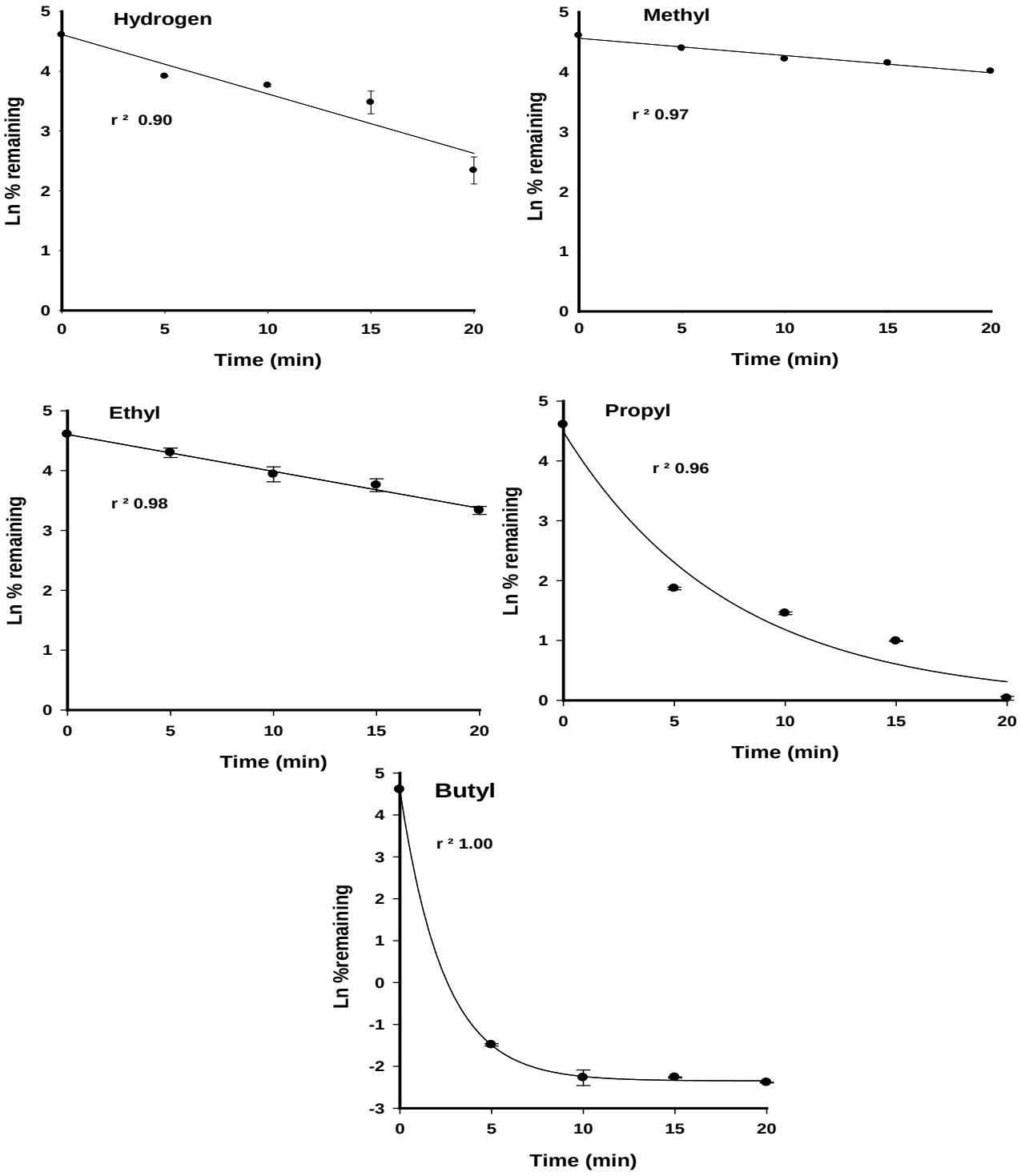

Figure 3.5 Concentration-time profiles of benzonaphthyridine analogues (hydrogen – butyl) following incubation in mouse (C57 Bl/6) liver microsomes. Results are mean ± s.e. (n = 3).

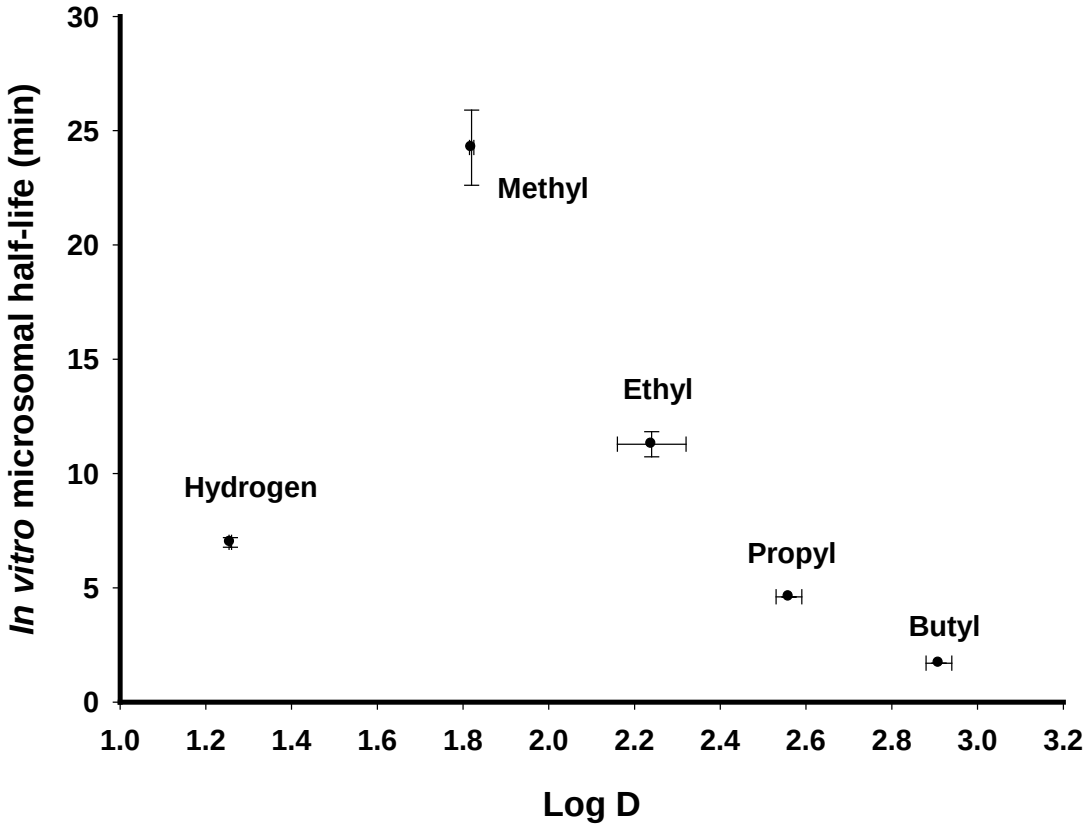

Figure 3.6 *In vitro* microsomal half-life of the benzonaphthyridine analogues (hydrogen – butyl) *vs* their Log D. Results are mean ± s.e. (n = 3).

3.4.5 Murine hepatic microsomal binding

Solutions of each benzonaphthyridine analogue (1 µM) were prepared using mouse liver microsomes and were equilibrated for 120 min. Aliquots were taken in triplicate at 5, 10, 20, 60 and 120 min from individual wells corresponding to each analogue and measured to establish the optimal equilibration time for binding to occur. The plots are shown in Figure 3.7. The bound fractions of each benzonaphthyridine derivatives were calculated in triplicate after 20 min of equilibration and their relationship to lipophilicity is shown in Figure 3.8. In addition, unbound fraction values were used to correct the total microsomal intrinsic clearance (CL_{int}) values generated from the concentration-time data shown in Figure 3.5 to produce the corresponding unbound clearance values for each analogue. The results are shown in Figure 3.9 and Table 3-3.

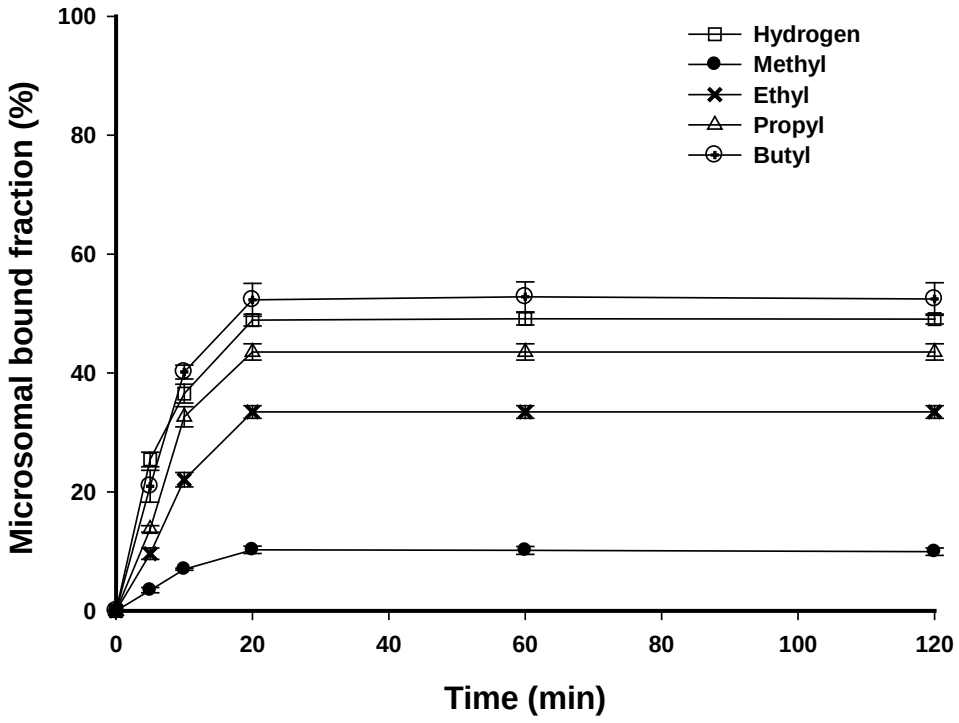

Figure 3.7 Bound fractions of benzonaphthyridine analogues (hydrogen – butyl) in mouse liver microsomes. Results are mean ± s.e. (n = 3).

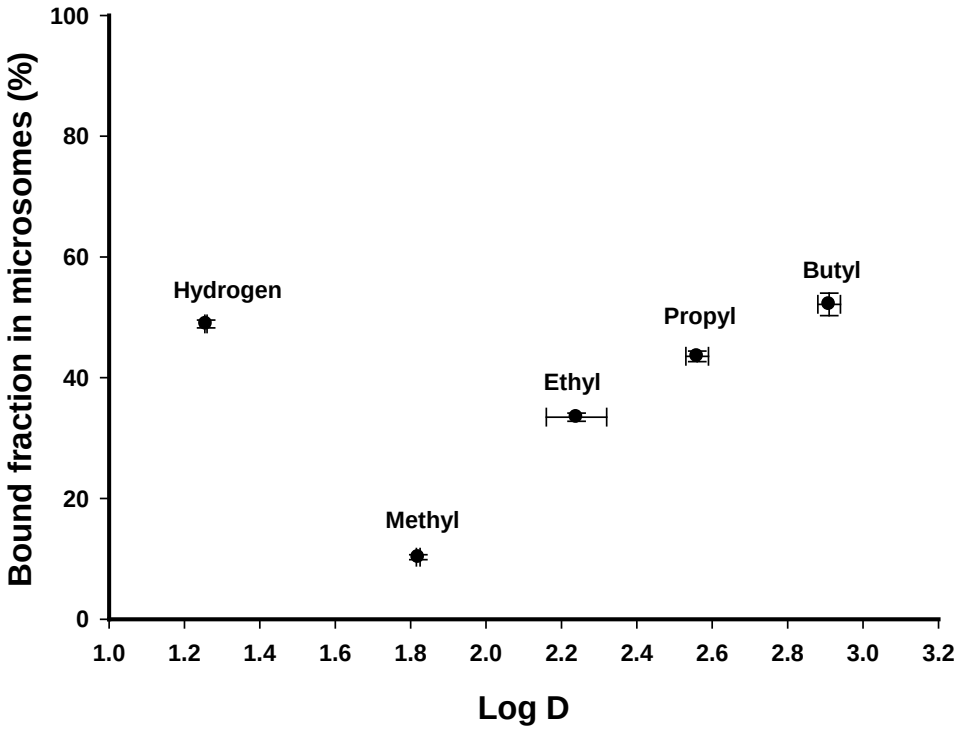

Figure 3.8 Bound fraction in mouse (C57 Bl/6) liver microsomes *vs* Log D for the benzonaphthyridine analogues (hydrogen – butyl). Results are mean ± s.e. (n = 3).

Table 3-3 Bound and unbound intrinsic clearances of the benzonaphthyridine analogues (hydrogen – butyl). Results are mean ± s.e.

Analogue	CL_{int} (µl/min/mg)	Unbound CL_{int} (µl/min/mg)
Hydrogen	15.8 ± 0.3	8.1 ± 0.2
Methyl	4.6 ± 0.2	4.1 ± 0.2
Ethyl	9.9 ± 0.3	6.5 ± 0.3
Propyl	24.6 ± 0.4	13.5 ± 0.1
Butyl	67.4± 0.3	32.3 ± 0.3

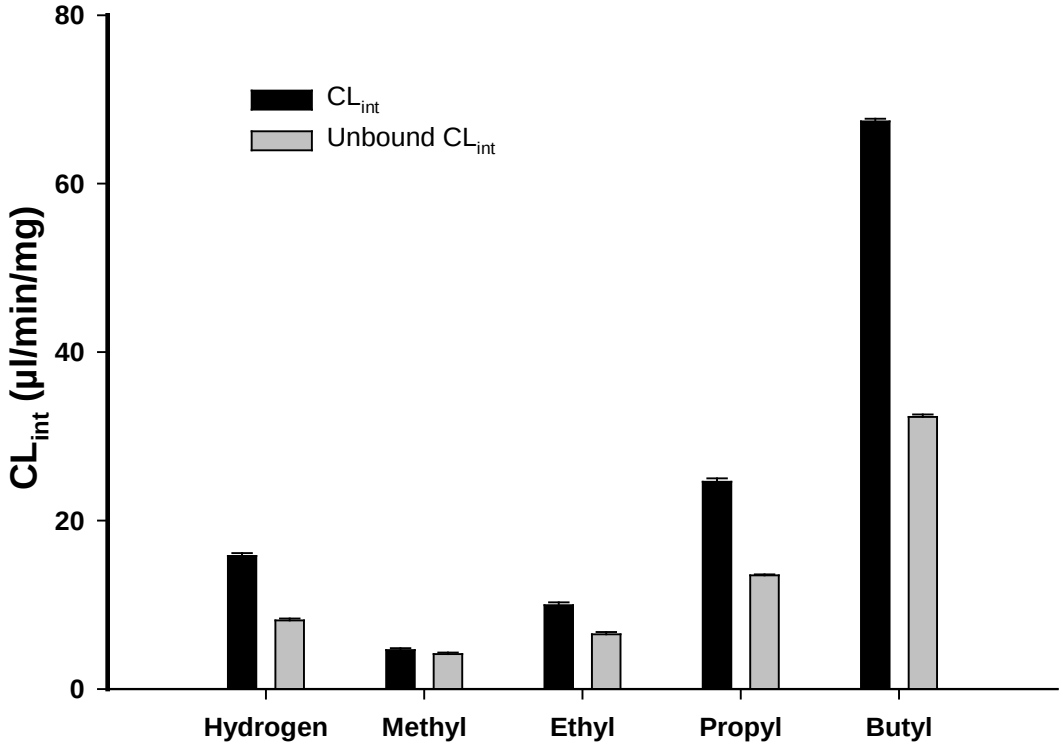

Figure 3.9 Total and unbound clearance of benzonaphthyridine analogues in mouse liver microsomes. Results are mean ± s.e (n = 3).

3.4.6 In vitro – in vivo extrapolation

The hepatic clearances (CL_H) were calculated by extrapolation for all the five analogues utilising a well-stirred model as previously described (section 3.3.7). The clearances are as shown in Table 3-4.

Table 3-4 Predicted *in vivo* hepatic clearances for benzonaphthyridine analogues (hydrogen – butyl). Results are mean ± s.e. (n =3).

Analogue	CL_H (l/h/kg)
Hydrogen	4.1 ± 0.04
Methyl	2.1 ± 0.1
Ethyl	3.4 ± 0.1
Propyl	7.2 ± 0.2
Butyl	16.6 ± 0.6

3.4.7 Tumour binding *in vitro*

Bound fraction in tumour was calculated using Equation 3-3 after a 12 h equilibration. A significant correlation with increasing lipophilicity ($r = 0.86$; $P = 2 \times 10^{-7}$) was observed as shown in Figure 3.10.

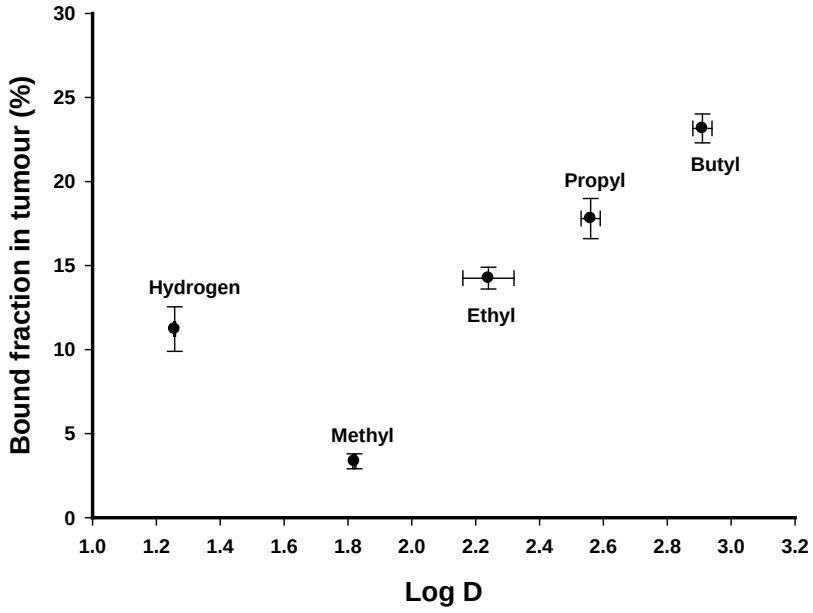

Figure 3.10 Bound fractions of benzonaphthyridine analogues in tumour homogenate after 12 h of equilibration. Results are mean ± s.e (n = 3).

3.5 Discussion

The evaluation of *in vitro* stability along with the determination of physicochemical properties, such as Log D, are well known factors in facilitating the selection of drugs with favourable properties for further development. Plasma protein binding is also another important factor in the screening of compounds in drug development as the free (unbound) drug is the available fraction for activity. The results demonstrated that all five analogues are highly bound to plasma proteins and that the degree to which they are bound increased with their increasing lipophilicity. This is consistent with other reported findings regarding the relationship between increases in protein binding and lipophilicity [146]. Overall, plasma protein binding of these analogues was greater in human compared to mouse plasma. In comparison to the other DNA binding drugs (Table 3-5) the methyl analogue was found be less bound to the plasma proteins with the exception of doxorubicin.

Table 3-5 Bound fractions (%) of the DNA binding drugs in mouse and human plasma.

Drug	Mouse plasma	Human plasma
Amsacrine	93.3 ± 0.7 [147]	97.0 ± 0.5 [148]
Amsalog	99.3 ± 0.2 [147]	99.9 ± 0.001 [149]
Doxorubicin	65.0 ± 0.1 [150]	72.4 ± 2.8 [151]
DACA	85.2 ± 0.8 [152]	96.7 ± 0.6 [152]
SN 28049/ methyl	87.3 ± 0.4	91.0 ± 0.9

Microsomal binding was evaluated using the high throughput (96-well format) methodology and was used to correct for the free fraction of the CL_{int} estimated the concentration-time data of the analogues in the microsomes. The unbound CL_{int} appears to increase with the lipophilicity ($r = 0.70$, $P = 4 \times 10^{-3}$). This along with the microsomal stability data indicates the higher lipophilic analogues in the series (propyl and butyl) have higher clearance.

Tumour binding studies presented used the similar high throughput approach, but were performed with a 12 h equilibration time, as the maximal concentrations were observed in previous studies [130]. The bound fraction in tumour homogenates was significantly less when compared to plasma and liver microsomal preparations (Figure 3.11). This may possibly indicate that higher fractions of benzonaphthyridine derivatives are available for activity.

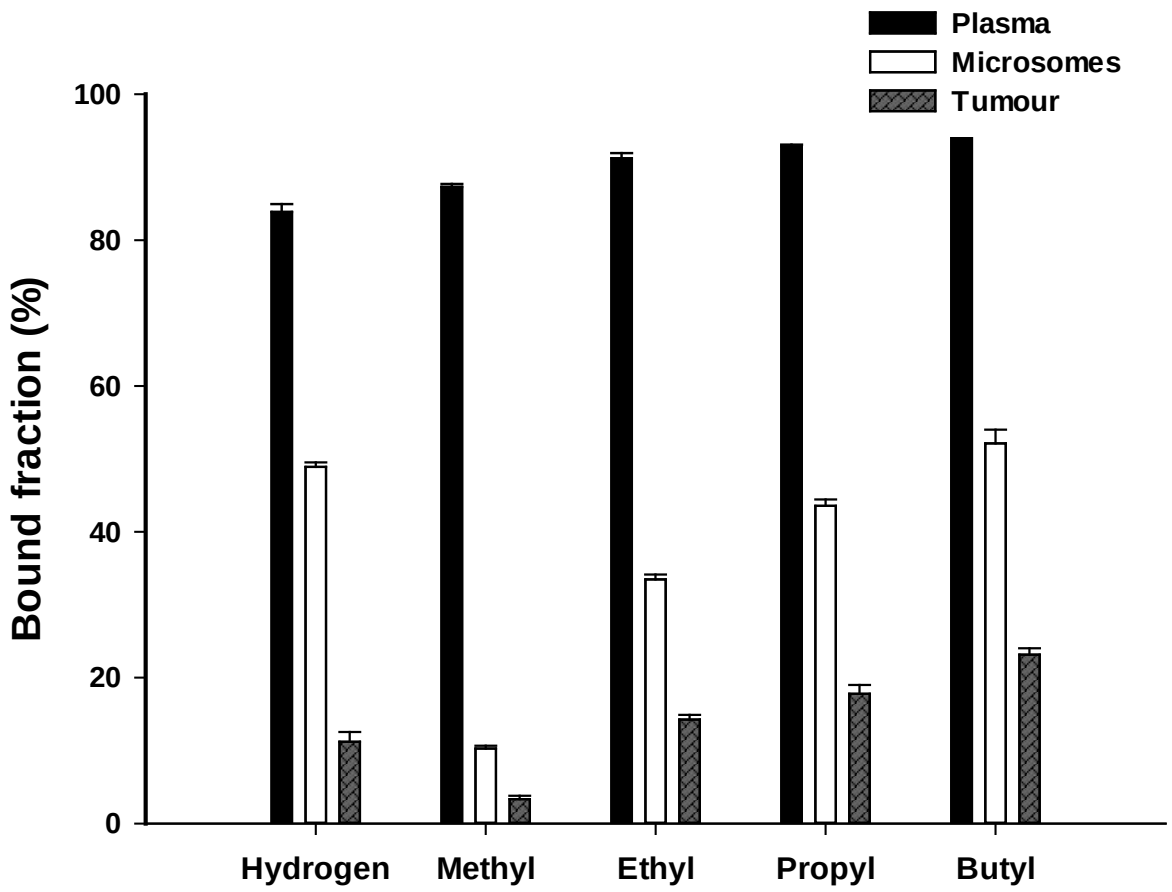

Figure 3.11 Comparison of bound fractions in mouse plasma, liver microsomes and Colon-38 tumour homogenate. Results are mean ± s.e.

The hepatic microsomal half-life was calculated for these analogues and subsequently, their intrinsic clearance, allows the prediction of *in vivo* clearance. SN 28049 (methyl) analogue had the longest half-life (24 min) compared to the others. It is important to note that minor structural changes may result in substantial changes in the pharmacokinetic properties of the drug. This is consistent with other reports where increasing chain length (i.e., increased lipophilicity) results in increased metabolic clearance and hence, a shorter elimination half-life. The microsomal intrinsic clearance data was further used to predict *in vivo* hepatic clearance, which correlated with lipophilicity ($r = 0.70$; $P = 4 \times 10^{-3}$) and allowed selection of favourable analogues. The validity of this approach needs further verification by comparing these to the experimentally determined *in vivo* clearances (see chapter 4) as it is well known, that these models based on microsomal kinetics usually under-estimate the *in vivo* clearances [153].

To summarise, the results from these studies of *in vitro* screening may aide partially in selecting a suitable candidate for further evaluation. The most important factor was the

microsomal stability study which suggests the methyl analogue is the most suitable with its longer half-life and moderate intrinsic clearance from the microsomes. While, on the other hand, the protein binding studies in human and mouse plasma serve as proof-of-concept that an increase in the chain length (lipophilicity) an increases protein binding, but does not provide a clear insight into whether protein binding is an important factor that can be used in predicting *in vivo* tumour pharmacokinetics.

Chapter 4

In vivo pharmacokinetics of benzonaphthyridine derivatives in mice

4.1 Introduction

The benzonaphthyridine derivative N-[2-(dimethylamino)ethyl]-2,6-dimethyl-1-oxo-1,2-dihydrobenzo[b]-1,6-naphthyridine-4-carboxamide (SN 28049) is a DNA intercalating drug that binds selectively to GC-rich DNA and exhibits poisoning to varying degrees of both topoisomerase I and II [129]. In addition, SN 28049 shows curative activity against the Colon-38 adenocarcinoma in mice, a tumour model which is relatively resistant to DNA intercalating topoisomerase poisons such as amsacrine, doxorubicin and etoposide. It was superior in this respect to all other analogues within the same benzonaphthyridine series [113]. We have previously reported that SN 28049 exhibited selective *in vivo* tumour retention in the murine Colon-38 tumour, resulting in a tumour tissue AUC approximately 30-fold higher than the healthy normal tissues [130].

As part of on-going studies to establish why this compound exhibited exceptional tumour retention, analogues have been synthesised with differing substituents at N-2 position of the benzonaphthyridine ring. Alteration of this substituent affected not only anti-tumour activity but also dose potency [113, 128]. The compounds selected for this study were hydrogen, ethyl, propyl and butyl N-2 analogues of SN 28049. Results from the *in vitro* studies reported in chapter 3 demonstrated that the methyl analogue (SN 28049) was the most metabolically stable when exposed to mouse microsomes, suggesting perhaps that this compound had a pharmacokinetic advantage when compared to the other derivatives in the series. In contrast *in vitro* studies of plasma protein and tumour binding indicated that the degree of binding correlated with lipophilicity with no individual compound exhibiting atypical binding. The influence of lipophilicity and these *in vitro* characteristics on the *in vivo* pharmacokinetics in healthy and tumour-bearing mice were examined in this chapter.

4.2 Aims and approach

The aims were:

1. Pharmacokinetic evaluation of each of the benzonaphthyridine analogues in healthy and Colon-38 tumour mouse (C57 Bl/6) model.

2. Relate tumour exposure to anti-tumour activity and to explore the role played by lipophilicity in plasma and tumour disposition.

4.3 Materials and methods

4.3.1 Chemicals and reagents

Acetonitrile (MeCN; LC-MS grade) and formic acid were purchased from Merck, KGaA, Darmstadt, Germany. Ethylene disodium tetra acetic acid (EDTA) was from Bio Chemed (Winchester, VA, USA). Water used in all experiments was purified by filtering through an ion exchange column and a 0.22 µ filter (Milli-Q purification system, Millipore Corporation, Bedford, MA, USA).

4.3.2 Animal model

C57 Bl/6 female mice (20 - 25 g; 8 - 12 week old) were bred by the Vernon Jansen Unit at The University of Auckland and housed under constant temperature (20 ± 2ºC) with a 12 h light/dark cycle. Mice were fed *ad libitum* UV-treated Milli-RO water (Millipore Corporation, Billerica, MA, USA) and a sterilized rodent diet (Harlan Teklad, Madison, WI, USA). Healthy and tumour-bearing mice were used for pharmacokinetic and distribution studies. All experimental procedures, which included blood collection in mice from the ocular sinus under isofluorane anaesthesia, were approved by The University of Auckland Animal Ethics Committee and conformed to the Guidelines for the Welfare of Animals in Experimental Neoplasia, as set out by the United Kingdom Co-ordinating Committee on Cancer Research.

4.3.3 Subcutaneous Colon-38 tumour transplantation

Refer section 2.3.2.

4.3.4 Formulation and dosing

All analogues (hydrogen – butyl) were dissolved in PBS (dose: 25 µmol/kg) and injected (10 µl/g of body weight) via intravenous (i.v.) and intraperitoneal (i.p.) routes to mice (n = 3 per time point). Healthy female mice were used for the i.v. and i.p. pharmacokinetic and tissue distribution studies. Blood and tissue samples were collected at various time points (0.08, 0.5, 1, 2, 4, 8, 12 and 24 h). Female tumour-bearing mice were used to study the pharmacokinetics and distribution in the tumour after i.p. injection. Blood and tissue samples were collected at various time points up to 72 h (0.08, 0.5, 1, 2, 4, 8, 12, 24, 48 and 72 h).

4.3.5 Mouse plasma and tissue homogenates

Refer section 2.3.3.

4.3.6 Mass spectral analysis

All analytes were measured by a validated LC-MS/MS assay as previously described (section 2.3.4)

4.3.7 Pharmacokinetic methodology and data analysis

The concentration-time course (plasma and tissues) was fitted to a non-compartmental model using WinNonlin® version 5.3 (Pharsight, Sunnyvale, CA, USA). Area under the concentration-time profile curve (AUC) was calculated by the log trapezoidal rule by log-linear regression and was extrapolated to infinity by addition of the value Ct/λ_Z, where Ct is the concentration at the last time point and λ_Z, the terminal slope (determined by linear regression) of the log concentration-time curve. The terms C_{max} and T_{max} represent the maximum concentration achieved and the time to maximum concentration respectively and were determined from the concentration-time profiles. The bioavailability (F) was calculated as the ratio of the AUC after i.p. dosing to the AUC after i.v. dose (all at the same dose, 25 µmol/kg). The elimination half-life ($T_{½}$) was calculated by the equation $T_{½} = \ln(2)/\lambda_Z$. The model-independent pharmacokinetic parameters, clearance (CL), volume of distribution at steady state (V_{SS}) and mean residence time (MRT) were calculated by the following equations: CL = F x Dose/AUC; V_{SS} = (F x Dose x AUMC)/$(AUC)^2$ and MRT = AUMC/AUC; where AUMC represents the total area under the first moment of the concentration-time curve, computed in a similar fashion to that used for AUC. All results were expressed as mean ± s.e. Statistical analysis procedures were previously described (section 3.3.9).

4.4 Results

4.4.1 Plasma pharmacokinetics, bioavailability and tissue distribution in healthy mice

Plasma concentration-time profiles of the 5 benzonaphthyridine analogues after i.v. and i.p. administration to healthy mice are shown in Figure 4.1 and the pharmacokinetic parameters are reported in Table 4-1. After i.v. administration the least lipophilic hydrogen analogue produced the highest plasma AUC and this parameter decreased with increasing lipophilicity (Log D) in this series of analogues ($r = –0.95$, $P = 2 \times 10^{-7}$). Both plasma CL and V_{SS} showed a significant positive correlation with Log D ($r = 0.95$, $P = 2 \times 10^{-7}$ and $r = 0.95$, $P = 2 \times 10^{-7}$, respectively). Similar correlations were observed between these pharmacokinetic parameters and Log D values after i.p. administration. The bioavailability after i.p. administration varied considerably with values of 37.6 ± 1.7 %, 84.6 ± 1.8 %, 60.4 ± 4.1 %, 46.1 ± 5.4 % and 38.8 ± 2.1 % corresponding to the hydrogen, methyl, ethyl, propyl and butyl analogues respectively.

The tissue concentrations were determined after i.p. administration in healthy mice (Figure 4.2) and the tissue to plasma AUC ratios are shown in Figure 4.3. Overall, tissue concentrations were much greater than those in plasma for all 5 analogues, with tissue to plasma AUC ratios ranging from 1.6 to 53 with the exception of the hydrogen analogue whose brain AUC was less than plasma (0.5-fold). There was a significant positive correlation ($r = 0.91$, $P = 2 \times 10^{-7}$) between the brain to plasma AUC ratios and Log D values, indicating an increasing brain exposure with increasing lipophilicity of these compounds. With the other tissues examined, the tissue to plasma ratios were several fold greater than those for the brain and there was a tendency for the tissue to plasma ratio to be smallest for the hydrogen analogue and greatest for the butyl, with the exception of the lung where the hydrogen analogue had by far the greatest ratio.

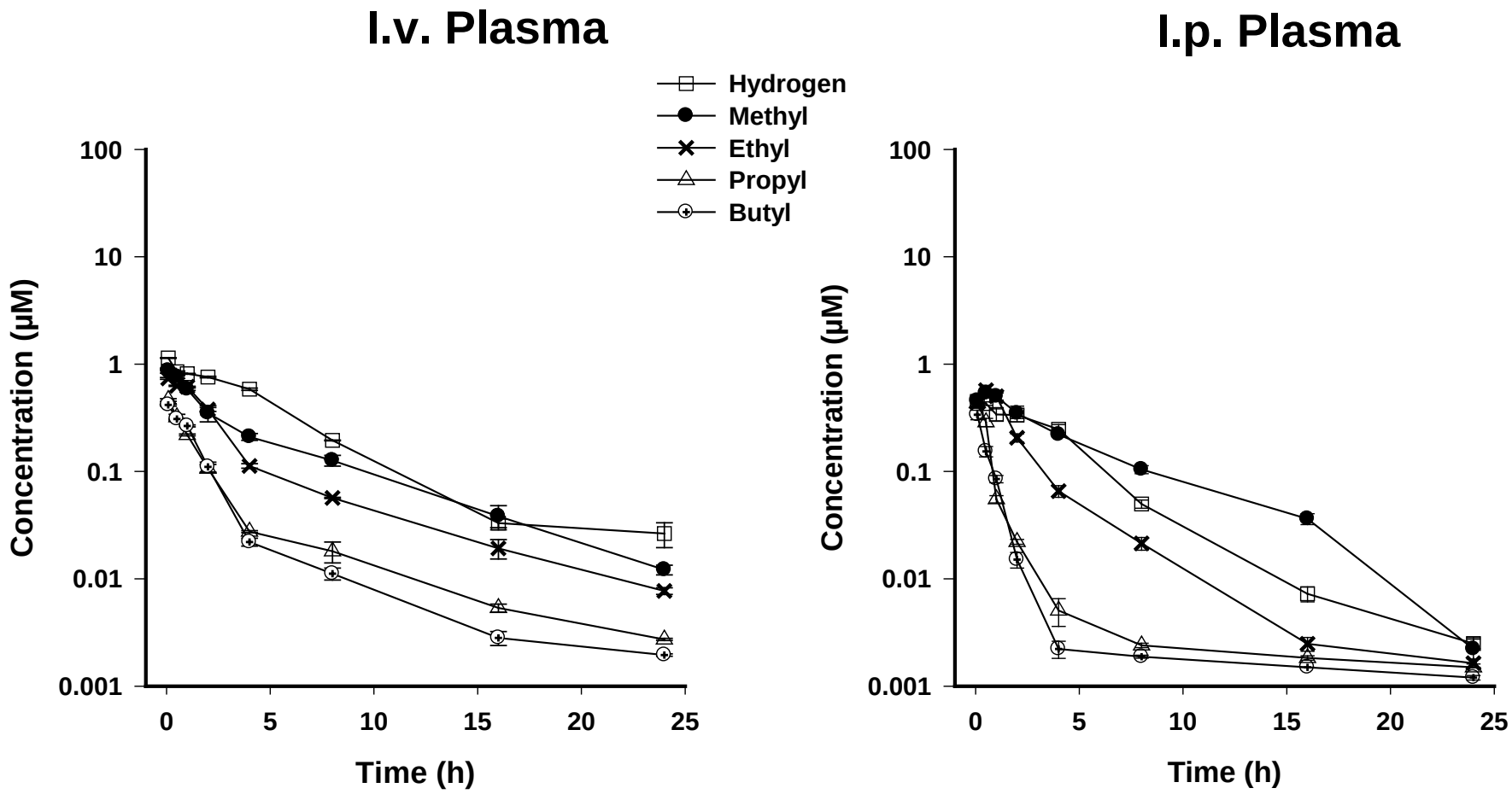

Figure 4.1 Plasma concentration-time profiles after i.v. and i.p. administration of benzonaphthyridine analogues (hydrogen – butyl; 25 µmol/kg) to healthy female mice (n = 3 per time point). Results are mean ± s.e.

Table 4-1 Pharmacokinetic parameters calculated using non-compartmental analysis from concentration-time profiles of plasma after i.v. and i.p. administration of benzonaphthyridine analogues (hydrogen – butyl; 25 µmol/kg) to C57 Bl/6 female mice (n=3 per time point). Results are mean ± s.e.

Analogue (route)	AUC (µM.h)	C_{max} (µM)	T_{max} (h)	$T_{½}$ (h)	Mean Residence Time (h)	CL (l/h/kg)	V_{SS} (l/kg)	Bioavailability (F %)
Hydrogen (i.v.)	5.7 ± 0.1	1.2 ± 0.02	0.08	4.2 ± 0.1	5.6 ± 0.2	4.2 ± 0.1	22.0 ± 0.9	--
(i.p.)	2.2 ± 0.1	0.5 ± 0.1	0.5	3.2 ± 0.1	3.9 ± 0.1	11.4 ± 0.6*	53.0 ± 2.2*	37.6 ± 1.7
Methyl (i.v.)	3.3 ± 0.2	0.9 ± 0.04	0.08	4.8 ± 0.3	5.3 ± 0.2	7.5 ± 0.2	37.0 ±1.2	--
(i.p.)	2.8 ± 0.15	0.6 ± 0.01	1	3.2 ± 0.04	5.0 ± 0.1	9.3 ± 0.5*	42.6 ± 2.6*	84.6 ± 1.8
Ethyl (i.v.)	2.3 ± 0.03	0.7 ± 0.02	0.08	4.3 ± 0.02	4.4 ± 0.02	10.6 ± 0.2	47.3 ± 2.0	--
(i.p.)	1.4 ± 0.1	0.6 ± 0.05	0.5	2.7 ± 0.07	2.4 ± 0.02	18.0 ± 1.0*	83.8 ± 15.3*	60.4 ± 4.1
Propyl (i.v.)	0.9 ± 0.1	0.4 ± 0.01	0.08	2.5 ± 0.1	3.2 ± 0.14	29.7 ± 0.8	108.8 ± 8.1	--
(i.p.)	0.4 ± 0.05	0.4 ± 0.03	0.08	2.5 ± 0.01	1.8 ± 0.6	65.7 ± 8.1*	194.5 ± 5.1*	46.1 ± 5.4
Butyl (i.v.)	0.7 ± 0.02	0.4 ± 0.03	0.08	2.0 ± 0.01	2.5 ± 0.1	32.6 ± 0.9	172.7 ± 3.7	--
(i.p.)	0.3 ± 0.005	0.3 ± 0.01	0.08	2.3 ± 0.03	1.1 ± 0.07	84.0 ± 2.1*	305.3 ± 25.9*	38.8 ± 2.1

**** For i.p. administration CL and V_{SS} values are uncorrected for bioavailability (i.e. represent CL/F and V_{SS}/F).***

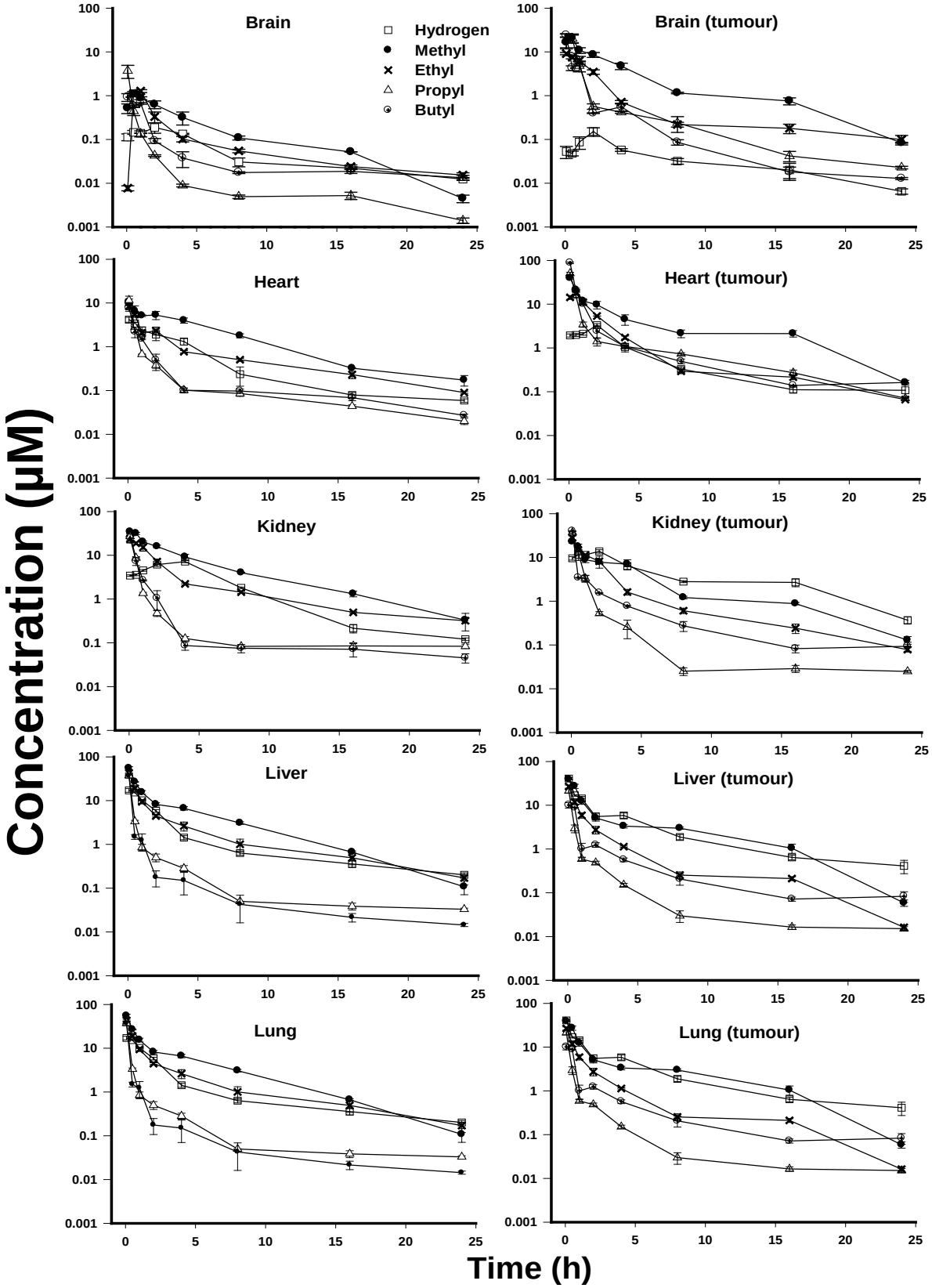

Figure 4.2 Concentration-time profiles in female (n = 3 mice per time point) healthy and tumour-bearing (Colon-38) mouse tissues after i.p. administration (25 µmol/kg) of benzonaphthyridine analogues (hydrogen – butyl). Results are mean ± s.e.

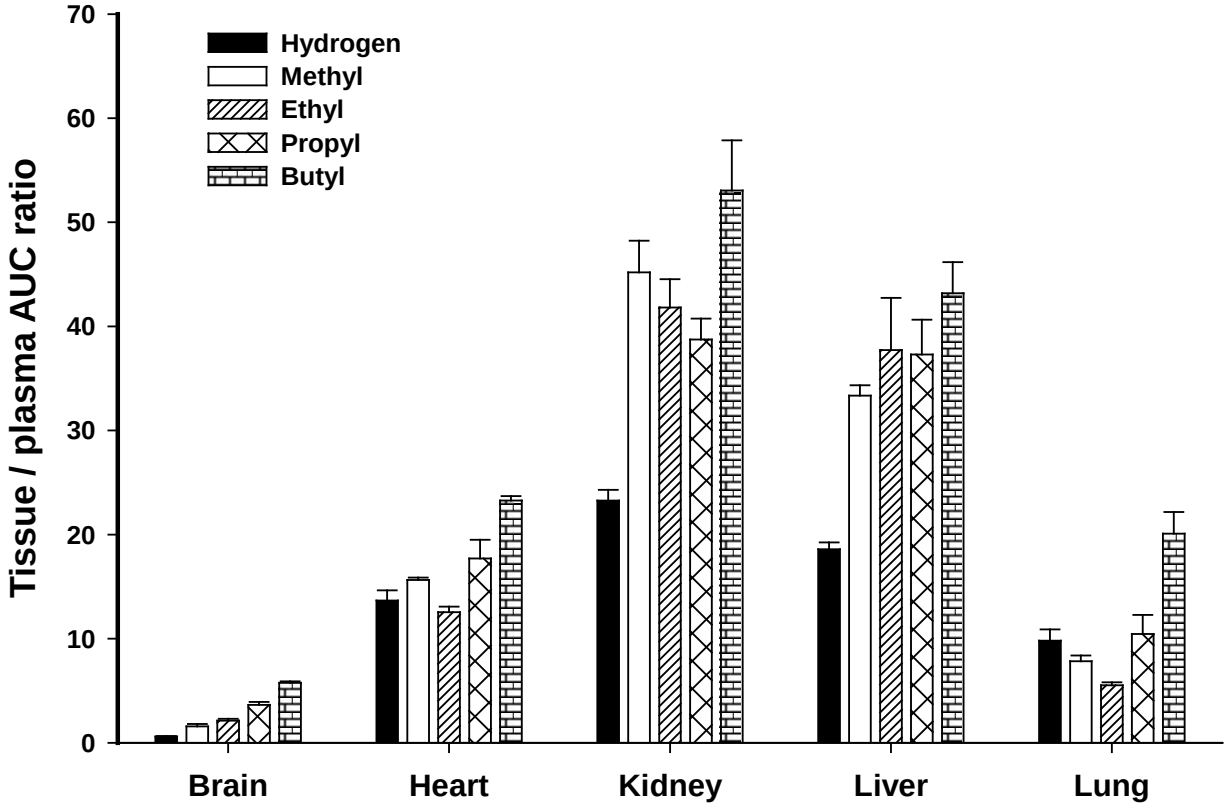

Figure 4.3 Tissue to plasma AUC ratios after i.p. administration of benzonaphthyridine analogues (hydrogen – butyl; 25 µmol/kg) to healthy female mice (n = 3 per time point). Results are mean ± s.e.

4.4.2 Plasma pharmacokinetics and tissue distribution in tumour-bearing mice

Plasma and tumour concentration-time profiles following i.p. administration of the benzonaphthyridine analogues in tumour-bearing mice are shown in Figure 4.4 and the corresponding pharmacokinetic parameters are reported in Table 4-2. Tissue concentration-time profiles are shown in Figure 4.3. As observed in the previous study in healthy mice, plasma CL and V_{SS} increased significantly with increasing lipophilicity, r = 0.97, P = 2 x 10^{-7} and r = 0.85, P = 2 x 10^{-7}, respectively. This resulted a significant decrease in the AUC with increasing lipophilicity (r = –0.96; P = 2 x 10^{-7}). Comparison of the pharmacokinetic parameters between healthy and tumour-bearing mice after i.p. administration of these analogues indicated a significant reduction in CL/F (P < 1 x 10^{-3}) and V_{SS}/F (P < 1 x 10^{-3}) in tumour-bearing mice, resulting in a significant increase in the plasma AUC (P < 1 x 10^{-3}) in the latter. This was particularly noticeable for the more lipophilic analogues (i.e. propyl and butyl), but was much less for the hydrogen and methyl analogues.

Despite having the largest plasma AUC, the hydrogen analogue exhibited the smallest tumour AUC (26.3 ± 3.5 µM.h). In contrast, the methyl analogue exhibited the greatest tumour AUC (2334 ± 60 µM.h) with an 825-fold tumour to plasma ratio. The ethyl, propyl and butyl had tumour to plasma AUC ratios of 150, 80 and 142-fold respectively. Uptake into the tumour tissue was relatively rapid achieving maximal concentrations (T_{max}) by 1 h for the most lipophilic analogue (butyl) followed by the propyl and ethyl at 2 h and the hydrogen and methyl, the slowest at 8 h. Of all the analogues, the methyl had the longest tumour elimination half-life (17.5 ± 1.5 h) with ethyl, the least (7.9 ± 0.3 h). The tumour $T_{½}$ for the hydrogen, propyl and butyl were 11.2 ± 1.1, 13.2 ± 1.6 and 13.2 ± 2.6 h, respectively with no correlation with lipophilicity (r = 0.04; P = 87 x 10^{-1}). The tumour $T_{½}$s however were significantly longer than those observed in plasma (P < 1 x 10^{-3}). Tissue to plasma ratios of brain, heart, liver, lung and kidney were of similar magnitude to those observed in healthy mice (Figure 4.5). With all analogues, brain tissue had the least uptake. Highly vascularised organs such as heart, kidney, liver and lung were found to have higher uptake but were less than the tumour with the exception of the hydrogen analogue, which had the highest uptake in kidney.

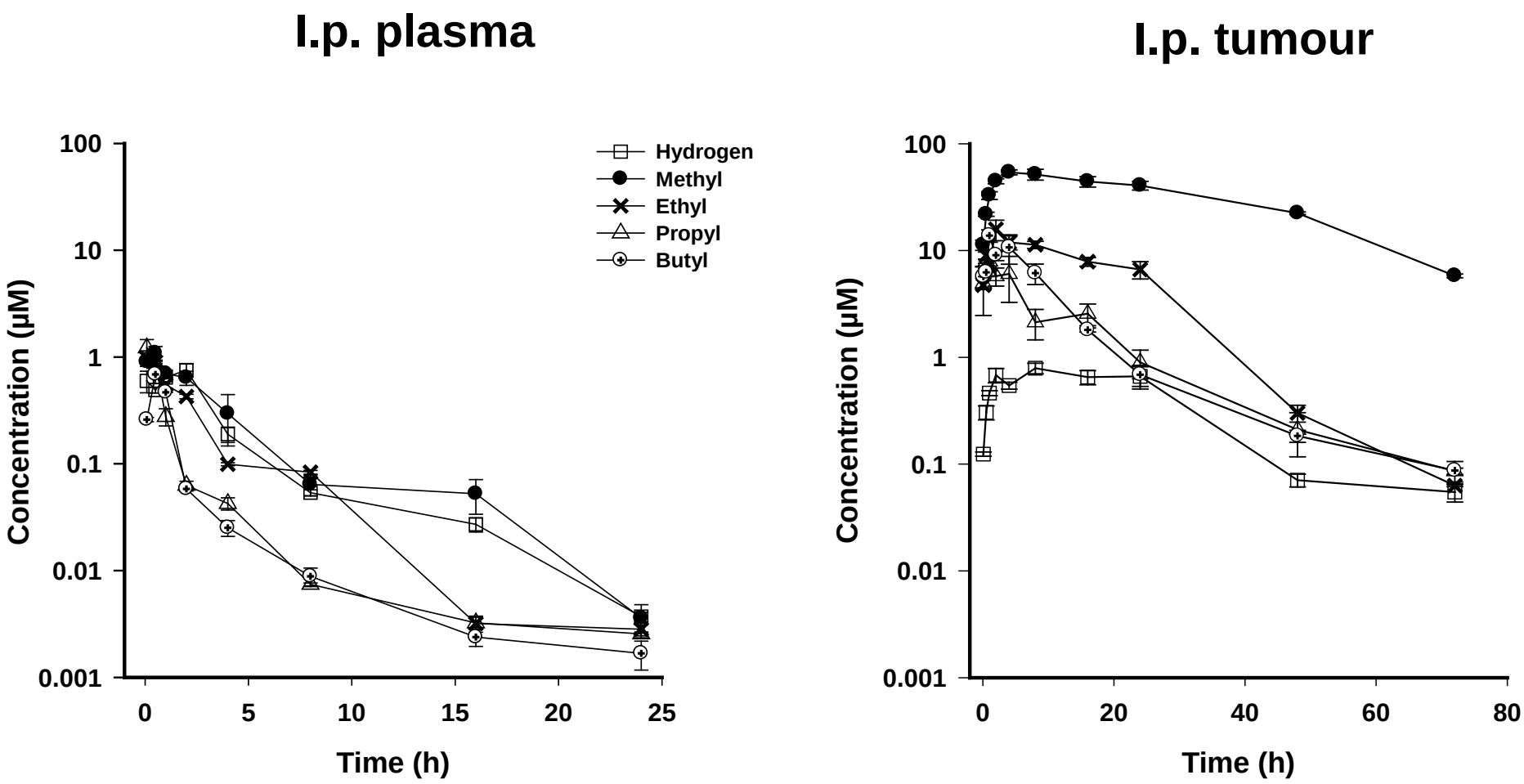

Figure 4.4 Plasma and tumour concentration-time profiles after i.p. administration of benzonaphthyridine analogues (hydrogen – butyl; 25 μmol/kg) to female tumour-bearing mice (n = 3 per time point). Results are mean ± s.e.

Table 4-2 Pharmacokinetic parameters calculated using non-compartmental analysis from concentration-time profiles of tumour and plasma after i.p. administration of benzonaphthyridine analogues (hydrogen – butyl; 25 µmol/kg) to tumour-bearing female mice (n = 3 per time point). Values are means ± s.e. CL and Vss values are uncorrected for bioavailability.

Analogue	(matrix)	AUC (µM.h)	C_{max} (µM)	T_{max} (h)	$T_{½}$ (h)	Mean Residence Time (h)	CL/F (l/h/kg)	V_{SS}/F (l/kg)
Hydrogen	**tumour**	26.3 ± 3.5	0.9 ± 0.1	8	11.2 ± 1.1	21.5 ± 0.3	--	--
	plasma	3.3 ± 0.1	0.8 ± 0.1	2	3.7 ± 0.1	4.0 ± 0.3	8.0 ± 0.5	47.3 ± 7.5
Methyl	**tumour**	2334.6 ± 60.2	58.4 ± 0.7	8	17.5 ± 1.5	23.2 ± 1.3	--	--
	plasma	2.9 ± 0.2	0.6 ± 0.01	1	3.2 ± 0.1	5.1 ± 0.1	9.3 ± 0.5	42.3 ± 2.6
Ethyl	**tumour**	315.0 ± 24.0	17.2 ± 2.1	2	7.9 ± 0.3	14.8 ± 0.8	--	--
	plasma	2.1 ± 0.1	0.8 ± 0.06	0.08	2.3 ± 0.4	2.5 ± 0.02	14.3 ± 0.3	49.6 ± 1.2
Propyl	**tumour**	96.0 ± 5.0	10.2 ± 0.9	2	13.2 ± 1.6	12.6 ± 0.6	--	--
	plasma	1.2 ± 0.03	0.9 ± 0.03	0.08	2.1 ± 0.1	1.8 ± 0.1	20.1 ± 0.3	86.6 ± 7.2
Butyl	**tumour**	128.1 ± 15.1	15.0 ± 1.0	1	13.2 ± 2.6	11.4 ± 1.1	--	--
	plasma	0.9 ± 0.03	0.6 ± 0.07	0.5	1.8 ± 0.1	1.1 ± 0.1	23.3 ± 0.9	105.3 ± 2.4

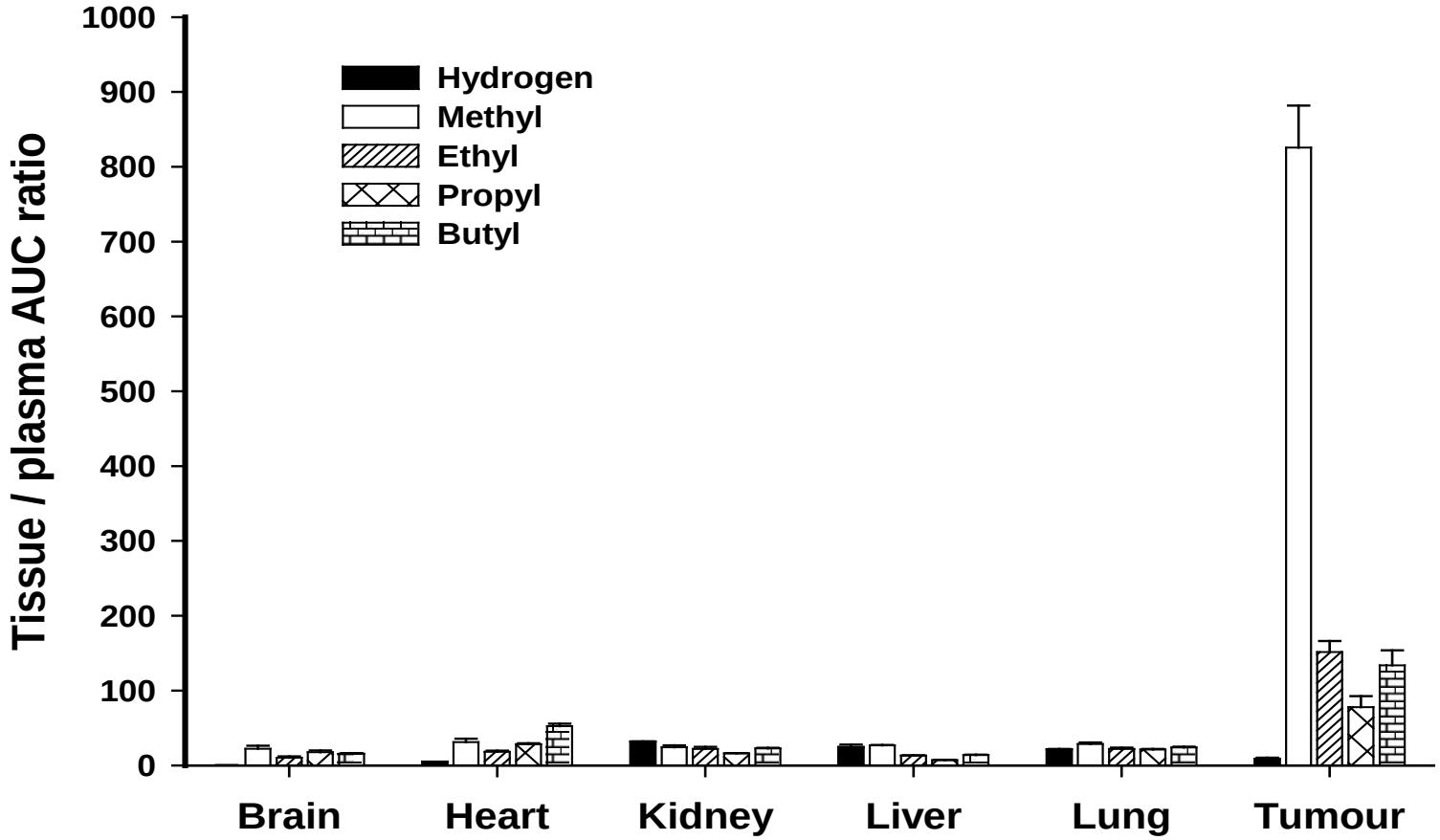

Figure 4.5 Tissue to plasma AUC ratios after i.p. administration of benzonaphthyridine analogues (hydrogen – butyl; 25 μmol/kg) to female tumour-bearing (Colon-38) mice (n = 3 per time point). Values are mean ± s.e.

4.5 Discussion

This study has employed a homologous series of benzonaphthyridine derivatives to show that while plasma and normal tissue pharmacokinetics are related to lipophilic character, tumour pharmacokinetics for the Colon-38 murine adenocarcinoma show a non-linear relationship which is highly dependent on the nature of the N-2 substituent of the benzonaphthyridine ring structure. For instance, the tumour to plasma AUC ratio for the methyl analogue is 825-fold, but only 8-fold for the hydrogen analogue. The corresponding ratio in the Colon-38 tumour for the anthracycline antibiotic, such as doxorubicin [154] is 164-fold respectively. The relative degree of uptake and retention of these drugs in Colon-38 adenocarcinoma tumour tissue, particularly when compared to that of other DNA intercalating topoisomerase poisons, is likely to be a major factor contributing to the high cure rate in this tumour model. There was a significant correlation ($r = –0.98$; $P = 2 \times 10^{-7}$) between tumour exposure and the dose required for a 14-day tumour regression observed upon treatment with these analogues in the murine Colon-38 tumour model [113, 128]. The ethyl and butyl analogues had greater exposures than the hydrogen analogue but had similar anti-tumour activity. The hydrogen analogue had the least tumour exposure (26.3 ± 3.5 µM.h) and had significantly less anti-tumour activity (no cures at 30 mg/kg) compared to the other analogues. The non-linear relationship between lipophilicity and anti-tumour activity bears some similarity to the parabolic relationship reported for another series of DNA binding anticancer drugs [110].

The results indicate that within this series, the methyl analogue exhibited the most outstanding tumour pharmacokinetic characteristics. These were not apparent from its plasma pharmacokinetics and could not have been predicted from the physicochemical properties such as lipophilicity.

No correlation was observed between lipophilicity and i.p. bioavailability across this series. SN 28049 exhibited the greatest i.p. bioavailability and the most prolonged microsomal elimination $T_{½}$, perhaps suggesting that this increased microsomal stability may lead to a reduction in first-pass metabolism after i.p. administration, which may be an important factor contributing to its enhanced bioavailability. It was also of interest that a significant reduction in CL/F and V_{SS}/F was observed with these analogues (particularly the more lipophilic, propyl and butyl analogues) in the tumour-bearing compared to healthy mice. Many mechanisms may be responsible for the latter, including down-

regulation of various drug metabolising enzymes resulting from the increased production of pro-inflammatory cytokines and nitric oxide, or reduction of blood flow to the liver and other tissues [155-157].

Comparison of CL after i.v. administration with the extrapolated hepatic clearance (CL_H) (section 3.4.6), the extrapolated predictions were 2.0 to 4.1-fold less than the observed CL_H while, the predicted value for the hydrogen analogue is similar. It can be inferred that other clearance mechanisms such as, renal elimination of these analogues may account for these differences.

In conclusion, these results clearly support the concept that while lipophilicity is an important determinant for plasma pharmacokinetics and blood brain barrier penetration of these analogues, other factors appear to influence tumour exposure. The study also illustrates the potential limitations of plasma pharmacokinetic studies in selecting and optimizing anti-cancer drug development and is in agreement with previously reported anti-cancer agents like N-[2-(dimethylamino)ethyl]acridine-4-carboxamide (DACA) [158]. Very little is known on transport-mediated drug uptake on intracellular concentrations in tumours and their role in determining anti-tumour response at the cellular level. Further work needs to be undertaken to investigate the mechanisms involved in the uptake of SN 28049's outstanding anti-tumour properties in this Colon-38 tumour model.

Chapter 5

Pharmacokinetics of the methyl derivative in murine and human xenograft tumour models

5.1 Introduction

The methyl benzonaphthyridine derivative (SN 28049) exhibited a more favourable tumour pharmacokinetic profile with an apparent selective uptake and retention in a syngeneic murine Colon-38 tumour, compared to the other benzonaphthyridine analogues (chapter 4). This raised the question of whether this behaviour was specific to the Colon-38 tumour or occurred with other tumours *in vivo* in the mouse.

Establishing xenograft tumour models from patient-derived tumour tissue is believed to conserve original tumour characteristics such as heterogeneous histology, clinical biomolecular signature, malignant phenotypes and genotypes, tumour architecture and tumour vasculature. Based on this prevalent hypothesis, patient-derived tumour grafts are believed to offer relevant predictive insights into clinical outcomes when evaluating the efficacy of novel cancer therapies. However, successful xenografting of human tumours in mice requires immunodeficiency in the host animal to prevent rejection of the transplanted foreign tissues and this was accomplished with nude mice in the late 1960s [159, 160]. Since the discovery of the ragged mouse, many strains of immunodeficient mice containing single mutations (e.g. nude, scid, beige, xid, rag-1 null, rag-2 null) or combined mutations, (e.g. bg/nu, bg/nu/xid, nude/scid, nod/scid) were developed and extensively used in cancer research [161, 162].

In vitro evaluation of the methyl derivative in cell lines developed from murine LLTC tumour and human melanomas (NZM4, NZM10 and NZM52) indicated potent activity with growth inhibitory concentrations (IC_{50}) of 1.0 nM (LLTC), 19.0 nM (NZM4), 2.3 nM (NZM10) and 0.97 nM (NZM52) (B. Baguley, unpublished data). Assessment of *in vivo* anti-tumour activity of the methyl derivative in Rag-1 mice inoculated with NZM4, NZM10 and NZM52 (17.4 µmol/kg i.p. on day 0 and 7) and C57 Bl/6 mice inoculated with LLTC

tumours (26.3 µmol/kg dosed on day 0) gave growth delays of 14 (NZM10), 21 (NZM52) and 9 days (LLTC), but no activity in NZM4 (B. Baguley, unpublished data). Potent *in vitro* and *in vivo* anti-tumour activity of SN 28049 in these tumour models provided the basis for further pharmacokinetic evaluation of SN 28049. The rationale was to determine whether the tumour pharmacokinetics of SN 28049 in these models correlated with the observed *in vivo* activity, and whether the 825-fold tumour to plasma AUC ratio detected with the Colon-38 tumours was also found in other tumour models.

5.2 Aims and approach

The aims were:

1. Pharmacokinetic evaluation of the methyl derivative in C57 Bl/6 mice inoculated with LLTC tumours and comparison with Colon-38 tumours.

2. Pharmacokinetic evaluation of the methyl derivative in immunodeficient Balb/c Rag-1 mice inoculated with various human melanoma xenograft tumours (NZM4, NZM10, NZM52 and LOX IMVI).

5.3 Materials and methods

5.3.1 Tumours

The LLTC cell line, developed from the Lewis lung tumour at the Southern Research Institute, Birmingham, AL, USA, was obtained from Dr R.C. Jackson (Warner-Lambert Company, Ann Arbor, MI, USA) [163]. The melanoma cell lines, NZM4, NZM10 and NZM52 were cultured from tumour samples collected from patients and have been previously described [164]. Procedures involved in the collection and development of LOX IMVI (human amelanotic melanoma tumour) tumours have been previously described [165].

5.3.2 Cell culture

All cell lines were cultured in alpha minimal essential medium (α-MEM) supplemented (Gibco, Life Technologies, Grand Island, NY, USA) with 10 % v/v foetal bovine serum (Gibco, Life Technologies, Grand Island, NY, USA) (FBS), penicillin (60 µg/ml) and streptomycin sulfate (100 µg/ml), (Sigma-Aldrich, St Louis, MO, USA) and maintained in a humidified chamber containing 5 % carbon dioxide (CO_2) and air, at 37°C.

5.3.3 Animal model

C57 Bl/6 mice were used for the inoculation of LLTC cell line. Immunodeficient Balb/c Rag-1 female mice were used for inoculating the human melanoma xenograft (NZM4, NZM10, NZM52 and LOX IMVI) tumours. All experimental procedures, which included blood collection in mice from the ocular sinus under isoflurane anaesthesia, were approved by the University of Auckland Animal Ethics Committee and conformed to the Guidelines for the Welfare of Animals in Experimental Neoplasia, as set out by the United Kingdom Co-ordinating Committee on Cancer Research.

5.3.4 Tumour inoculation in mice

Cultured cells were trypsinised (0.05 %, Gibco, Grand Island, NY, USA) in phosphate buffered saline (PBS) and collected by centrifugation. Cells were quantitated by Coulter counter. The medium was replaced by medium without FBS to give a concentration of 10^8 cells/ml. A 100 µl volume of cells was injected subcutaneously into each mouse.

Experiments were carried out when tumours reached 8-10 mm in diameter, 15 - 20 days after inoculation.

5.3.5 Pharmacokinetic studies

C57 Bl/6 female mice with LLTC tumours received a 25 µmol/kg dose. Immunodeficient Rag-1 female mice inoculated with NZM4, NZM10, NZM52 or LOX IMVI tumours were administered i.p. with the methyl derivative (17.4 µmol/kg). This lower dose (17.4 µmol/kg) was the maximum tolerated dose in Rag-1 mice.

5.3.6 Sample collection and analysis

Blood and tissues (heart, kidney and liver) from anaesthetised mice were collected at predetermined time points (0.08, 0.5, 1, 2, 4, 8, 16 and 24 h). Tumour was collected for an additional two time points, 48 and 72 h from C57 Bl/6 mice with LLTC tumours; 0.08 (only NZM4), 1, 4 and 24 h for Rag-1 mice (n = 3 mice per time point)]. Fewer time points were chosen for the latter due to limited supply of Rag-1 mice. Plasma was separated from blood by centrifugation and tissues (washed with PBS) were homogenised in PBS as described previously (section 2.3.3). Sample deproteination was performed as described in section 2.3.6. Concentrations were measured using a validated LC-MS/MS method (section 2.3.4).

5.3.7 Pharmacokinetic and statistical analysis

Non-compartmental analysis was performed on the plasma and tissue concentration-time data following procedures previously described (see section 4.3.7). AUC in tumour tissue was extrapolated to infinity from time points up to 72 h for murine tumours (LLTC and Colon-38) and only up to 24 h for the melanoma xenografts. Statistical analysis procedures were previously described (section 3.3.9).

5.4 Results – Murine tumours

5.4.1 Plasma pharmacokinetics

Plasma concentration-time profiles after i.p. administration of the methyl derivative (25 µmol/kg) to C57 Bl/6 tumour-bearing female mice are shown in Figure 5.1 and the pharmacokinetic parameters calculated from these profiles are presented in Table 5-1.

The plasma AUCs were similar, 2.7 ± 0.02 (LLTC) *vs* 2.9 ± 0.2 µM.h (Colon-38) ($P = 8 \times 10^{-1}$). Maximal concentrations [0.9 ± 0.05 (LLTC) *vs* 0.6 ± 0.01 µM (Colon-38)] were achieved within 1 h. There was no significant difference in the total plasma i.p. CL/F between the mice with LLTC or Colon-38 tumours, but in the former, the plasma $T_{½}$ and the V_{SS}/F were significantly greater ($P = 9 \times 10^{-3}$; 4.6 ± 0.4 *vs* 3.2 ± 0.1 h and $P < 1 \times 10^{-3}$; 96.5 ± 4.6 *vs* 42.3 ± 2.6 l/kg).

Comparison of plasma pharmacokinetic parameters between mice with LLTC tumours and healthy C57 Bl/6 mice administered 25 µmol/kg of the methyl derivative i.p. (data in Table 5-1) demonstrated that the AUCs, CL/F were not significantly different ($P = 8 \times 10^{-1}$). Significant differences were observed with $T_{½}$s ($P = 9 \times 10^{-3}$; 4.6 ± 0.4 *vs* 3.2 ± 0.04) and V_{SS}/F ($P < 1 \times 10^{-3}$) which were 1.4 and 2.3-fold greater than those observed in healthy and Colon-38 tumour-bearing (C57 Bl/6) mice.

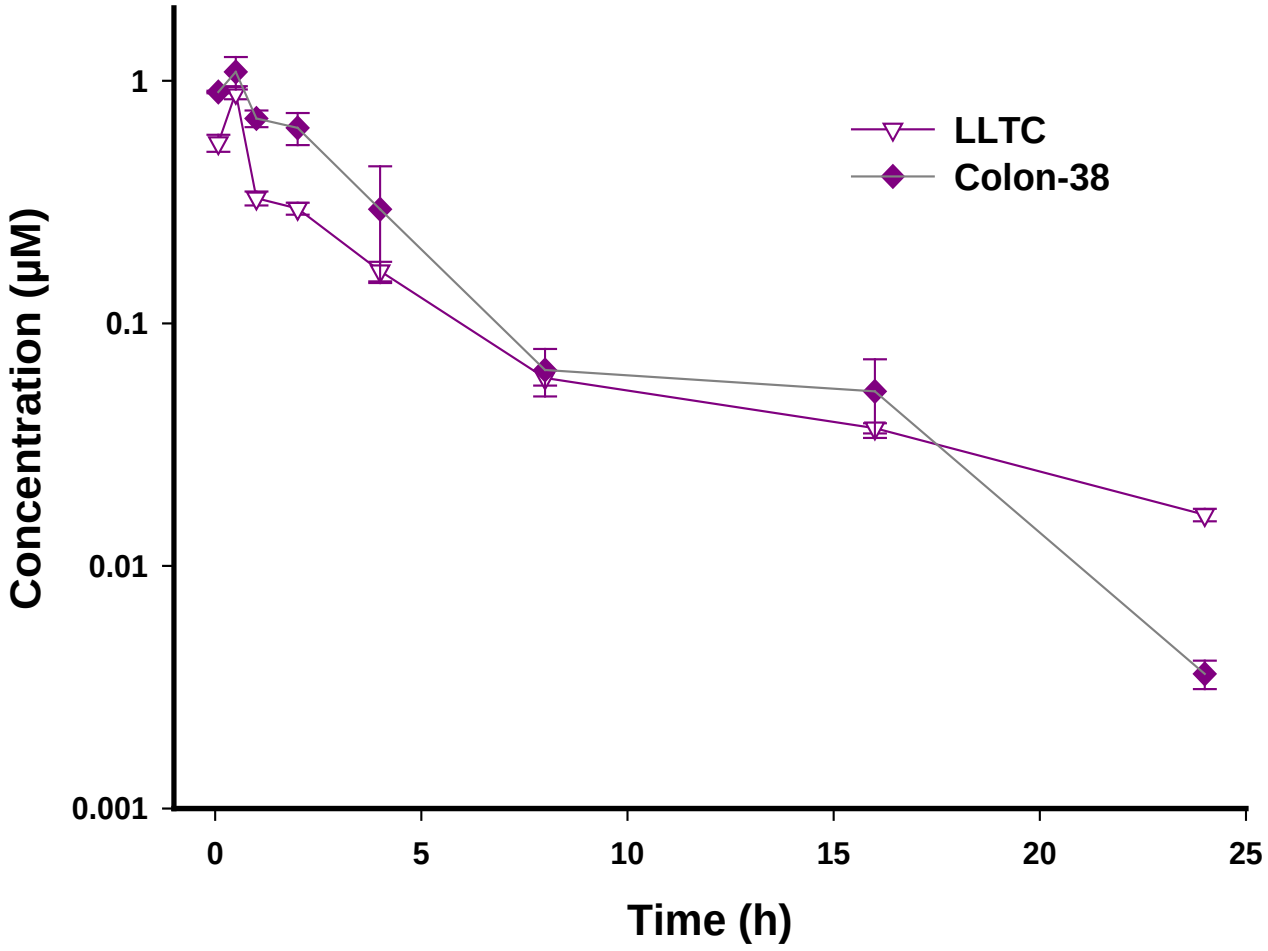

Figure 5.1 Plasma concentration-time profiles after i.p. administration of the methyl derivative (25 µmol/kg) to female tumour-bearing C57 Bl/6 mice (n = 3 per time point). Values are mean ± s.e.

Table 5-1 Plasma pharmacokinetic parameters calculated using non-compartmental analysis from concentration-time profiles after i.p. administration of the methyl derivative (25 µmol/kg) to C57 Bl/6 tumour-bearing mice (n = 3 per time point). Values are mean ± s.e. Data from healthy mice (C57 Bl/6) after i.p. administration of the methyl derivative (25 µmol/kg) included for comparison

Tumour	AUC (µM.h)	C_{max} (µM)	T_{max} (h)	$T_{½}$ (h)	Mean Residence Time (h)	CL/F* (l/h/kg)	V_{SS}/F* (l/kg)
LLTC	2.7 ± 0.02	0.9 ± 0.05	1	4.6 ± 0.4	5.5 ± 0.2	10.3 ± 0.1	96.5 ± 4.6
Colon-38	2.9 ± 0.2	0.6 ± 0.01	1	3.2 ± 0.1	5.1 ± 0.1	9.3 ± 0.5	42.3 ± 2.6
Healthy C57 mice	2.8 ± 0.2	0.6 ± 0.01	1	3.2 ± 0.04	5.0 ± 0.1	9.3 ± 0.5	42.6 ± 2.6

CL/F and V_{SS}/F values are uncorrected for bioavailability.

5.4.2 Tissue and tumour distribution

Tissue (heart, kidney, liver and tumour) concentration-time profiles after i.p. administration of the methyl derivative (25 µmol/kg) to C57 Bl/6 mice are shown in Figure 5.2 and the pharmacokinetic parameters are presented in Table 5-2.

The tissues AUCs were 21 to 94-fold greater than the plasma. The uptake into tissues (heart, liver and kidney) was rapid in these mice with Colon-38 (T_{max}, 0.08 h) compared to mice with LLTC tumours (0.5 h). Highest AUCs in normal tissues (heart, kidney and liver) were observed in mice with LLTC tumours (Table 5-2). The AUCs in liver and heart were 2.5 and 3.2-fold higher in mice with LLTC tumours compared to mice with Colon-38 tumours while differences in kidney were moderate (1.1-fold) and the variations were significant ($P < 1 \times 10^{-3}$).

In mice with LLTC tumours, tumour AUC was 83-fold higher ($P < 1 \times 10^{-3}$) than plasma and similar in magnitude to the heart (84-fold; $P = 8.1 \times 10^{-1}$), while liver was 1.1-fold greater ($P < 1 \times 10^{-3}$) than tumour. The tumour $T_{½}$ was 2-fold greater than plasma and was significantly different ($P < 1 \times 10^{-3}$). Tissue to plasma ratio (TPR) in Colon-38 tumour (Figure 5.3) was 825-fold greater than plasma and 34-fold higher than the other tissues and 11-fold higher than LLTC tumour demonstrating selectivity to a greater magnitude which was unique to this tumour model.

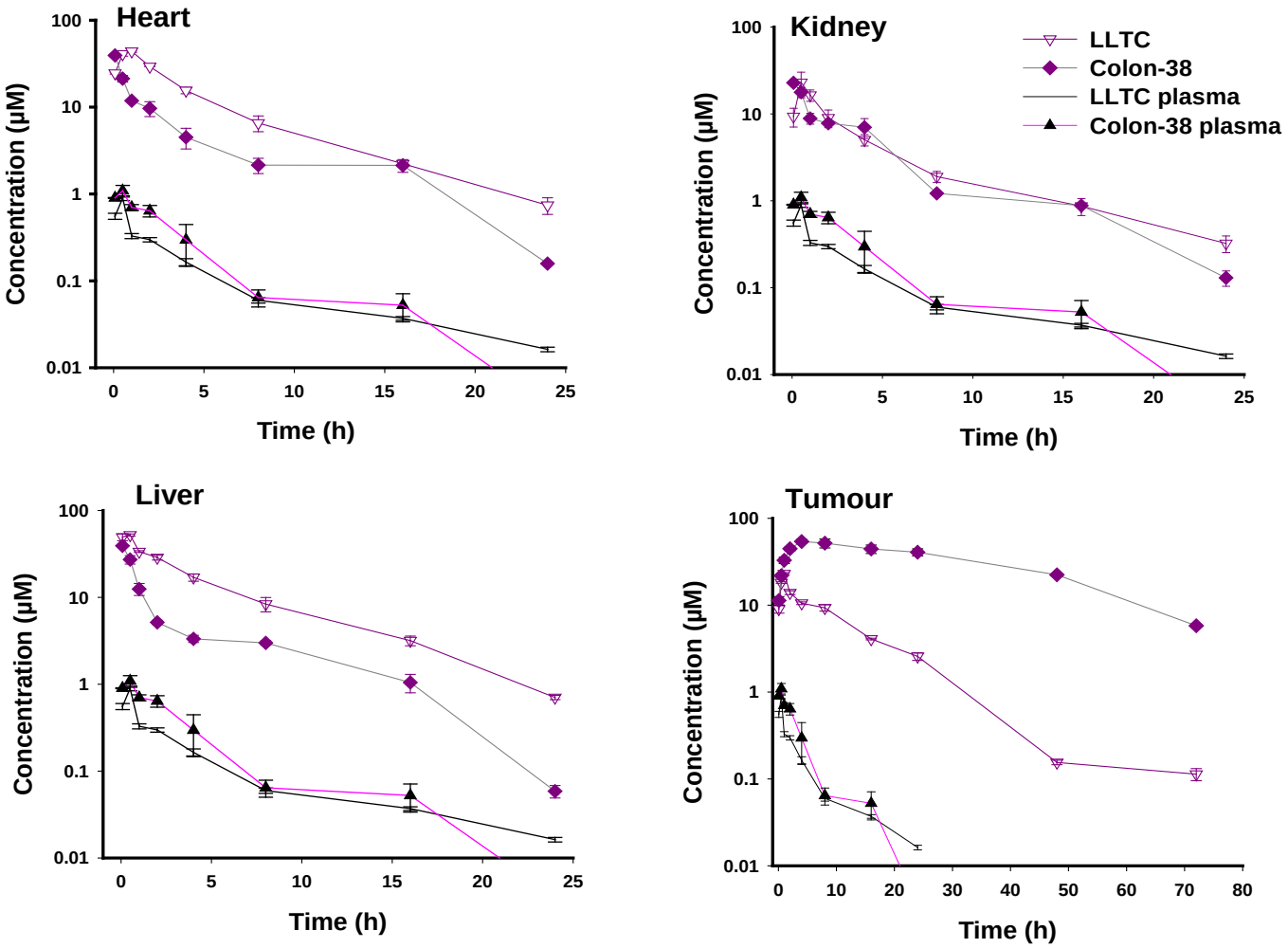

Figure 5.2 Tissue (heart, kidney, liver and tumour) concentration-time profiles after i.p. administration of the methyl derivative (25 μmol/kg) to tumour-bearing C57 Bl/6 female mice (n = 3 per time point). Plasma profiles included for comparison. Values are mean ± s.e.

Table 5-2 Pharmacokinetic parameters calculated using non-compartmental analysis from concentration-time profiles of heart, kidney, liver and tumour after i.p. administration of the methyl derivative (25 µmol/kg) to tumour-bearing C57 Bl/6 female mice (n = 3 per time point). Values are mean ± s.e.

Tumour	Tissue	AUC (µM.h)	C_{max} (µM)	T_{max} (h)	$T_{½}$ (h)	Mean Residence Time (h)
LLTC	Heart	220.1 ± 6.1	45.1 ± 0.2	0.5	4.7 ± 0.3	6.1 ± 0.3
	Kidney	78.3 ± 2.3	25.5 ± 5.8	0.5	5.4 ± 0.4	6.1 ± 0.5
	Liver	246.3 ± 13.3	54.1 ± 1.4	0.5	4.5 ± 0.2	6.5 ± 0.1
	Tumour	216.5 ± 7.2*	23.1 ± 0.6	1	9.3 ± 0.3	11.6 ± 0.2
Colon-38	Heart	87.8 ± 10.8	39.3 ± 1.7	0.08	3.7 ± 0.03	5.7 ± 0.3
	Kidney	68.7 ± 8.3	22.8 ± 1.8	0.08	3.5 ± 0.2	4.7 ± 0.2
	Liver	76.1 ± 5.1	39.2 ± 0.8	0.08	3.1 ± 0.02	4.7 ± 0.2
	Tumour	2334.6 ± 60.2*	58.4 ± 0.7	8	17.5 ± 1.5	23.2 ± 1.3

AUC was calculated using concentrations up to 72 h and extrapolated to infinity (∞).

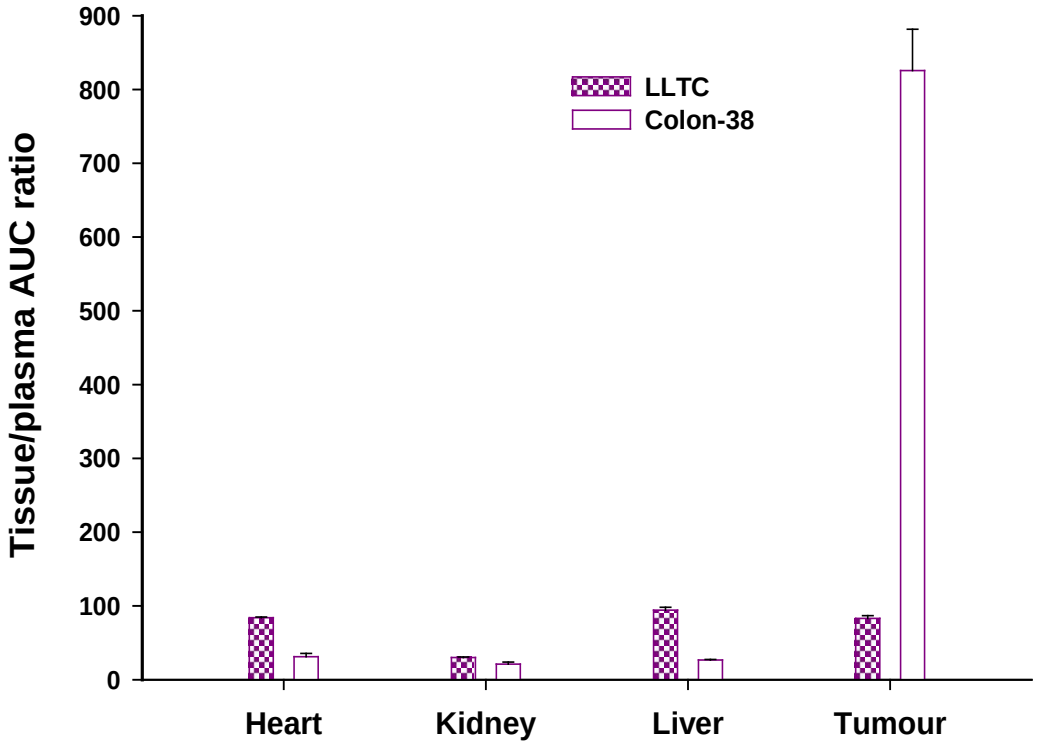

Figure 5.3 Tissue to plasma AUC ratios after i.p. administration of the methyl derivative (25 µmol/kg) to C57 Bl/6 tumour-bearing female mice (n = 3 per time point). Values are mean ± s.e.

5.5 Results – Human xenograft tumours

5.5.1 Plasma pharmacokinetics

Plasma concentration-time profiles for the four xenograft tumours (NZM4, NZM10, NZM52 and LOX IMVI) in Rag-1 mice are shown in Figure 5.4 and the pharmacokinetic parameters calculated from these profiles are presented in Table 5-3. There was considerable variation between the plasma AUCs observed in Rag-1 mice with melanoma tumours, varying from 3.3 ± 0.2 (NZM4) to 5.0 ± 0.1 µM.h (NZM52). Plasma CL/F ranged from 3.5 (NZM52) to 5.3 (NZM4) l/h/kg and were significantly different ($P = 4 \times 10^{-3}$). Similarly, V_{SS}/F varied from 16.7 ± 1.0 (NZM52) to 24.9 ± 3.4 (NZM4) l/kg ($P = 4 \times 10^{-3}$). Moderate $T_{½}$s - 3.0 ± 0.1 (LOX IMVI) to 3.7 ± 0.2 (NZM10) h were observed.

Despite receiving a smaller dose (17.4 *vs* 25 µmol/kg in C57 mice) the total plasma AUCs in Rag-1 mice were significantly higher ($P < 1 \times 10^{-3}$) than those observed in C57 mice with either Colon-38 or LLTC tumours. Consequently, the tumour-bearing Rag-1 mice had plasma i.p. clearance and volume of distribution values approximately 50 % of those observed in tumour-bearing C57 mice (CL/F: 3.5 – 5.3 *vs* 9.3 – 10.3 l/h/kg; V_{SS}/F: 16.7 – 24.9 *vs* 42.3 – 96.5 l/kg). Despite this, the elimination $T_{½}$s were of similar magnitude, 3.0 – 3.7 in Rag-1 mice *vs* 3.2 – 4.6 h in C57 mice.

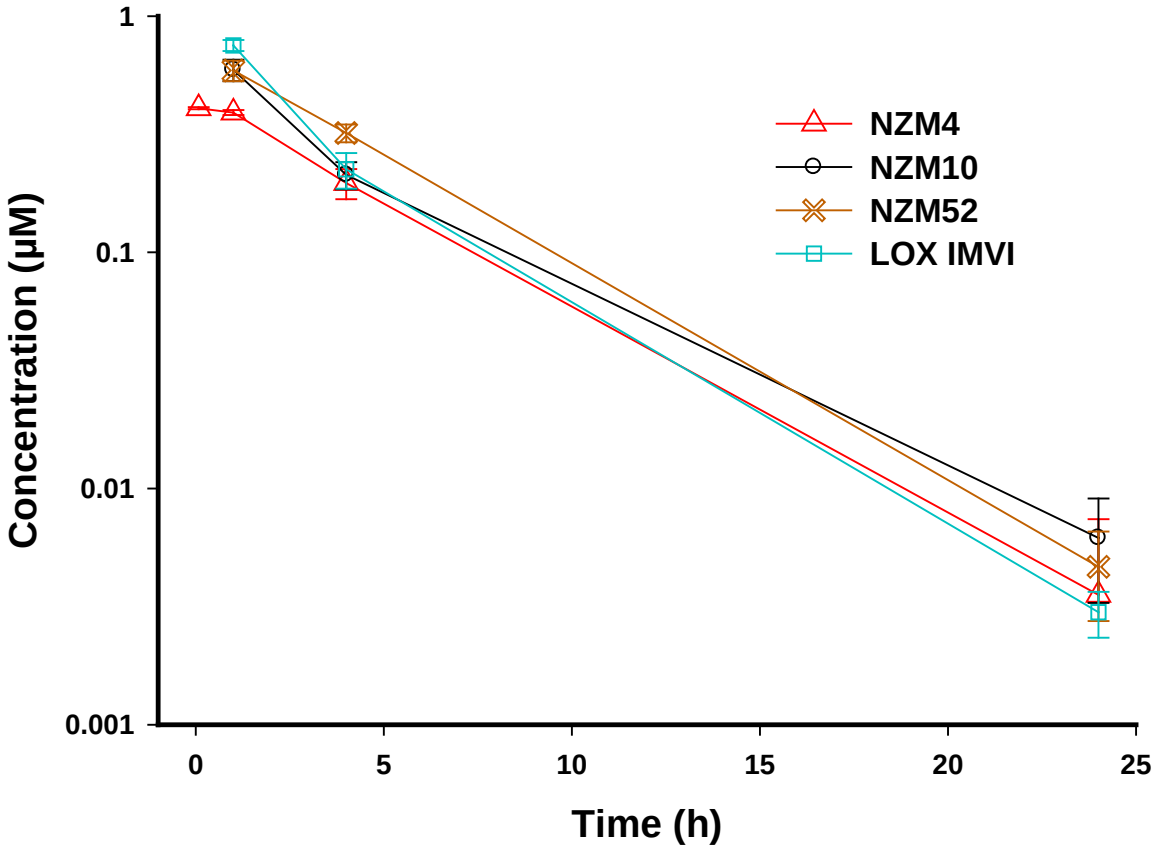

Figure 5.4 Plasma concentration-time profiles after i.p. administration of the methyl derivative (17.4 µmol/kg) to female tumour-bearing Rag-1 mice (n = 3 per time point). Values are mean ± s.e.

Table 5-3 Plasma pharmacokinetic parameters calculated using non-compartmental analysis from concentration-time profiles after i.p. administration of the methyl derivative (17.4 µmol/kg) to Rag-1 tumour-bearing mice (n = 3 per time point). Values are mean ± s.e. Data from C57 Bl/6 with Colon-38 tumours after i.p. administration of the methyl derivative (25 µmol/kg) included for comparison.

Tumour	AUC (µM.h)	C_{max} (µM)	T_{max} (h)	$T_{½}$ (h)	Mean Residence Time (h)	CL/F (l/h/kg)	V_{SS}/F (l/kg)
NZM4	3.3 ± 0.2	0.4 ± 0.002	0.08	3.3 ± 0.5	3.4 ± 0.3	5.3 ± 0.3	24.9 ± 3.4
NZM10	4.0 ± 0.3	0.6 ± 0.03	1	3.7 ± 0.2	3.6 ± 0.2	4.7 ± 0.3	24.3 ± 1.1
NZM52	5.0 ± 0.1	0.6 ± 0.03	1	3.3 ± 0.2	3.6 ± 0.1	3.5 ± 0.1	16.7 ± 1.0
LOX IMVI	4.3 ± 0.2	0.8 ± 0.02	1	3.0 ± 0.1	3.1 ± 0.1	4.2 ± 0.2	18.3 ± 1.1
Colon-38	2.9 ± 0.2	0.6 ± 0.01	1	3.2 ± 0.1	5.1 ± 0.1	9.3 ± 0.5	42.3 ± 2.6

CL/F and V_{SS}/F values are uncorrected for bioavailability.

5.5.2 Tissue and tumour distribution

Tissue (heart, kidney, liver and tumour) concentration-time profiles after i.p. administration of the methyl derivative (17.4 µmol/kg) are shown in Figure 5.5 and the pharmacokinetic parameters are presented in Table 5-4. Rag-1 mice with LOX IMVI tumours had the greatest uptake and retention into kidney (AUC: 674.5 ± 8.5 µM.h) with a C_{max}, 77.6 ± 1.3 µM. This trend of higher kidney AUC was consistent with other tumour models and was significant between the tumour model ($P = 1 \times 10^{-3}$). The methyl derivative was also concentrated in heart and liver to a greater extent than plasma with all the tumour models. Heart AUCs were the higher in NZM10 (217.4 ± 8.1 µM.h) and NZM52 (197.8 ± 6.4 µM.h) followed by NZM4 (182.8 ± 14.8 µM.h) and LOX IMVI (136.2 ± 3.5 µM.h). These differences in accumulation were significant ($P = 1 \times 10^{-3}$). The liver AUCs varied from 67.5 ± 2.2 (NZM4) to 220.4 ± 29.6 µM.h (NZM10) and were significantly different ($P = 1 \times 10^{-3}$). The order of AUCs in these xenograft models can be given as follows: NZM4: kidney>heart>liver; NZM10: kidney>liver>heart; NZM52: kidney>heart>liver; LOX IMVI: kidney>liver>heart. $T_{½}$s were 2.3 ± 0.1 (heart, NZM52) to 4.6 ± 0.3 h (kidney, NZM52 and LOX IMVI). Overall, the tissue AUCs were 20 (liver, NZM4) to 165-fold (kidney, LOX IMVI) higher than the plasma.

Tumour AUCs were very variable, ranging over 36-fold, from a high of 320.7 ± 33.1 µM.h in NZM10 down to a low of 8.9 ± 0.3 µM.h in the NZM4 tumour. As with the LLTC and Colon-38 tumours, tumour concentrations were much greater than plasma, with tumour/plasma AUC ratios ranging from 86 in NZM10 down to 2.8 in NZM4. Tumour $T_{½}$s (6.3 ± 0.4 – 8.8 ± 0.4 h) were approximately 2-fold greater compared to plasma (3.0 ± 0.1 – 3.7 ± 0.2 h) and the other tissues (2.3 ± 0.1 – 4.6 ± 0.3 h). The TPRs for the individual tumours and all tissues investigated are illustrated in Figure 5.6. The greatest ratios were observed in the kidney, followed by the heart and liver (similar magnitude), with the smallest ratio in the tumour (with the exception of NZM10).

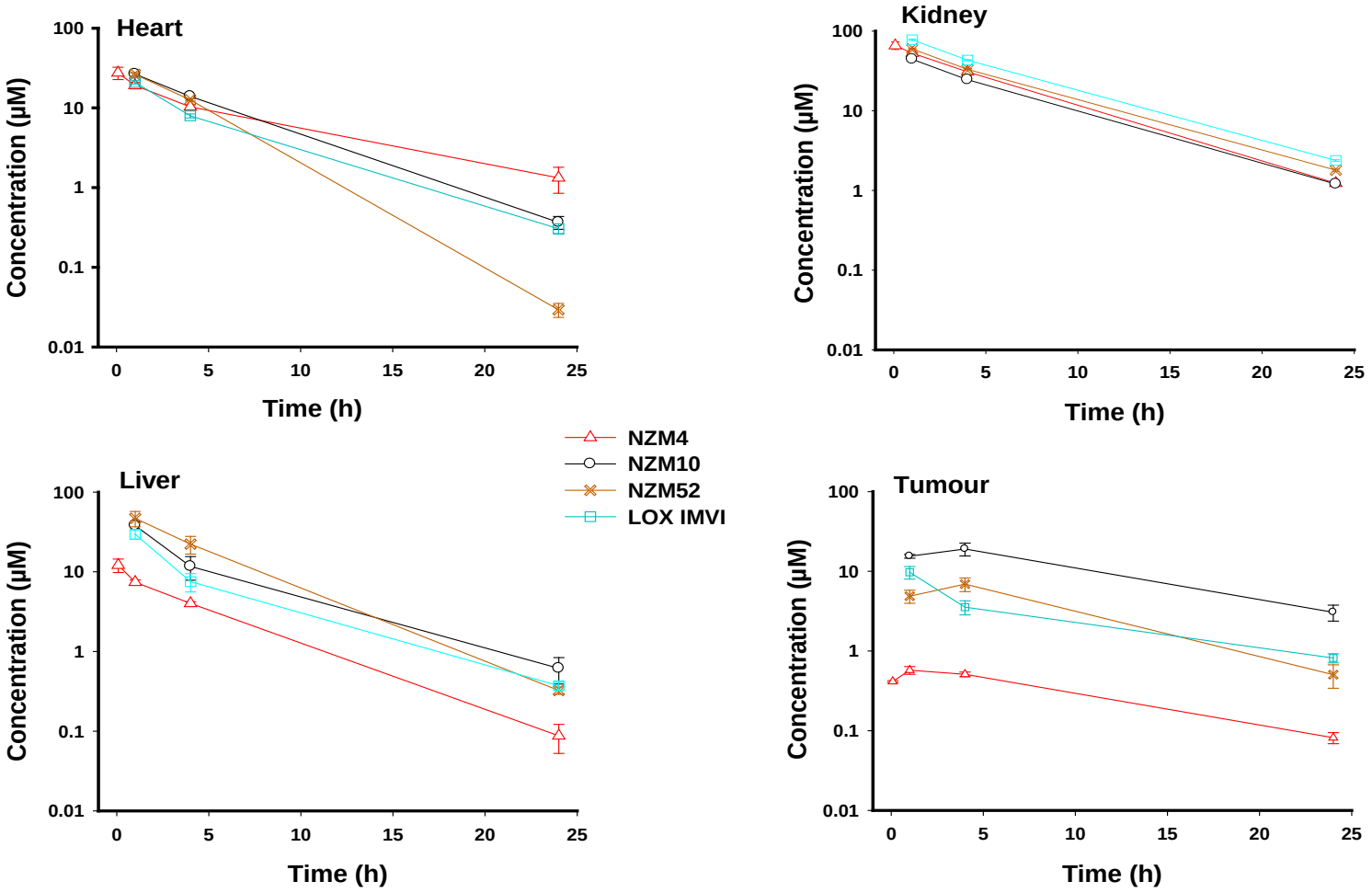

Figure 5.5 Tissue (heart, kidney, liver and tumour) concentration-time profiles after i.p. administration of the methyl derivative (17.4 µmol/kg) to tumour-bearing Rag-1 female mice (n = 3 per time point). Values are mean ± s.e.

Table 5-4 Pharmacokinetic parameters calculated using non-compartmental analysis from concentration-time profiles of heart, kidney, liver and tumour after i.p. administration of the methyl derivative (17.4 µmol/kg) to tumour-bearing Rag-1 female mice (n = 3 per time point). Values are mean ± s.e.

Tumour	Tissue	AUC (µM.h)	C_{max} (µM)	T_{max} (h)	$T_{½}$ (h)	Mean Residence Time (h)
NZM4	Heart	182.8 ± 14.8	27.5 ± 1.0	1	4.3 ± 0.1	4.5 ± 0.4
	Kidney	502.0 ± 41.0	67.3 ± 6.3	0.08	4.3 ± 0.1	4.0 ± 0.1
	Liver	67.5 ± 2.2	12.1 ± 1.3	0.08	3.6 ± 0.2	3.5 ± 0.1
	Tumour	8.9 ± 0.3	0.6 ± 0.03	1	7.9 ± 0.3	8.6 ± 0.5
NZM10	Heart	217.4 ± 8.1	26.5 ± 1.0	1	3.7 ± 0.1	3.7 ± 0.2
	Kidney	441.0 ± 6.5	44.2 ± 0.7	1	4.3 ± 0.1	4.6 ± 0.05
	Liver	220.4± 29.6	38.1 ± 0.3	1	4.1 ± 0.3	3.9 ± 0.3
	Tumour	320.7 ± 33.8	19.1 ± 2.0	4	8.8 ± 0.4	9.7 ± 0.8
NZM52	Heart	197.8 ± 6.4	26.3 ± 1.2	1	2.3 ± 0.1	3.2 ± 0.02
	Kidney	517.7 ± 6.1	59.6 ± 0.8	1	4.6 ± 0.05	4.6 ± 0.1
	Liver	354.2 ± 41.5	46.8 ± 5.9	1	3.4 ± 0.1	3.5 ± 0.1
	Tumour	98.8 ± 10.4	6.9 ± 0.8	4	6.3 ± 0.4	11.4 ± 1.1
LOX IMVI	Heart	136.2 ± 3.5	21.0 ± 1.0	1	3.9 ± 0.2	3.5 ± 0.02
	Kidney	674.5 ± 8.5	77.6 ± 1.3	1	4.6 ± 0.3	4.6 ± 0.03
	Liver	151.7 ± 11.9	29.6 ± 1.3	1	3.9 ± 0.2	3.6 ± 0.1
	Tumour	77.2 ± 5.7	9.7 ± 1.0	1	7.3 ± 0.2	8.6 ± 0.3

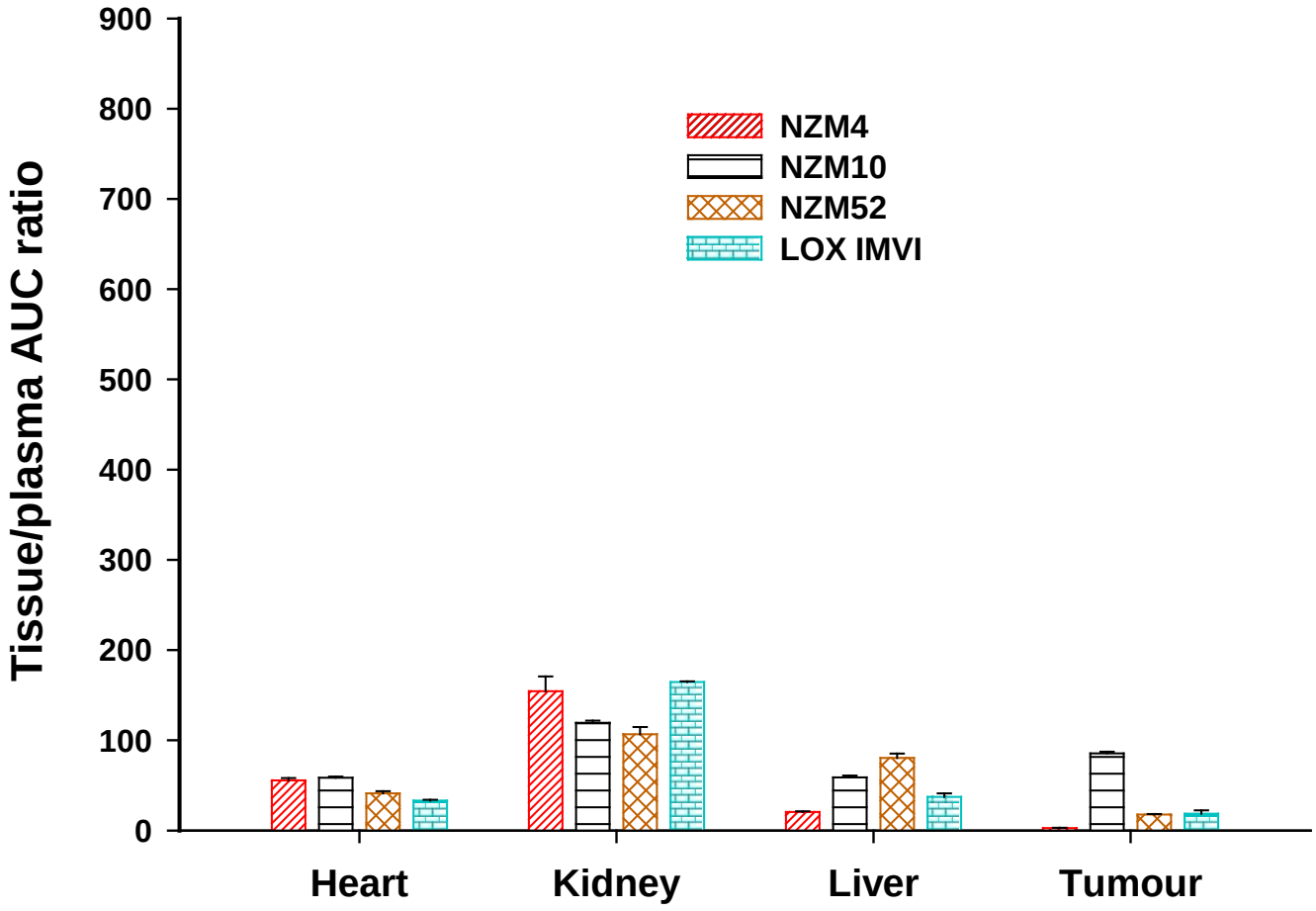

Figure 5.6 Tissue to plasma AUC ratios after i.p. administration of the methyl derivative (17.4 µmol/kg) to Rag-1 tumour-bearing female mice (n = 3 per time point). Values are mean ± s.e.

5.6 Discussion

These studies indicated that both the plasma CL/F and V_{SS}/F of the methyl derivative pharmacokinetic parameters in Rag-1 mice with melanoma tumours are approximately 50% of the same parameters in tumour-bearing C57 mice (Figure 5.7). As the pharmacokinetics of the methyl derivative were not investigated in healthy Rag-1 mice, it is not known whether these pharmacokinetic differences are due to the strain of mice or to the tumour. Earlier studies with benzonaphthyridine series (chapter 4) have demonstrated that the tumour had an influence on the pharmacokinetics of these analogues, although this more or less disappeared with the methyl derivative. Further evidence for the modulation of plasma pharmacokinetics by the presence of a tumour is given by the observation of the more than doubling of the V_{SS}/F parameter in C57 mice with the LLTC tumours, compared to C57 mice with Colon-38 tumours.

As with previous studies, tissue and tumour concentrations in Rag-1 mice were considerably greater than plasma. However, in contrast to C57 mice, Rag-1 mice exhibited the greatest concentrations in the kidney, even greater than their tumour concentrations. Lack of immune system in the Rag-1 mice, while promoting tumour growth, may also lead to reduced renal function due to inflammation [166]. This may result in the higher AUCs in kidney and plasma despite a lower dose. These increases in circulating concentrations may possibly be a reason for the lower maximum tolerated dose of the methyl derivative (17.4 *vs* 26.3 µmol/kg). Another notable feature of the tissue profiles of the methyl derivative in Rag-1 mice was the great variability in the liver and in particular the tumour AUCs. Within these melanoma tumours, there was a 36-fold difference in tumour exposure from the same i.p dose of drug. Interestingly this appeared to correlate with anti-cancer activity in these melanoma tumour models as the methyl derivative had no *in vivo* activity against NZM4 which had the lowest tumour AUC of 8.9 ± 0.3 µM.h, compared to growth delays of 21 and 14 days for NZM52 (AUC, 98.8 ± 10.4) and NZM10 (AUC, 320.7 ± 33.8) respectively. The mean residence times were at least 2 to 4.5-fold greater in tumour than plasma and other tissues indicating a selective and longer retention in tumour ($P < 1 \times 10^{-3}$; Figure 5.8). Additionally the mean residence time of the methyl derivative in Colon-38 tumour was at 2-fold longer compared to the other tumours. The tissue to plasma AUC ratio (Figure 5.9) in the Colon-38 tumour was far greater than any other tumour tested confirming the unique retention of the methyl derivative in this tumour.

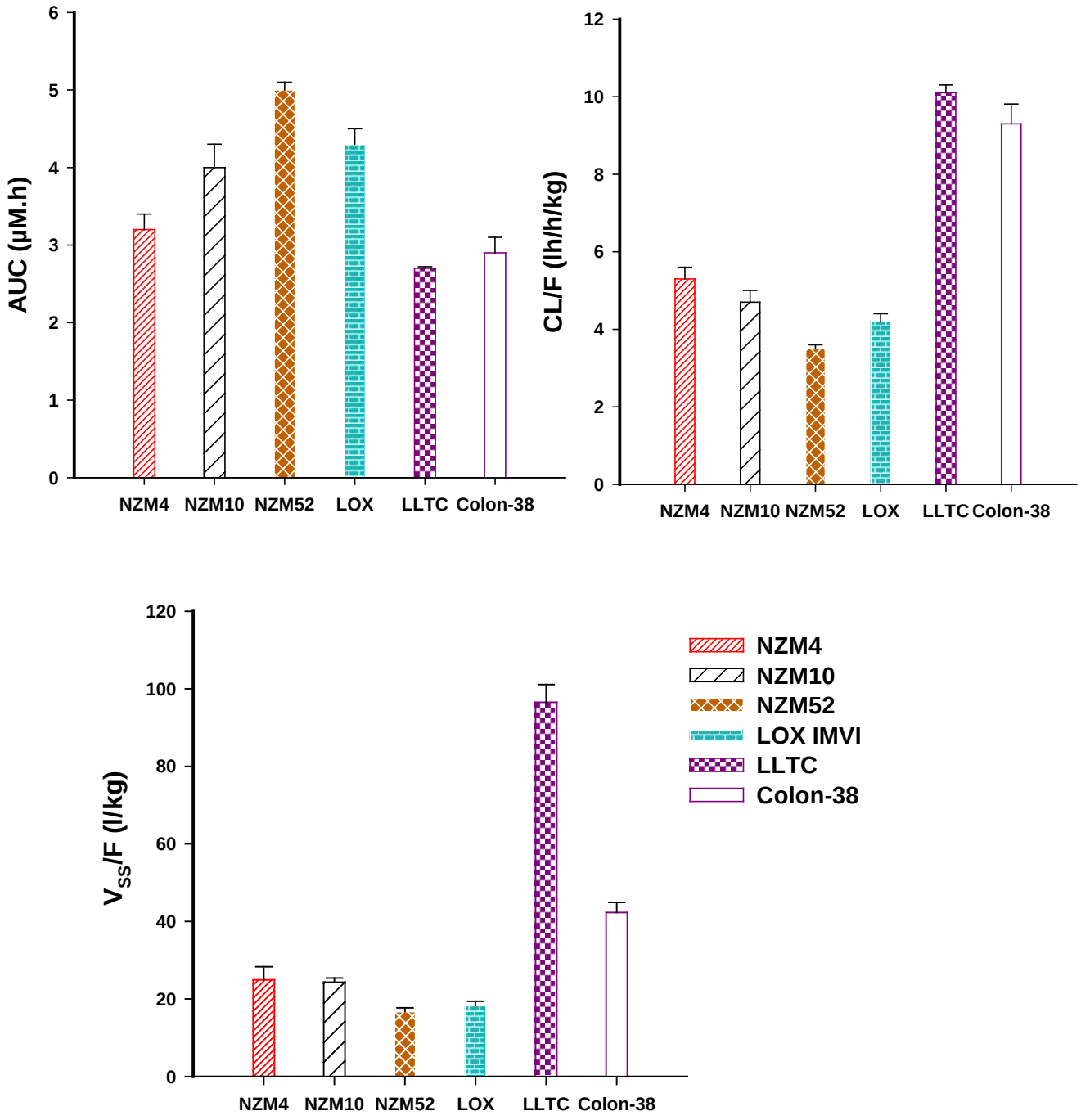

Figure 5.7 Plasma AUC, CL/F and V_{SS}/F plots after i.p. administration of the methyl derivative to Rag-1 (17.4 µmol/kg) or C57 Bl/6 (25 µmol/kg) female tumour-bearing mice (n = 3 per time point). Values are mean ± s.e.

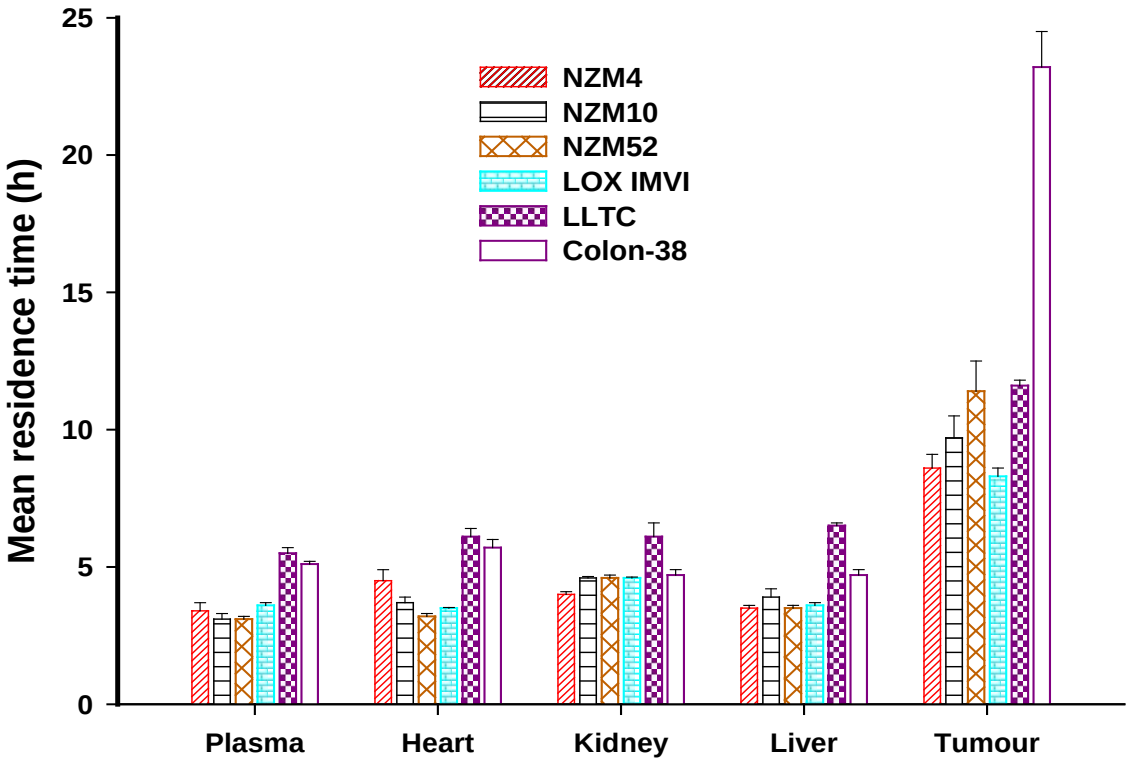

Figure 5.8 Mean residence times after i.p. administration of the methyl derivative to Rag-1 (17.4 µmol/kg) or C57 Bl/6 (25 µmol/kg) tumour bearing female mice (n = 3 per time point). Values are mean ± s.e.

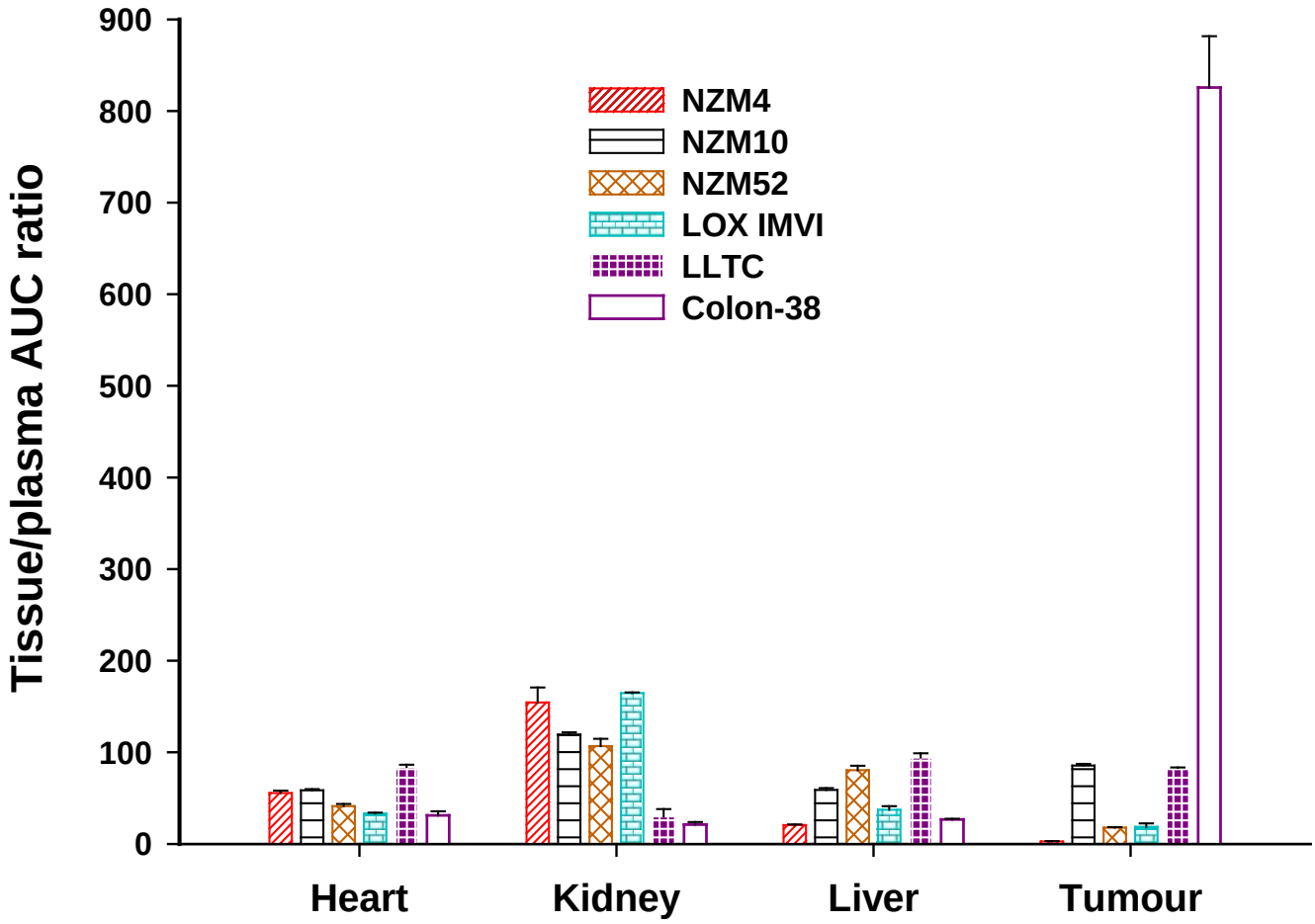

Figure 5.9 Tissue to plasma AUC ratios after i.p. administration of the methyl derivative to Rag-1 (17.4 µmol/kg) or C57 Bl/6 (25 µmol/kg) tumour-bearing female mice (n = 3 per time point). Values are mean ± s.e.

Chapter 6

Tumour cell kinetics and cytotoxicity of the benzonaphthyridine derivatives

6.1 Introduction

Pharmacological evaluation of the benzonaphthyridine series (as described in chapter 4) demonstrated an apparent greater tumour uptake and longer retention in Colon-38 tumours in mice compared to the lipophilic variants in the series (ethyl – butyl). The selectivity of Colon-38 tumours for the methyl derivative was confirmed by the pharmacokinetic studies in other human and murine xenograft tumour models (chapter 5). However the reasons for the apparent greater uptake and retention of the methyl derivative in the Colon-38 tumours *in vivo* are unknown. The *in vivo* tumour microenvironment which is influenced by factors such as blood flow, the tumour acidity, the number of stromal cells and the composition of the extracellular matrix, all of which vary from tumour to tumour, may influence tumour drug distribution and retention to varying degrees [36, 167-170]. In addition, such selective uptake and retention may occur at the tumour cellular level. To answer this question, further *in vitro* studies were undertaken using the individual cell lines from the tumours utilised in the *in vivo* evaluation of these derivatives (chapters 4 and 5). An indication of differences in uptake/retention at the individual cell line level would provide a basis for further studies to identify the transport mechanism, which may be responsible for such uptake/retention of these benzonaphthyridine derivatives. One of the objectives here was to obtain evidence for or against the hypothesis that differences *in vivo* tumour pharmacokinetics were caused by differences in cell kinetics.

Transporter molecules in the cell membranes may limit or enhance drug entry in to the tumour cell, thus modifying drug action. Multi-drug resistance (MDR) of cancer cells to chemotherapeutic drugs may occur by numerous mechanisms, including increased drug efflux or decreased drug uptake, activation of detoxifying systems, activation of DNA repair mechanisms, and evasion of drug-induced apoptosis. These mechanisms are reviewed in detail elsewhere [171-174]. The modulation of the cellular efflux of lipophilic drugs mediated by energy-dependent transporters, known as ATP-binding cassette (ABC)

transporters, such as P-gp, MRP1 and BCRP [175, 176] may play a role in the different degrees of uptake and retention observed for these lipophilic benzonaphthyridines. Colon carcinomas are known to express transporters such as P-gp and MRP1 which are actively involved in the efflux of anti-cancer drugs [177, 178]. Since variants of Colon-38 tumour cell lines overexpressing multi-drug resistant transporters were not available, alternative cell cultures over-expressing P-gp, (human lymphoblastic leukaemia cell line resistant to vinblastine), CEM/VLB_{100} and MRP1 (resistant to epirubicin), CEM/E_{1000} were used for this evaluation [179-181].

Thus *in vitro* studies were performed to further investigate the cellular accumulation of the benzonaphthyridine derivatives in Colon-38, CCRF-CEM, CEM/VLB_{100} and CEM/E_{1000} cell cultures. Cellular uptake and retention of the methyl derivative was further evaluated in Colon-38, LLTC and New Zealand melanoma (NZM) cultures (NZM4, NZM10 and NZM52).

6.2 Aims and approach

The aims were:

1. To assess the cell uptake, retention and antiproliferative activity of the methyl derivative following short-term drug exposure up to 48 h in Colon-38, Lewis Lung (LLTC) and melanoma (NZM4, NZM10 and NZM52) cell cultures.

2. To estimate the antiproliferative activity and cellular retention of benzonaphthyridine derivatives (hydrogen – butyl) in the human leukaemia cell line (CCRF-CEM) and its drug resistant variants (CEM/VLB_{100} and CEM/E_{1000}) and determine their susceptibility to efflux transporters.

6.3 Materials and methods

6.3.1 Cell culture maintenance

6.3.1.1 Cell lines

Cultures from murine tumours including, Colon-38 [182], LLTC [163] and human melanoma cell lines, NZM4, NZM10 and NZM52 (cultured from tumour samples collected from patients were previously described [164]) were maintained as adherent cultures. The leukaemia cell line, CCRF-CEM (developed from tumour samples collected from patients with lymphoblastic leukaemia) [179] and the two drug resistant sub-lines (of CCRF-CEM) were developed by treatment with either vinblastine, CEM/VLB_{100} [180] or epirubicin, CEM/E_{1000} [181]. The latter were maintained as suspension cultures. The leukaemia cell lines, CCRF-CEM, CEM/VLB_{100} and CEM/E_{1000} were kindly provided by Professor R. A. Davey, University of Sydney, NSW, Australia.

6.3.1.2 Culture medium

α-MEM was prepared by dissolving α-MEM powdered medium in Milli Q water and adding sodium bicarbonate ($NaHCO_3$) (2.2 g/l). The pH was adjusted to 7.2 using 12 N hydrochloric acid (HCl) or 5 M sodium hydroxide (NaOH). The medium was filter-sterilized under pressure and aliquoted into sterile Schott Duran bottles (Schott AG, Mainz, Germany). Medium was stored at 4°C and used within 1-month of preparation. Medium was warmed in a 37°C water bath prior to use and was supplemented with 10 % (v/v) FBS and penicillin and streptomycin (60 µg/ml and 100 µg/ml respectively). Cultures were maintained in T75 (75 cm^2) flasks (BD Falcon, Bedford, MA, USA) in a humidified incubator (Thermo Scientific, Asheville, NC, USA) at 37°C with 5 % CO_2.

6.3.1.3 Growth and maintenance of cell cultures

Cell cultures were propagated by weekly passage. Prior to harvesting, cells were checked for fungal or bacterial contamination by an inverted phase-contrast microscope (Olympus, Tokyo, Japan). For adherent cultures, the medium was aspirated and the surface of the T75 flask was coated with 1 ml of trypsin-EDTA (0.05 % / 1X) (Gibco, Grand Island, NY, USA) and placed in the incubator for 5 min to detach the cells from the flask. Following this, 7 ml of α-MEM was added to the flask, mixed gently and cells were collected in a 15 ml tube. Cell density was assessed by a Coulter Counter (Z2 Coulter Particle Counter and Size Analyzer, Beckman Coulter Inc, Miami, FL, USA). After centrifugation, cells (10^6/ml) were seeded in T75 flasks containing 15 ml supplemented culture medium (α-MEM + 10 % FBS + penicillin/streptomycin). For suspension cultures, 0.1 ml aliquots of cell suspension were pipetted and diluted with 9.9 ml of PBS in a plastic cuvette. The cell count for all cultures was determined by Coulter Counter and viability by trypan blue (0.4 %) incorporation method by Countess Auto cell counter (Invitrogen, Carlsbad, CA, USA). Aliquots of the suspension (0.1 to 0.5 ml) were transferred into a new T75 flask containing 20 ml supplemented culture medium as needed.

6.3.1.4 Cryopreservation and recovery of cells

Cells were cultured in T75 flasks until confluent to maintain them in an exponential growth phase. Adherent cells were trypsinised (see section 6.3.1.3). For suspension cultures, the contents were transferred to a 40 ml tube and centrifuged. Medium was aspirated and the cell pellet was suspended in fresh medium. A volume of (0.9 ml) was placed into cryovials (Nunc A/S, Roskilde, Denmark) at a concentration of 10^6 cells/ml, containing 0.9 ml of freezing mixture [90 % FBS, 10 % dimethyl sulfoxide (DMSO) in α-MEM] .These cryovials were placed in a Nalgene Mr Frosty freezing container, (Nalgene, Thermo Scientific, Rochester, NY, USA) and chilled overnight in a –80°C freezer allowing the cryovials to freeze at a slow rate, about 1°C/min. These vials were then transferred to a liquid nitrogen (–196°C) for long-term storage. To reconstitute cells from liquid nitrogen storage, each vial of cells was thawed in a 37°C water bath. Contents were transferred to 15 ml tubes containing 10 ml supplemented culture medium and centrifuged at 1000 × *g* for 5 min. The supernatant was aspirated and cells were resuspended in culture medium and seeded into a T25 flask. Medium was replaced the next day. Subcultures were maintained in T75 flasks as needed.

6.3.2 IC_{50} assay

Growth inhibition data were expressed as the IC_{50} value for each drug, where IC_{50} is defined as the drug concentration required to reduce cell growth to 50 % of control drug-free cultures. The (tritiated) [^{3}H]-thymidine incorporation assay [183, 184], which measures the amount of radioactive thymidine incorporated into cellular DNA during DNA replication, was used to determine the growth inhibitory potencies of cytotoxic drugs. Each treatment group was tested in triplicate in each experiment for consistency.

Drugs were prepared as 2 mM stock solutions solution in 50 % ethanol and subsequent dilutions were done using α-MEM. Supplemented culture medium (100 µl) was added to each well in a 96-well culture plate. 50 µl of drug (2700 nM) was added to the top concentration well. A set of five serial dilutions were performed by pipetting 50 µl from each well and adding to the subsequent well. Finally, 50 µl of cell suspension (1000 cells/well) was added to each well containing drug and were incubated for 72 h. This yields a top drug concentration of 600 nM serially diluted (5 sets) 3-fold across the 96-well plate. Two sets of triplicates were left untreated and 25 µl of culture medium were added instead. Each 96-well plate was used to assay 4 compounds.

[^{3}H]-thymidine incorporation was determined 72 h after adding drug. For the final 6 h of drug incubation, an aliquot (20 µl) of medium containing 5-Methyl-[^{3}H]-thymidine (20 Ci/mM, 0.04 µCi per well), unlabelled thymidine (TdR) (0.1 µM final concentration) and 5-fluoro-2'-deoxyuridine (FUdR) (0.1 µM final concentration) was added to each well. Cells were harvested using an automated multi-well harvester and transferred to a sheet of filter paper. Filter paper was dried overnight and sealed in a plastic bag with 10 ml scintillation fluid (Wallac, OY, Finland). The amount of tritium retained on the filter paper was measured by the beta (β)-plate liquid scintillation counter (Wallac, OY, Finland). The output was obtained as counts per min and plotted against the corresponding concentration of each drug. The IC_{50} value was calculated from the fitted curve (using a four parameter logistic curve) by SigmaPlot® 11. Experiments with adherent cultures were previously performed and data is included for comparison (Y. Chen & B. Baguley, unpublished data). Resistance factor was calculated by dividing the IC_{50} obtained for the resistant subline (CEM/VLB_{100} or CEM/E_{1000}) by the IC_{50} obtained for the parental cell line (CCRF-CEM).

6.3.3 Drug release after repeated washes following a 1 h exposure

Cultures (Colon-38) were used to verify the retention of the benzonaphthyridine derivatives (hydrogen – butyl) following repeated washes after a brief exposure (1 h). Experiments with other cultures (LLTC, NZM4, NZM10 and NZM52) were limited to the methyl derivative. Cells were seeded into P100 culture dishes (5 x 10^4 cells/ml; 15 ml) and incubated (37°C) overnight to attach. For each culture, 12 dishes (4 sets; triplicate for each set) were maintained and 0.5 µM drug (final concentration in each dish) was added and incubated for 1 h. After the incubation period, media from the first set (triplicate) was carefully removed and the cells were washed with 2 - 3 ml of supplemented α-MEM. For the second and the third set, cultures dishes were washed twice or thrice respectively. The fourth set was treated as control (no wash). The medium was discarded (after washes) and the cells were harvested by trypsinisation (section 6.3.1.3). Cells were collected in 1.5 ml tubes and centrifuged (1000 × *g,* 5 min). Cell pellets were separated by removal of extracellular medium and were extracted by adding 3-volumes of MeCN:MeOH mixture containing 0.05 µM d_7 internal standard. These were then centrifuged 13000 × *g* (5 min, 4°C) and a 25 µl supernatant was diluted with equal volume of mobile phase B (0.01 % formic acid in Milli Q water) and were analysed by LC-MS/MS (section 2.3.4).

6.3.4 Drug efflux over 48 h

These experiments with Colon-38, NZM4, NZM10 and NZM52 cultures were limited to the methyl derivative. Cells were seeded into P100 culture dishes (5 x 10^4 cells/ml; 15 ml) and incubated (37°C) overnight to attach. For each culture, 21 dishes (6 sets; triplicate for each set) were exposed to 0.5 µM drug (final concentration in each dish) for 1 h. After this period, the culture dishes were washed thrice with 2 - 3 ml supplemented α-MEM and cultured with fresh medium for the duration of the time-course (up to 48 h). One set of untreated controls (no drug; triplicate) were processed similarly and harvested at the first time point (1 h). At pre-determined time points (1, 4, 8, 16, 24 and 48 h) triplicate dishes withdrawn, medium was removed and cells were harvested by trypsinisation (section 6.3.1.3). Cells collected in 1.5 ml tubes were centrifuged to separate the cell pellets from extracellular medium. Sample preparation and analysis was performed as described previously (sections 6.3.3 and 2.3.4). Area under the concentration-time curve (AUC) was calculated from the concentration-time data up to 48 h using a similar approach as described previously (section 4.3.7).

6.3.5 Cell uptake studies

Cell uptake was assessed with the benzonaphthyridine derivatives (hydrogen – butyl) in CCRF-CEM, CEM/VLB_{100} and CEM/E_{1000} cultures. Cell densities at 10^7/ml were achieved by propagating in T175 flasks at least four days prior to the experiment. Drugs were prepared as 2 mM stocks prepared in 50 % ethanol and diluted in α-MEM. Cell suspensions (10^7/ml; 12 ml) in α-MEM were maintained in sterilised glass bottles with magnetic stirrers and the suspension was stirred at 5 rpm to maintain a homogenous suspension. The glass bottles were sealed with screw caps with perforations for sampling and gas ports. The gas supply had mixture of 5 % CO_2, 95 % O_2, passed through a Dreschel bottle (AM Glassware, Aberdeen, Scotland) with Milli Q water to humidify the gas before its entry into each glass bottle. The entire assembly was immersed in a temperature controlled (37°C) water bath. Drug (50 µl, 0.3 µM; final concentration) was added to the stirred suspension and samples (0.5 ml) were collected at various time points (5, 10, 15, 20, 30 and 60 min). DMSO was added to the control bottle. Each drug was measured in triplicate. Cell viability was determined by trypan blue (0.4 %) incorporation method as described previously (section 6.3.1.3) in samples collected at each time point. Samples were immediately centrifuged (13,000 × *g*, 45 sec) and cell pellets was separated by aspirating the extracellular medium into separate tubes. Cell pellets were subjected to another brief centrifugation to remove any residual medium adhering to the tube wall [185]. Both cell pellets and extracellular medium were precipitated by 3-volumes of ice cold MeCN:MeOH (3:1) containing 0.05 µM d_7 internal standard. These separated samples were further centrifuged and a 25 µl volume was diluted with equal volume of mobile phase B (0.01 % formic acid in Milli Q water) and injected into LC–MS/MS. The extracellular concentrations and the cell-associated drug concentrations were measured by LC-MS/MS (section 2.3.4). Traces of extracellular medium stuck to the walls of the tube in addition to the medium trapped within the actual cell pellet were corrected for by measuring the phenol red peak area by diode array detector.

6.3.6 Statistical analysis

Statistical analysis procedures were previously described (section 3.3.9).

6.4 Results – Evaluation in Colon-38, LLTC, NZM cultures

6.4.1 Cellular uptake and retention by Colon-38, LLTC and NZM cultures

The cell-associated drug was measured after a 1 h exposure of the benzonaphthyridine series (hydrogen – butyl) to Colon-38 cultures and for the methyl derivative in melanoma (NZM4, NZM10 and NZM52) and LLTC cultures. (Figure 6.1). The concentration measured was expressed as the percentage of drug remaining following each wash (Table 6-1). The methyl derivative was taken up in the cells to a greater extent compared to hydrogen and the more lipophilic ethyl – butyl analogues. The loss after each wash from the culture was significant for all the derivatives ($P = 1 \times 10^{-3}$ to 1×10^{-2}) except for the methyl indicating the greatest retention in this culture. However, the percentage of drug retained after each wash correlated poorly with drug lipophilicity (Log D) over the series ($r = –0.54$; $P = 3 \times 10^{-2}$), Figure 6.2.

Table 6-1 Percentage of cell-associated drug remaining after each wash from Colon-38 culture following a 1 h incubation with the benzonaphthyridine derivatives (hydrogen – butyl). Values are mean ± s.e. Significance calculated by One Way ANOVA between no wash and the third wash (n = 3).

Analogue	% remaining			P value
	Wash 1	Wash 2	Wash 3	Significance ($P < 5 \times 10^{-2}$)
Hydrogen	93.8 ± 11.0	85.3 ± 10.5	57.5 ± 5.7	2×10^{-3}
Methyl	98.0 ± 1.3	94.4 ± 2.2	92.0 ± 2.0	7×10^{-2}
Ethyl	86.5 ± 1.0	65.0 ± 6.0	63.7 ± 7.8	1×10^{-2}
Propyl	85.2 ± 4.1	75.4 ± 4.9	62.5 ± 3.3	1×10^{-3}
Butyl	75.2 ± 3.6	66.5 ± 5.5	47.0 ± 6.5	1×10^{-3}

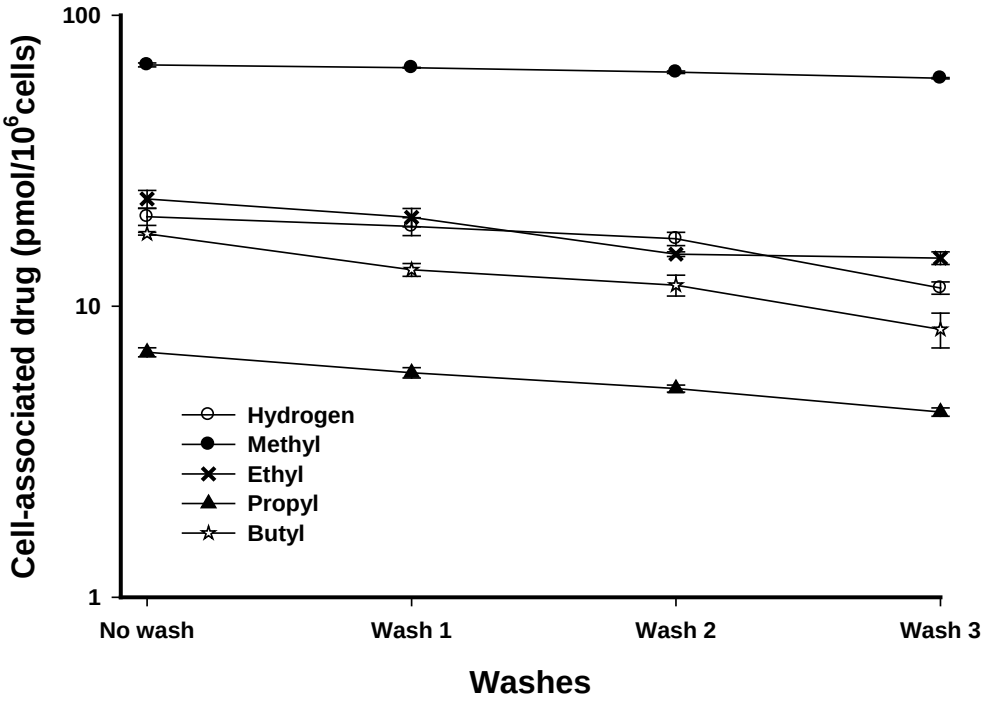

Figure 6.1 Cell-associated drug (hydrogen – butyl) after each wash from Colon-38 culture *in vitro.* Values are mean ± s.e (n = 3).

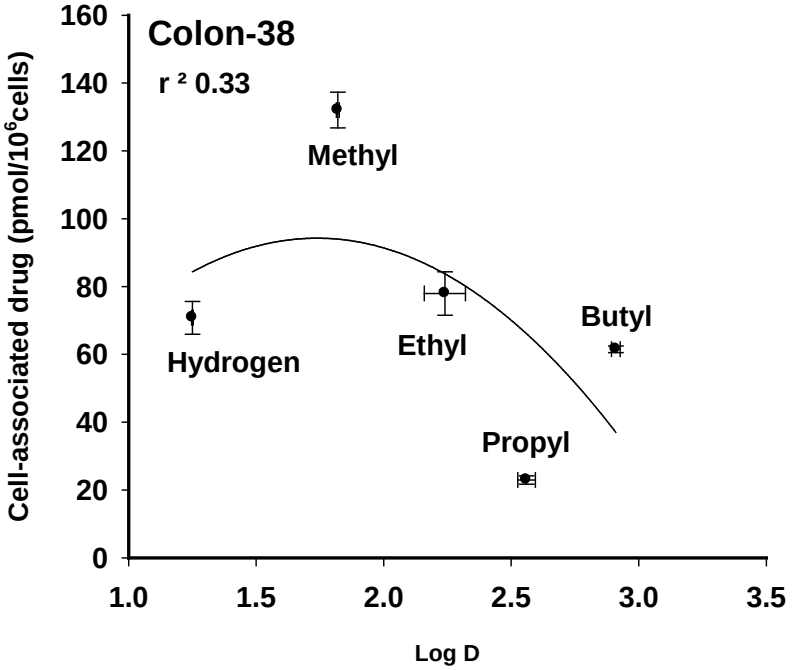

Figure 6.2 Cell-associated drug (pmol/10^{6}cells) at equilibrium *vs* Log D in Colon-38 cultures upon incubation with 0.5 µM of benzonaphthyridine (hydrogen – butyl) derivatives. Values are mean ± s.e (n = 3).

The percentage of the methyl derivative remaining after each wash was compared across Colon-38, LLTC and NZM (4, 10 and 52) cultures (Table 6-2). The drug uptake was maximal for the LLTC cultures (90.3 ± 0.4 µmol/10^6 cells). However, the loss of drug following each wash was more pronounced in this cell line ($P < 1 \times 10^{-3}$) than the Colon-38 culture (Table 6-2). The melanoma cultures also did not appear to retain the methyl derivative as effectively as the Colon-38 culture. The retention following the third wash was in the order: Colon-38 > LLTC > NZM10 > NZM4 > NZM52.

Table 6-2 Percentage of the methyl derivative retained after each wash from Colon-38, LLTC, NZM4, NZM10 and NZM52 cultures following a 1 h incubation. Values are mean ± s.e. (n = 3). Significance calculated by One Way ANOVA between no wash and the third wash.

Cell line	% remaining			P value
	Wash 1	Wash 2	Wash 3	Significance ($P < 5 \times 10^{-2}$)
Colon-38	98.0 ± 1.3	94.4 ± 2.2	92.0 ± 2.0	$= 7 \times 10^{-2}$
LLTC	92.3 ± 0.6	89.6 ± 0.5	75.0 ± 0.9	$< 1 \times 10^{-3}$
NZM4	72.4 ± 4.3	61.8 ± 5.0	54.7 ± 3.0	$< 1 \times 10^{-3}$
NZM10	74.5 ± 9.7	68.7 ± 8.3	66.9 ± 5.7	$< 1 \times 10^{-3}$
NZM52	61.7 ± 2.1	57.4 ± 3.7	44.2 ± 1.3	$< 1 \times 10^{-3}$

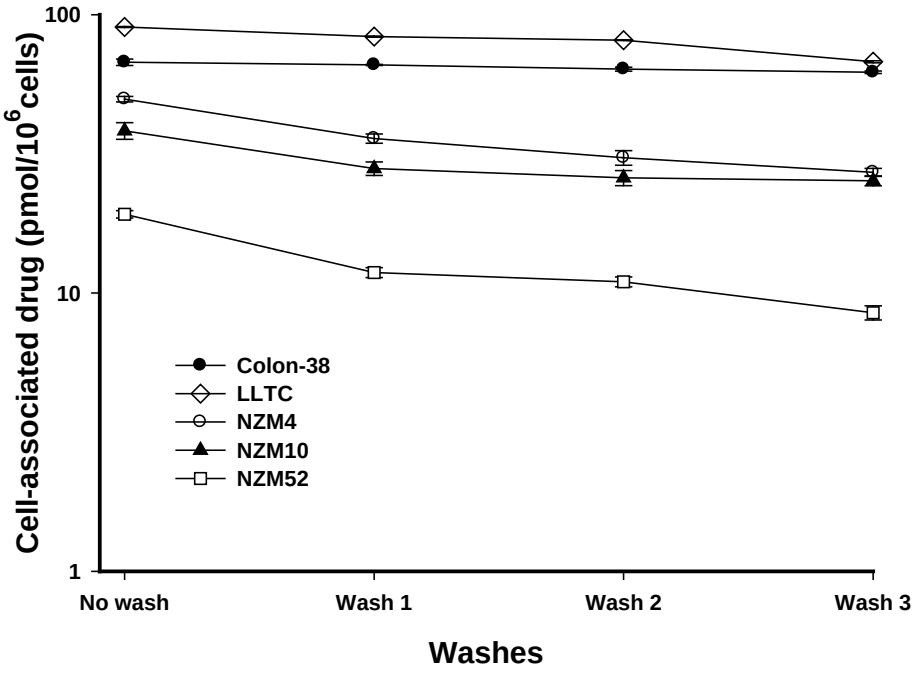

Figure 6.3 Cell-associated drug (methyl derivative) after each wash following a 1 h exposure in Colon-38, LLTC, NZM4, NZM10 and NZM52 cultures *in vitro.* Values are mean ± s.e. (n = 3).

6.4.2 Retention of the methyl derivative after 48 h exposure in Colon-38 and NZM cultures

Retention of the methyl derivative in Colon-38, NZM4, NZM10 and NZM52 cultures was examined over 48 h (Figure 6.4). Maximal concentrations were found in Colon-38 (73.2 ± 8.4 µM) at the first time point (1 h) which rapidly decreased by 2-fold over 8 h. These concentrations were significantly greater than those in the melanoma cultures (NZM4, NZM10 and NZM52) ($P < 1 \times 10^{-3}$). Among the melanoma cultures, the maximum retention was in NZM4 at the first time point (1 h) then NZM10 and NZM52 ($P = 1 \times 10^{-2}$), but the concentrations beyond 4 h were similar ($P = 8 \times 10^{-1}$). The AUCs calculated from these concentration-time curves as a measure of relative retention are presented in Figure 6.5 and Table 6-3. The AUC in Colon-38, (1143 ± 38 µM.h; $P < 1 \times 10^{-3}$) was the greatest while NZM52 (235 ± 8.7 µM.h) had the lowest.

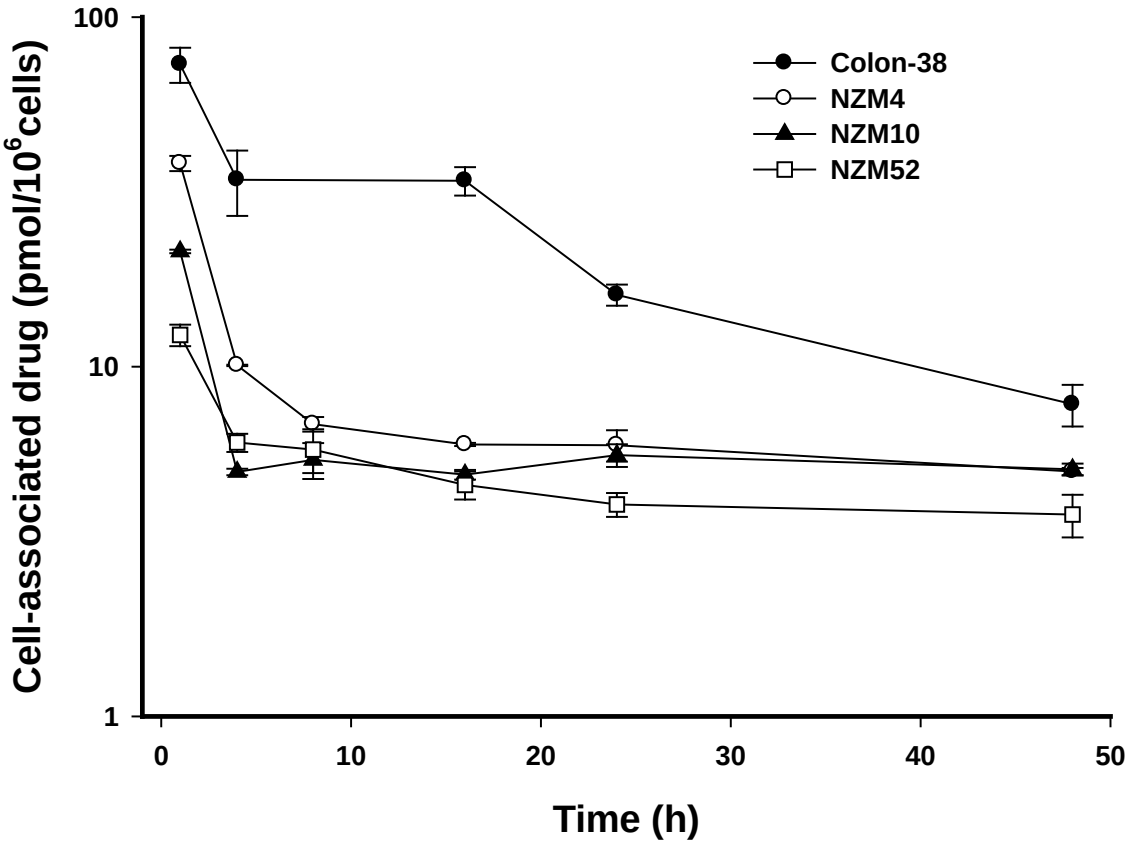

Figure 6.4 Retention of the methyl derivative in Colon-38, NZM4, NZM10 and NZM52 cell cultures over 48 h. Values are mean ± s.e. (n = 3).

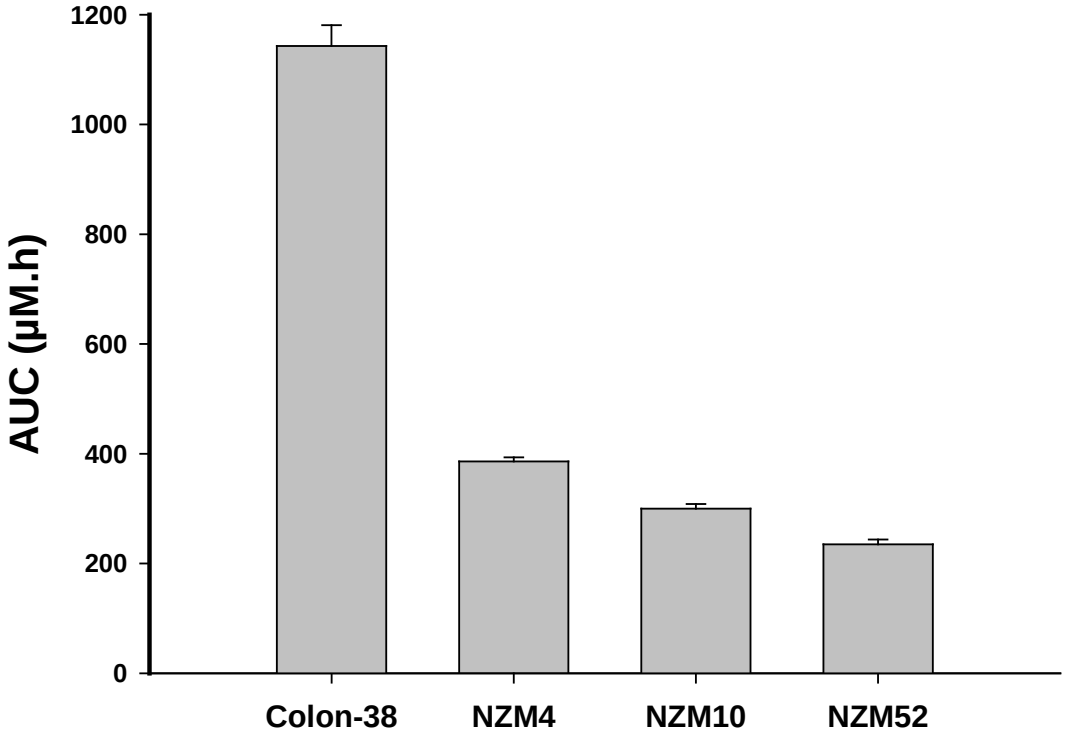

Figure 6.5 AUC values calculated from the concentration-time profiles after incubating 0.5 µM of the methyl derivative in Colon-38, NZM4, NZM10 and NZM52 cell cultures. Values are mean ± s.e. (n = 3).

Table 6-3 AUC values calculated from the concentration-time profiles after incubating with 0.5 µM of the methyl derivative in Colon-38, NZM4, NZM10 and NZM52 cell cultures. Values are mean ± s.e (n = 3).

Cell line	AUC (µM.h)
Colon-38	1143 ± 38
NZM4	386 ± 7.4
NZM10	300 ± 8.3
NZM52	235 ± 8.7

6.4.3 Relationship between lipophilicity and antiproliferative activity in Colon-38, LLTC and NZM cultures

The *in vitro* sensitivities of various cultures to the benzonaphthyridine series were assessed and data are presented in Table 6-4. The IC_{50} values plotted against lipophilicity (Log D) are shown in Figure 6.6. The methyl derivative was the most potent and had the lowest IC_{50} values in Colon-38 and LLTC cultures (1.3 ± 0.4 and 1.0 ± 0.1 nM in Colon-38 and LLTC, respectively). There were no significant differences between the IC_{50} values for the two cultures ($P = 5.4 \times 10^{-1}$). The trend was non-linear across the series and poor correlations with Log D were observed (Colon-38, $r = 0.49$; $P = 6 \times 10^{-2}$ and LLTC, $r = 0.69$; $P = 2 \times 10^{-2}$).

The IC_{50} values in the melanoma cultures (NZM4, NZM10 and NZM52) are only available for the methyl derivative and are included in Table 6-4. The NZM52 (0.97 nM) and NZM10 (2.3 nM) were found to be more sensitive to the methyl derivative compared to the NZM4, (19.0 nM).

Table 6-4 IC_{50} values (nM) of benzonaphthyridine analogues (hydrogen – butyl) in patient derived and murine cell cultures *in vitro*. Values are mean ± s.e. (n = 3).

Drug	Colon-38	LLTC	Cell line	Methyl
Hydrogen	8.6 ± 2.1*	5.5 ± 1.6*	**NZM4**	19.0[#]
Methyl	1.3 ± 0.4*	1.0 ± 0.1*	**NZM10**	2.3[#]
Ethyl	3.8 ± 0.9*	3.5 ± 0.6*	**NZM52**	0.97[#]
Propyl	9.9 ± 1.6*	8.1 ± 0.3*		
Butyl	12.9 ± 3.3*	12.3 ± 1.6*		

Y. Chen, unpublished data.

[#]***B. Baguley, unpublished data.***

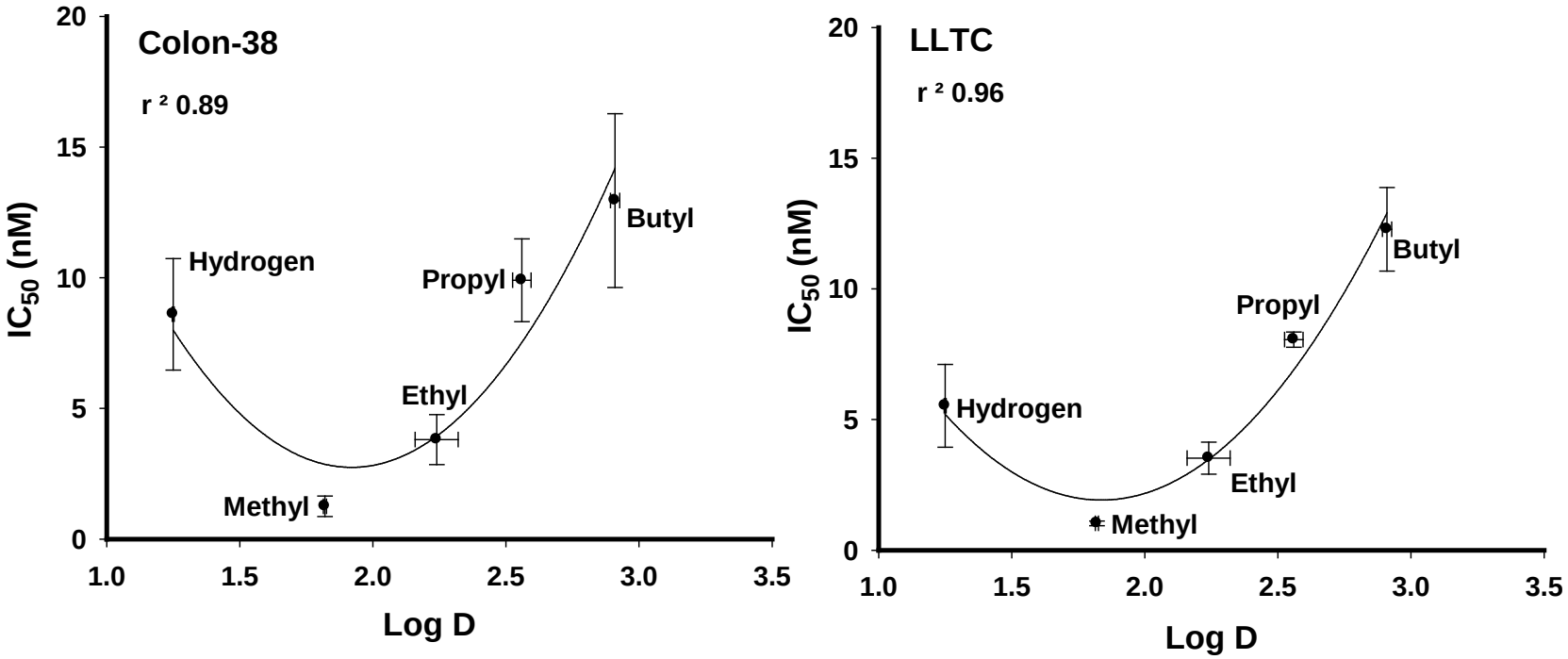

Figure 6.6 IC_{50} (nM) *vs* Log D of the benzonaphthyridine derivatives (hydrogen – butyl) in Colon-38 and LLTC cultures *in vitro.* Values are mean ± s.e. (n = 3).

6.5 Results - Evaluation in CCRF – CEM, CEM/VLB$_{100}$ and CEM/E$_{1000}$ cultures

6.5.1 Cellular uptake of benzonaphthyridines in CCRF-CEM and its drug resistant sublines

The cell-associated drug concentrations of the benzonaphthyridine derivatives (hydrogen – butyl) were measured in a leukaemia cell line (CCRF-CEM) along with the two drug resistant variants (CEM/VLB$_{100}$, expressing P-gp and CEM/E$_{1000}$, expressing MRP1) over a time course of 60 min (5, 10, 15, 20, 30 and 60 min). The cell-associated drug was plotted against time (Figure 6.7). The hydrogen analogue in CCRF-CEM was the slowest to reach equilibrium at 10 min compared to the rest of the series which had the highest cell-associated drug in the first time point sampled (5 min). Significant variability in uptake was only observed with the hydrogen analogue ($P < 1 \times 10^{-3}$; 5 min *vs* time points up to 60 min). The cell-associated drug of hydrogen, methyl and the ethyl derivatives were significantly lower in CEM/E$_{1000}$ than those observed in the CCRF-CEM and CEM/VLB$_{100}$ ($P < 1 \times 10^{-3}$). The cell-associated drug in all the three cell lines (CCRF-CEM, CEM/VLB$_{100}$ and CEM/E$_{1000}$) at equilibrium (10 min) for all 5 analogues (hydrogen – butyl) was plotted against their lipophilicity (Figure 6.8). All analogues in the series differed significantly ($P < 1 \times 10^{-3}$) and demonstrated a parabolic pattern of association with increasing order of lipophilicity for all three cultures. The CEM/E$_{1000}$ culture expressing MRP1 had the least cell-associated drug concentrations compared to CCRF-CEM and CEM/VLB$_{100}$, $P < 1 \times 10^{-3}$.

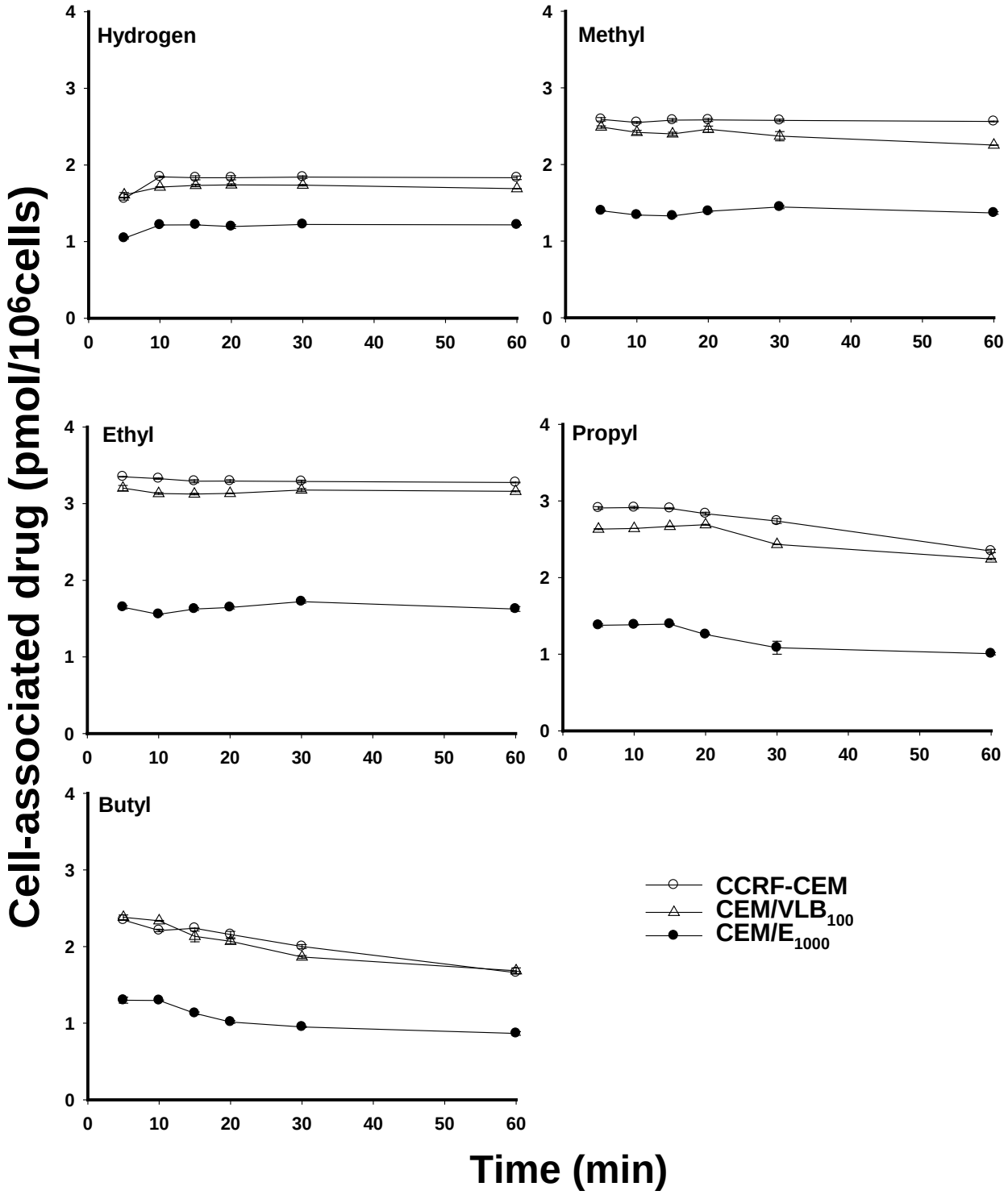

Figure 6.7 Cell-associated drug concentrations of benzonaphthyridine analogues (hydrogen – butyl) over 60 min in CCRF-CEM and the two drug resistant sublines, (CEM/VLB$_{100}$ and CEM/E$_{1000}$). Values are mean ± s.e. (n = 3).

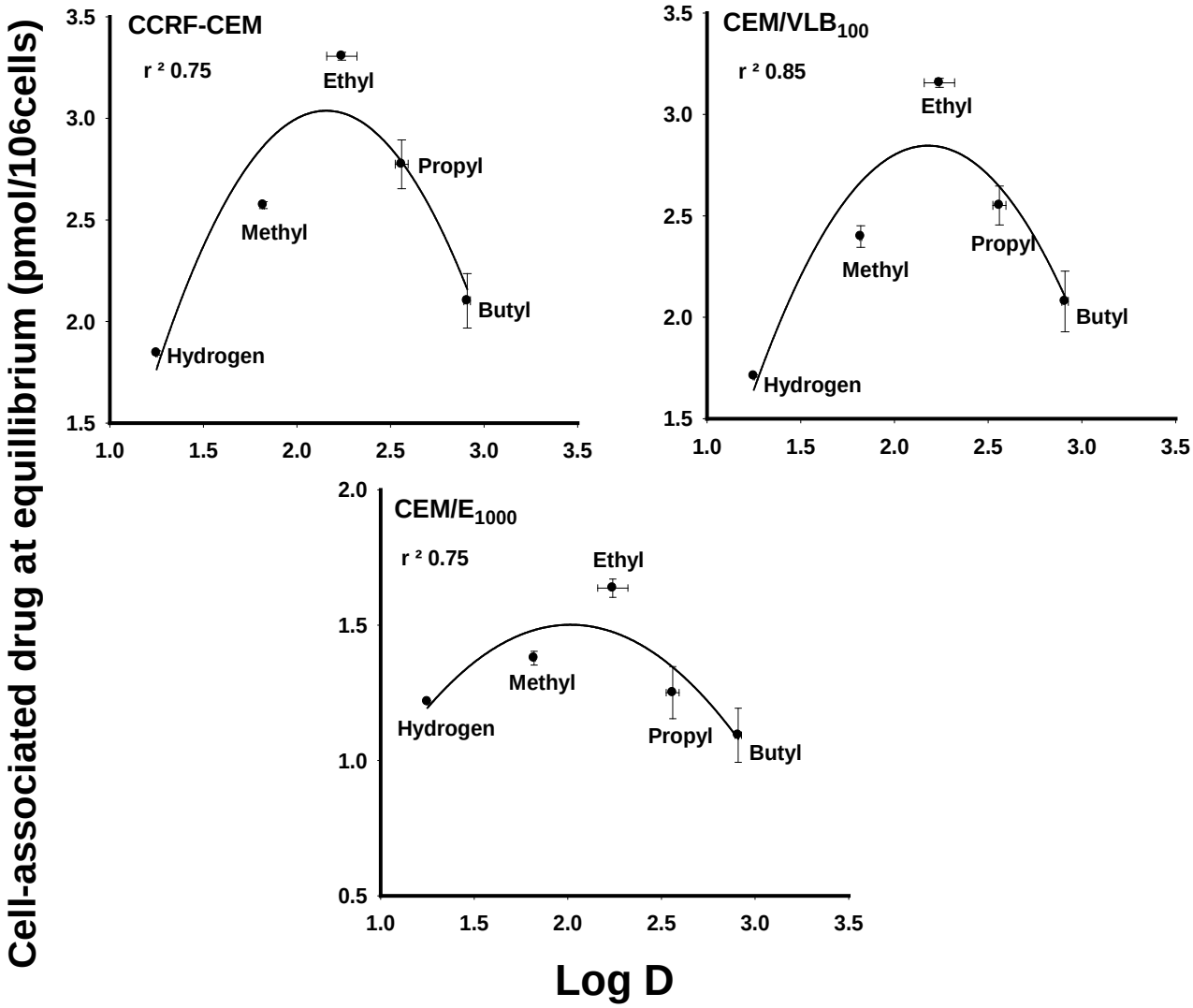

Figure 6.8 Cell-associated drug at equilibrium *vs* Log D of the benzonaphthyridine analogues (hydrogen – butyl) in CCRF-CEM and the two resistant sublines, CEM/VLB$_{100}$ and CEM/E$_{1000}$. Values are mean ± s.e. (n = 3).

6.5.2 Antiproliferative activity of benzonaphthyridine derivatives in CCRF- CEM, CEM/VLB$_{100}$ and CEM/E$_{1000}$ cultures

IC_{50} values for the CCRF-CEM and its two drug resistant sublines (CEM/VLB_{100} and CEM/E_{1000}) are presented in Table 6-5. With the CCRF-CEM cell line, the IC_{50} values ranged from 12.8 ± 0.3 (hydrogen) to 67.0 ± 2.0 nM (butyl) correlated significantly with the increasing order of lipophilicity of these analogues ($r = 0.95$; $P = 2 \times 10^{-7}$). A similar trend was observed with the epirubicin resistant variant (CEM/E_{1000}), ($r = 0.85$; $P = 2 \times 10^{-7}$). A non-linear trend was observed with the drug resistant variant, CEM/VLB_{100} where the hydrogen analogue was higher than the methyl (25.5 ± 0.9 *vs* 18.3 ± 0.4 nM) and yet correlated significantly with Log D ($r = 0.86$; $P = 2 \times 10^{-7}$) (Figure 6.9).

Table 6-5 IC_{50} values (nM) of benzonaphthyridine analogues (hydrogen – butyl) in patient derived cell cultures *in vitro.* Values are mean ± s.e. (n = 3).

Drug	CCRF-CEM	CEM/VLB_{100}	CEM/E_{1000}
Hydrogen	12.8 ± 0.3	25.5 ± 0.9*	17.2 ± 1.5*
Methyl	18.8 ± 1.5	18.3 ± 0.4	41.8 ± 1.2*
Ethyl	24.1 ± 1.5	32.6 ± 0.9*	52.3 ± 0.9*
Propyl	54.9 ± 3.4	63.0 ± 0.6	110.9 ± 3.0*
Butyl	67.0 ± 2.0	74.4 ± 1.1*	91.3 ± 1.5*

Significantly different from the IC_{50} value of the CCRF-CEM culture, $P < 1 \times 10^{-3}$.

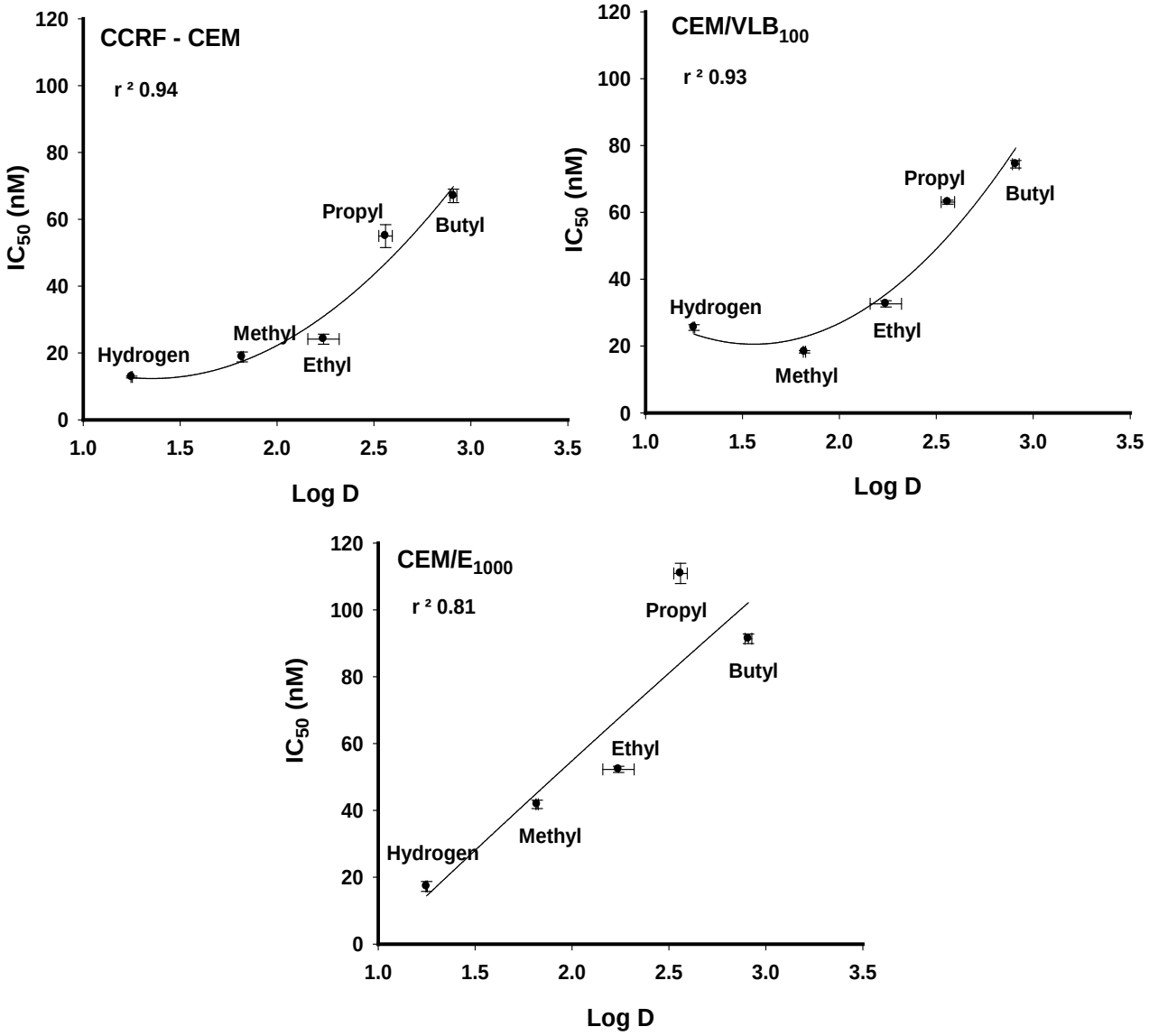

Figure 6.9 IC_{50} values (nM) *vs* Log D of the benzonaphthyridine derivatives (hydrogen – butyl) in leukaemia cultures *in vitro.* Values are mean ± s.e. (n = 3).

6.5.3 Resistance to P-gp and MRP1

The resistance factors (RF) (Table 6-6) of the 5 benzonaphthyridine derivatives were calculated for the two resistant variants, CEM/E_{1000} (epirubicin resistant) and CEM/VLB_{100} (vinblastine resistant) cultures of CCRF-CEM and plotted against Log D values (Figure 6.10). A non-linear correlation was observed in both the cultures with increasing lipophilicity. Significant differences were observed between the resistance factors of all the analogues between CEM/VLB_{100} and CEM/E_{1000} ($P = 3 \times 10^{-3}$).

Table 6-6 Resistance factors of benzonaphthyridine analogues (hydrogen – butyl) in CEM/VLB_{100} and CEM/E_{1000} cell cultures. Values are mean ± s.e. (n = 3).

Drug	Resistance factor (CEM/VLB_{100})*	Resistance factor (CEM/E_{1000})*
Hydrogen	2.0 ± 0.06	1.3 ± 0.1
Methyl	1.0 ± 0.09	2.3 ± 0.2
Ethyl	1.4 ± 0.08	2.2 ± 0.2
Propyl	1.2 ± 0.05	2.0 ± 0.2
Butyl	1.1 ± 0.04	1.4 ± 0.02

**** Drug resistance calculated relative to the parent cell line (CCRF-CEM).***

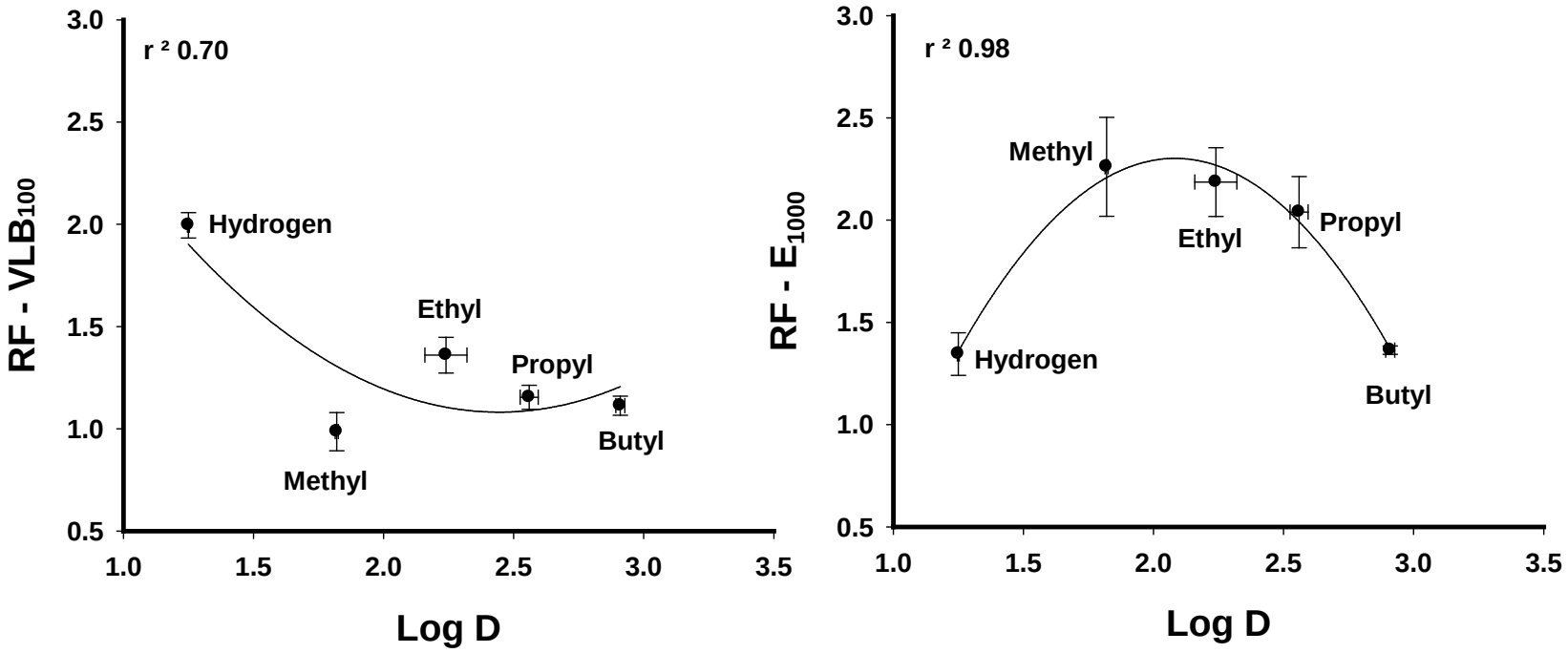

Figure 6.10 Resistance factors calculated from CEM/VLB_{100} and CEM/E_{1000} *vs* Log D of the benzonaphthyridine derivatives (hydrogen – butyl). Values are mean ± s.e. (n = 3).

6.6 Discussion

The cell-associated drug concentrations of the benzonaphthyridine derivatives were determined after a 1 h exposure to the Colon-38 cultures. Following the repeated washes, the concentrations of the hydrogen analogue and the more lipophilic derivatives (ethyl, propyl and butyl) decreased significantly ($P < 1 \times 10^{-3}$), while the methyl was retained in the cells. Among the panel of cell lines (Colon-38, LLTC, NZM4, NZM10 and NZM52) tested for retention of the methyl derivative, LLTC appeared to have the highest retention initially (first wash) but the loss was more pronounced upon repeated wash (third wash) compared to the loss in Colon-38 culture. A poor correlation was observed with the % of drug remaining following the third wash *vs in vivo* tumour AUCs. Comparing the cell-associated drug for the methyl derivative across the panel of cultures after 1 h incubation, the Colon-38 culture had the maximum while the leukaemia culture, CCRF-CEM and its two drug resistant sublines had the lowest (Figure 6.11). The higher retention of the methyl derivative correlated with the higher tumour AUC in the Colon-38 tumour *in vivo* in mice, while a correlation between lipophilicity and the IC_{50} values among the series was in conclusive. Drug efflux over 48 h, demonstrated that the exposure of the methyl derivative in Colon-38 cultures was significantly greater extent than the NZM (4, 10 and 52) resulting in the highest AUC *in vitro* which correlated significantly with the *in vivo* tumour AUCs (Figure 6.12, Table 6-7).

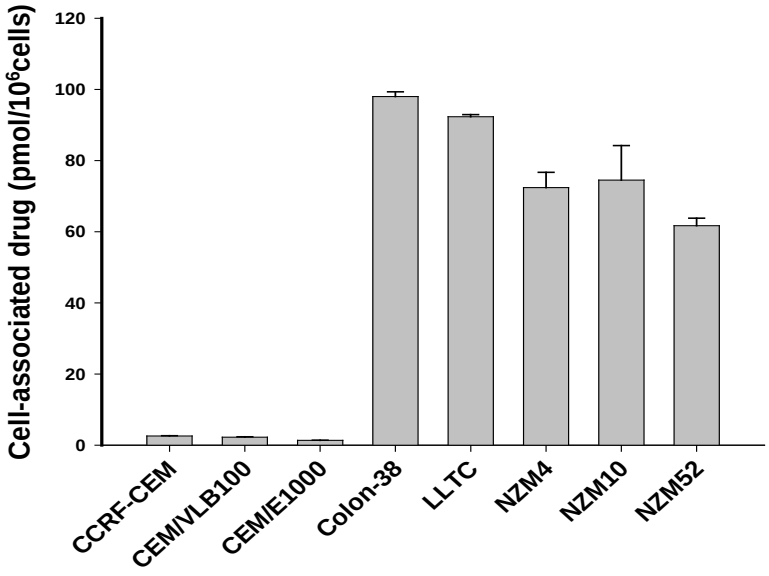

Figure 6.11 Cell-associated drug (methyl derivative) following a 1 h exposure to cultures. Values are mean ± s.e. (n = 3).

Table 6-7 *In vitro* (IC_{50}, AUC) and *in vivo* (tumour AUC, growth delay) in mice of the methyl derivative in Colon-38, NZM4, NZM10 and NZM52.

Cell line	*In vitro* IC_{50} (nM)	AUC *in vitro* (μM.h)	Tumour AUC *in vivo* (μM.h)	*In vivo* growth delay (days)
Colon-38	1.3 ± 0.4	1143 ± 38	2334 ± 60	Curative
NZM4	19	386 ± 7.4	8.9 ± 0.3	Inactive
NZM10	2.3	300 ± 8.3	220.4 ± 9.6	14
NZM52	0.97	235 ± 8.7	98.8 ± 10.4	21

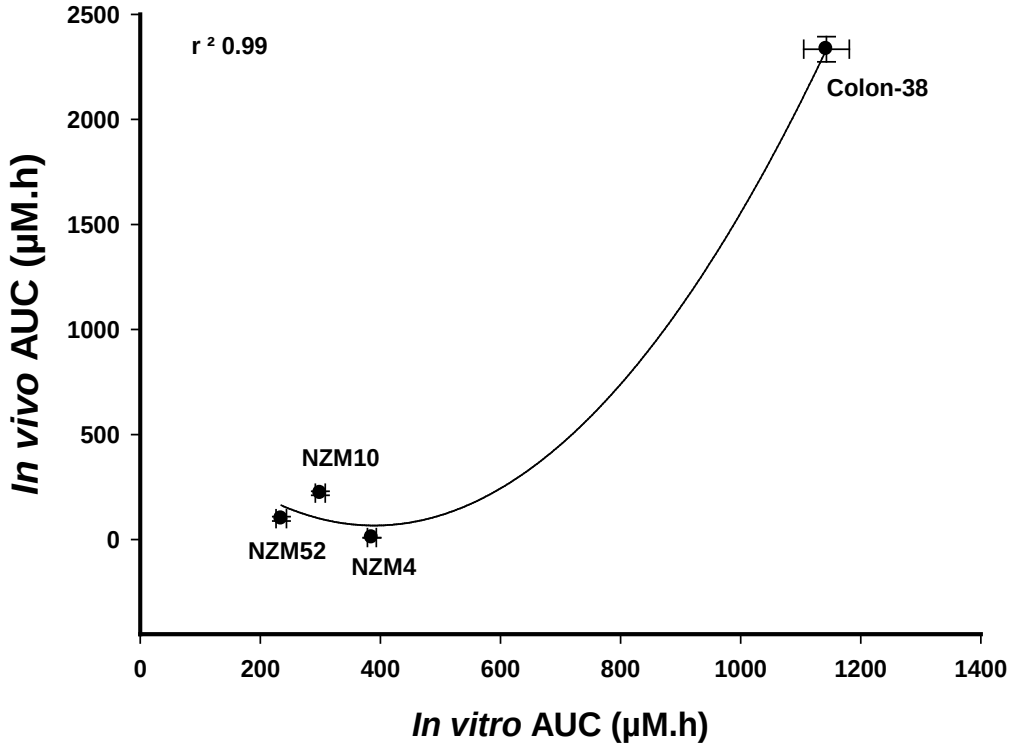

Figure 6.12 Correlation of the *in vitro* AUCs of the methyl derivative in Colon-38 and NZM (4, 10 and 52) cultures with the corresponding *in vivo* AUCs upon i.p. administration to tumour-bearing mice.

Both Colon-38 and LLTC cultures were sensitive to all analogues of the benzonaphthyridine series and the methyl derivative was the most potent in the series. A parabolic relationship was observed with increase in lipophilicity (Figure 6.6) and the IC_{50} values. Sensitivity of the methyl derivative in the melanoma cultures (NZM4, 10 and 52) varied 21-fold (0.97 – 19 nM) and correlated with the growth delays *in vivo* but had no correlation with the *in vitro* tumour AUCs (Table 6-7).

Susceptibility of benzonaphthyridine derivatives to multi-drug resistance was tested in leukaemia cultures transporters over-expressing either P-gp, or MRP1. The resistance factors were up to 2.3-fold higher than the corresponding sensitive culture (CCRF-CEM) and correlated with lipophilicity in a non-linear fashion. Comparing these results with the clinical topoisomerase poisons, these analogues were at least 4 to 34-fold less susceptible to P-gp or MRP1 (Table 6-8). Similar susceptibility to resistance with the drug-resistant variants of Jurkat Leukaemia cultures (amsacrine and doxorubicin) was observed with the methyl derivative; was moderately susceptible to both amsacrine and doxorubicin variants (resistance factors – 5.6 and 7.9 respectively) [113]. Susceptibility to other transporters such as BCRP [186], MRP5 [187] and solute carrier transporters such as OCT1, OCTN1 [188] expressed in the tumours may influence the uptake and/or retention as well as efflux of these derivatives. However, these tumour models (used in both *in vivo and in vitro;* chapters 4 and 5) are not characterised for overexpression of these transporters and is an avenue for future research.

Table 6-8 Resistance factors of benzonaphthyridine analogues (hydrogen – butyl) in CEM/VLB$_{100}$ and CEM/E$_{1000}$ cultures. Previously published data on resistance factors of the other topoisomerase poisons included for comparison [181, 189].

Drug	Resistance factor (CEM/VLB$_{100}$)	Resistance factor (CEM/E$_{1000}$)
Hydrogen	2.0 ± 0.06	1.3 ± 0.1
Methyl	1.0 ± 0.09	2.3 ± 0.2
Ethyl	1.4 ± 0.08	2.2 ± 0.2
Propyl	1.2 ± 0.05	2.0 ± 0.2
Butyl	1.1 ± 0.04	1.4 ± 0.02
DACA	1.1 ± 0.2*****	1.1 ± 0.2*
Daunorubicin	59 ± 19*	52 ± 14*
Doxorubicin	68 ± 0.1$^{\#}$	60 ± 0.1$^{\#}$
Amsacrine	8.6 ± 3.2*	16 ± 8.8*

Refer Davey et al, 1997 [189].

$^{\#}$***Refer Davey et al, 1995 [181].***

Cell-associated drug at equilibrium in Colon-38 and the leukaemia cultures were plotted against the IC_{50} values of this series (Figure 6.13). The Colon-38 and CCRF-CEM cultures appeared to correlate in a parabolic fashion while a poor correlation was observed with the drug-resistant variants (CEM/VLB$_{100}$ and CEM/E$_{1000}$). Further analysis

on this data comparing the cell-associated drug *vs* the resistance factors in CEM/VLB_{100} and CEM/E_{1000} demonstrated a lack of correlation (Figure 6.14).

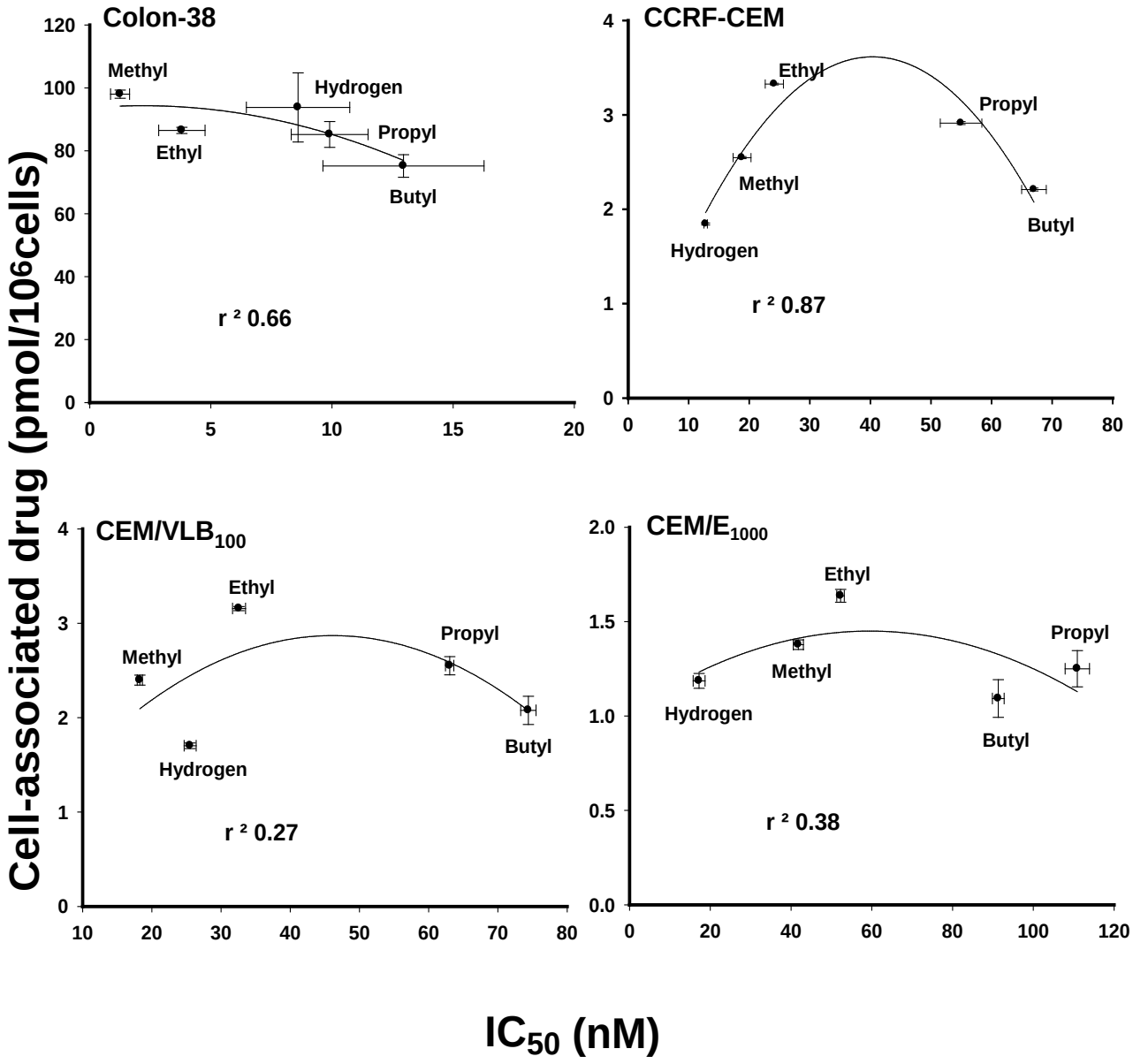

Figure 6.13 Cell-associated drug at equilibrium *vs* IC_{50} values of the benzonaphthyridine derivatives (hydrogen – butyl) in Colon-38, CCRF-CEM, CEM/VLB_{100}, CEM/E_{1000} cultures. Values are mean ± s.e (n = 3).

In conclusion, the methyl benzonaphthyridine derivative exhibited the greatest *in vitro* cellular retention among the series, in the Colon-38 cell line displaying the greatest retention from the panel of cultures tested.

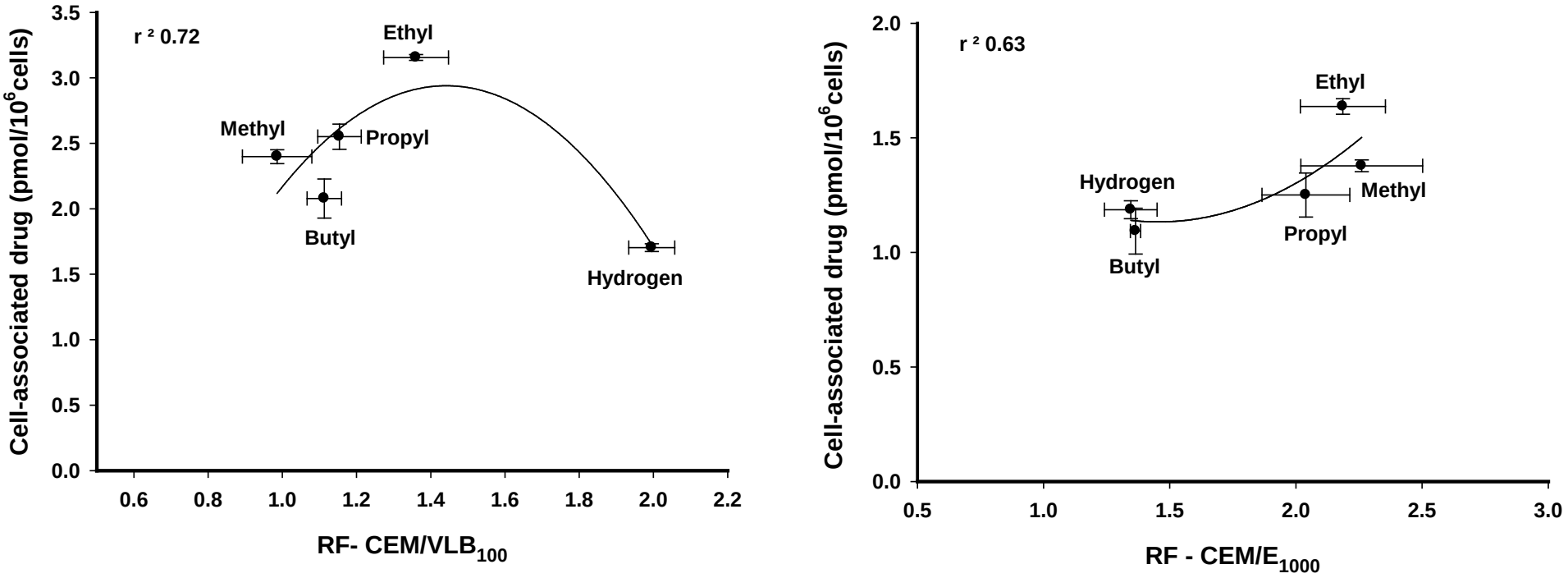

Figure 6.14 Cell-associated drug at equilibrium *vs* resistance factors of the benzonaphthyridine derivatives (hydrogen – butyl) in CEM/VLB$_{100}$ and CEM/E$_{1000}$ cultures. Values are mean ± s.e. (n = 3).

Chapter 7

Concluding discussion

The aim of this research was to identify the factors responsible for the exceptional tumour pharmacokinetics of the methyl benzonaphthyridine derivative (SN 28049). In particular, we wished to determine whether the differences in tumour pharmacokinetics were related to differences in lipophilicity and protein binding affinity, or possibly active cellular uptake/efflux rates.

7.1 Major findings

- Microsomal stability studies of this series demonstrated the methyl derivative to have the longest elimination $T_{½}$ (24 min).
- Plasma CL and V_{SS} after i.v. administration of the benzonaphthyridine series to healthy mice increased with increase in chain length and correlated with Log D resulting in a decrease in their AUCs.
- Reduced plasma CL/F and V_{SS}/F for this series in tumour-bearing mice compared to healthy mice.
- Tumour (Colon-38) AUCs of all the derivatives were greater than the corresponding plasma and tissue AUC.
- Exceptionally high tumour exposure and longer retention of the methyl derivative *in vivo* in mice is unique to Colon-38 tumour.
- Relatively high uptake and retention of the methyl derivative in melanoma and Lewis Lung tumour xenografts.
- Longer retention of the methyl derivative in Colon-38 cultures compared to melanoma (NZM4, 10 and 52) and LLTC cultures *in vitro*.
- Lack of susceptibility of the methyl derivative to cultures over-expressing P-gp, while moderately susceptible to MRP1 over-expression.

These findings strongly suggest that minor modifications in the chemical structure, which lead to changes in lipophilicity, cause a small but expected impact on plasma pharmacokinetics, but large unexpected effects on tumour pharmacokinetics. Plasma protein binding increased with lipophilicity. The highlights are presented in Figure 7.1. The binding constants for DNA copolymer poly (dG-dC)·poly (dG-dC) had no association with increasing chain length (B. Baguley, unpublished data). Several studies have previously reported the role of lipophilicity and its effects on cellular uptake and antiproliferative activity [86, 190]. However, there are no reports of an evaluation of tumour disposition of a series in an *in vivo* mouse tumour model.

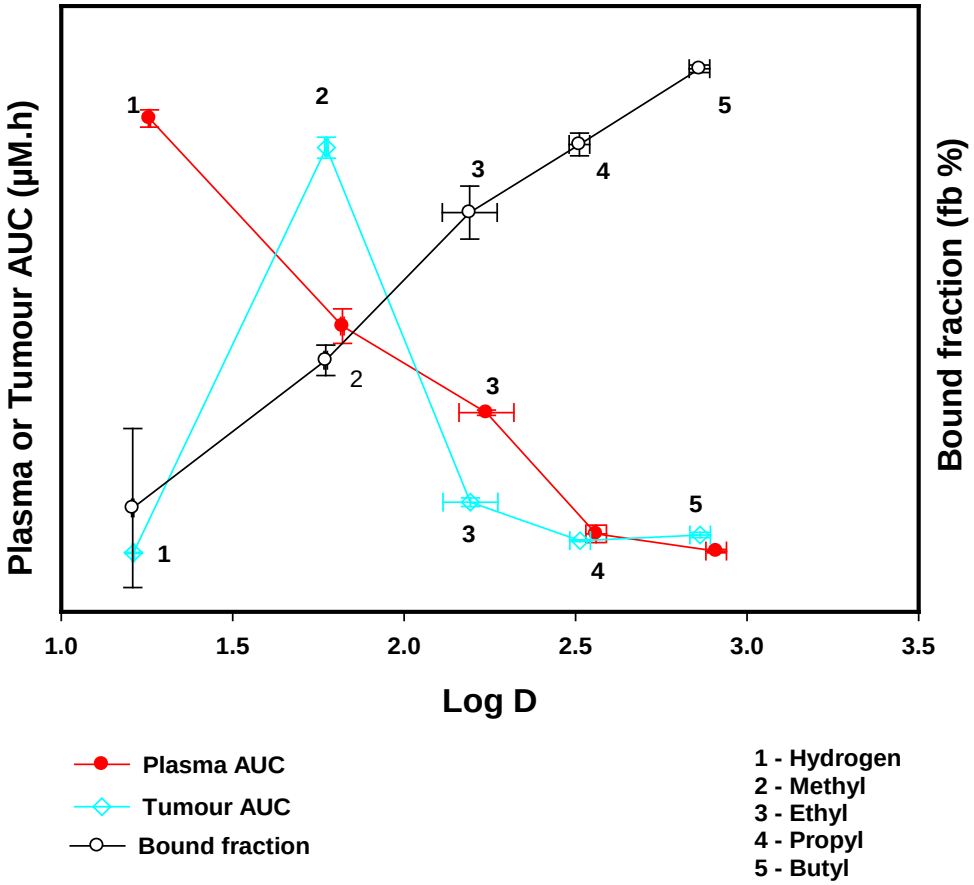

Figure 7.1 Log D *vs* plasma or tumour AUC and bound fraction (%) of the benzonaphthyridine derivatives in mouse plasma.

7.2 LC-MS/MS assay

Members of the benzonaphthyridine series were active at nanomolar plasma concentrations in mouse and human tumours inoculated in mice. A sensitive and high throughput method was required for investigating these compounds *in vivo*. A previously reported ion-trap LC-MS/MS method [132] for the measurement of the methyl derivative had an LOQ of 0.062 µM. The latter while acceptable, had insufficient sensitivity to measure the concentrations in samples of mouse plasma beyond 12 h post administration. Hence, improved sensitivity was needed to quantitate the methyl derivative for longer time points in the samples from the pharmacokinetic studies. The method developed (described in chapter 2) had a quantitation limit of 0.001 µM (1 nM), 62-fold more sensitive than the previously published method and was linear over a 300-fold range.

Samples from plasma and mouse tissue homogenates were collected after administration of different analogues in mice. The latter were pooled and processed as a single sample, allowing the simultaneous quantitation of 5 analogues in 7 min compared to the 12 min run time with the previous method. The extra sensitivity of the QqQ also aided in the rapid sample preparation where plasma or tissue homogenate samples from different analogues were pooled, precipitated with MeCN:MeOH and injected into the LC-MS/MS. In contrast, a 3 h drying and reconstitution of the dried extracts was needed with the ion-trap LC-MS/MS to even achieve the lower sensitivity of 0.062 µM.

This analytical method was successfully applied to the measurement of benzonaphthyridine derivatives in samples from studies ranging from *in vivo* mouse pharmacokinetics, *in vitro* protein binding, microsomal stability studies to microsomal and tumour binding and could be potentially utilised to analyse samples from a clinical trial.

7.3 *In vivo* pharmacokinetics

The pharmacokinetics of members of this series was determined in both healthy and tumour-bearing mice. Decreased plasma AUCs correlated negatively with increase in lipophilicity, which has been reported for a number of compounds [70]. Elimination half-lives were similar between plasma and tissues but, tumour half-lives were significantly longer, suggesting the presence of specific drug retention mechanisms for these benzonaphthyridine compounds in tumour tissue. Tumour tissue concentrations may be determined by a variety of factors, including blood perfusion, the presence of physiological barriers, tissue clearance, binding to proteins and the tumour matrix, the presence of specific receptors which may be tumour specific and the action of intracellular and extracellular influx and efflux transporters, both on cancer and stromal cells.

The use of a series of analogues of SN 28049 allowed the investigation of whether plasma and tissue pharmacokinetics were related to Log D as a measure of lipophilicity. Interestingly the AUCs in brain correlated with Log D, even though brain tissue had much smaller AUCs than other normal tissues and tumour. In general, more lipophilic compounds are thought to cross the blood brain barrier (BBB) via passive permeation. Although active efflux pumps such as P-gp and MRP1 are present, in the BBB previous studies with CNS drugs, demonstrated that the role of these efflux pumps may be moderate at best [191]. Hence, it can be hypothesised that benzonaphthyridines may enter the brain by passive diffusion and are not susceptible to these efflux mechanisms in the BBB. Further studies utilising P-gp or MRP knock-out mouse models may aid the confirmation or rejection of this hypothesis [192].

There are a few reported studies in the literature that examine the relationship between lipophilicity and drug exposure using a compound series. A previous study in rats reported increases in brain exposure with more lipophilic analogues of chlorambucil, an anti-cancer alkylating agent effective against chronic lymphocytic leukaemia, Hodgkin's and non-Hodgkin's lymphomas, as well as carcinomas of the breast and ovaries [193]. In this study, chlorambucil ester derivatives (Figure 7.2) with increasing lipophilicity were tested for their accumulation in brain [88]. The rationale was that esterification increases their lipid solubility and allows for better entry and diffusion across cellular membranes and biological barriers, such as the BBB [194, 195]. The plasma and brain pharmacokinetics of these esters after i.v. administration to female rats are summarised in Table 7-1. Brain to plasma ratios of the chlorambucil derivatives (Figure 7.3) demonstrated that increasing

lipophilicity resulted in an increased exposure in brain, while the plasma AUCs decreased. The results are consistent with our observations with the benzonaphthyridine series (see chapter 4).

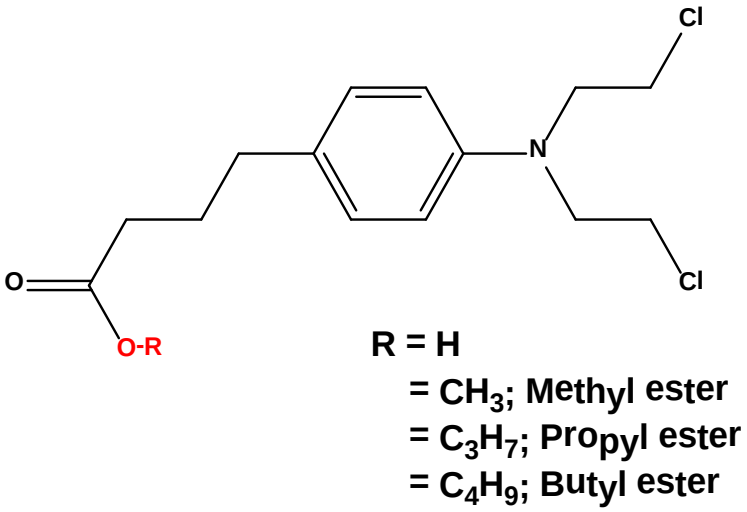

Figure 7.2 Chemical structure of chlorambucil and its ester derivatives.

Table 7-1 Pharmacokinetic parameters for chlorambucil derivatives after i.v. administration to female Wistar rats. Data from Genka et al [88].

Chlorambucil derivative (µmol/kg)	AUC (µM.h)	Brain to plasma AUC ratio
Methyl ester (31.4) Plasma	0.18	--
Brain	0.01	0.05
Propyl ester (28.9) Plasma	0.14	--
Brain	0.02	0.14
Butyl ester (27.7) Plasma	0.10	--
Brain	0.08	0.80

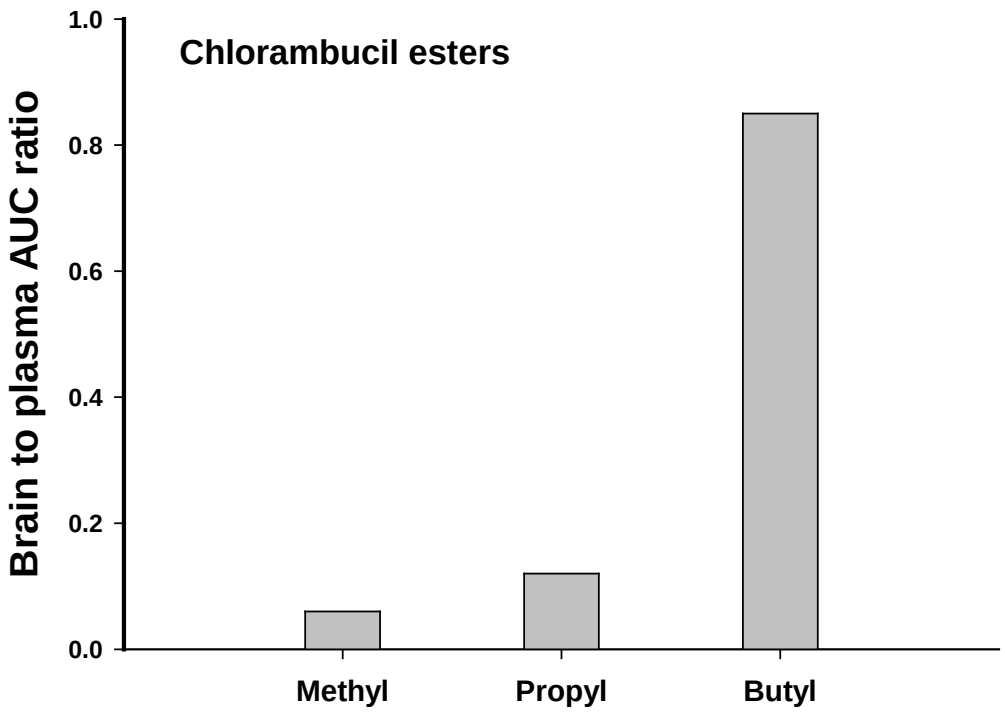

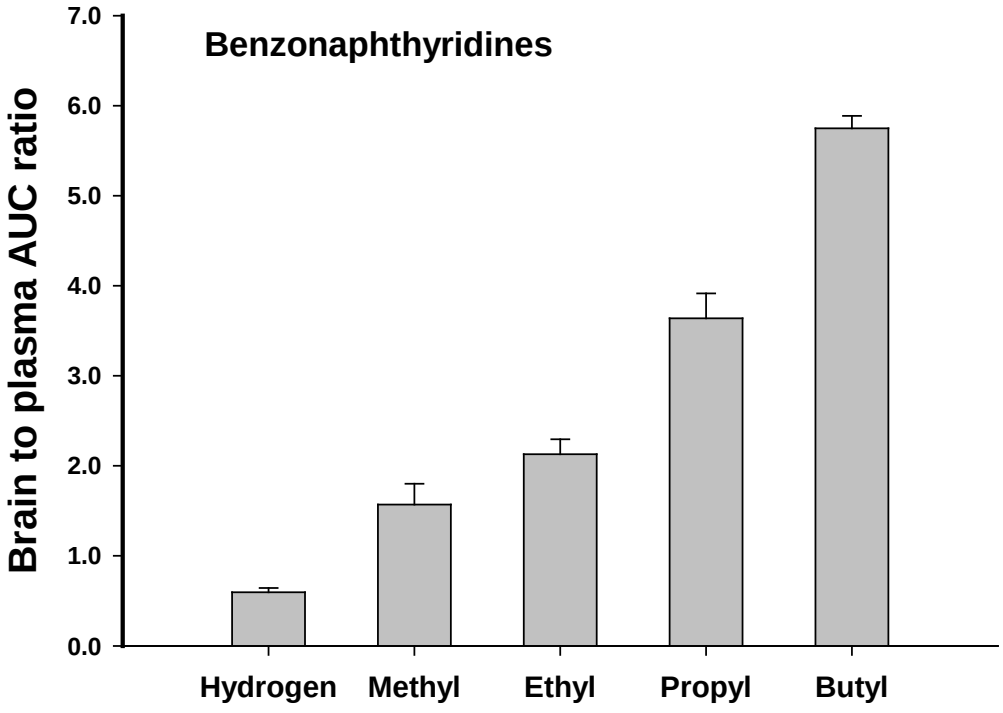

Figure 7.3 Brain to plasma AUC ratios after i.v. administration of chlorambucil ester derivatives [88], or benzonaphthyridine derivatives to rats or mice respectively.

Tissue distribution in normal tissues in healthy and tumour-bearing mice after i.p. administration of this series demonstrated that the tissue concentrations were greater than plasma concentrations. This has been observed with other DNA binding drugs such as doxorubicin and daunorubicin [196]. However, no patterns with increase in lipophilicity were identified except for brain tissue (discussed in chapter 4). Overall tissue accumulation of the benzonaphthyridines was a far less than tumour tissue, in contrast to doxorubicin which accumulated in heart tissue resulting in cardiotoxicity, a detrimental side effect of this drug [197].

Colon-38 tumour tissues in mice exhibited the greatest AUCs for all the benzonaphthyridine derivatives, as compared to plasma and other normal tissues. In particular, the methyl derivative had the greatest uptake and retention in tumour and this could be a potential reason for the observed high cure rates in this tumour model in mice. These results can be compared to the pharmacokinetic evaluation of doxorubicin and its two more lipophilic derivatives, 4-demethoxy-4'-O-methyldoxorubicin and 4-deoxy-4'-iododoxorubicin (Figure 7.4), in mice with Colon-38 tumours [154, 198]. The plasma and tumour AUCs after administration of these analogues (at optimal doses) are presented in Table 7-2. The tumour/plasma AUC ratio of this series of doxorubicin analogues showed a parabolic relationship (Figure 7.5), where a moderately lipophilic derivative, 4-demethoxy-4'-O-methyldoxorubicin had a more selective exposure in tumour resulting in the highest TPR. This ratio is similar to that of the methyl benzonaphthyridine derivative (moderately lipophilic among the series), which had the highest tumour AUC and TPR. It can be speculated that tumour uptake and retention mechanisms are unique and the selectivity of a tumour for a given analogue may partially depend on lipophilic/hydrophilic balance, but also may be affected by minor structural modifications. Also, it is known that the cellular uptake of primary amines, such as doxorubicin, may be reduced by 50 % with small changes in pH from 7.4 to 6.6 similar to what might be expected in the extracellular environment of tumours [45, 46]. Thus the degree of ionisation and pKa values for this weakly basic benzonaphthyridine series may be one of the physicochemical characteristics which may influence their cellular uptake and also their sequestration and entrapment in acidic vesicles such as lysosomes and endosomes within the cell. The intracellular distribution of anti-cancer drugs into such organelles and its relationship with their intended target and their function/toxicity is an area of limited knowledge but with advancing technology, such as confocal microscopy, will become a very active area of research.

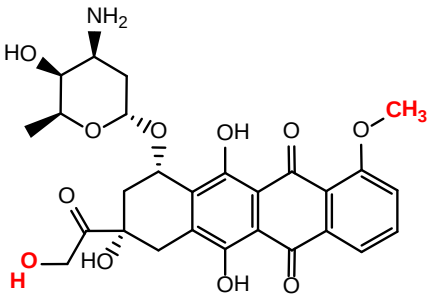

Doxorubicin

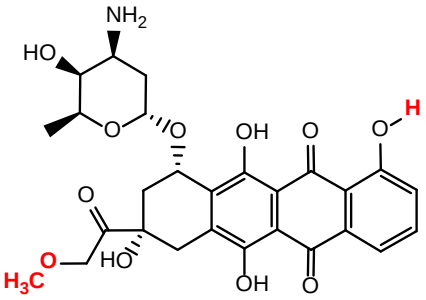

4-demethoxy-4'-O-methyldoxorubicin

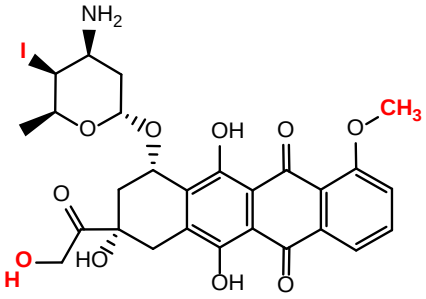

4-deoxy-4'-iododoxorubicin

Figure 7.4 Chemical structures of doxorubicin derivatives.

Table 7-2 Plasma and tumour AUC of doxorubicin derivatives after i.v. administration to mice with Colon-38 tumours [154, 198].

Drug (μmol/kg)	Plasma AUC (μM.h)	Tumour AUC (μM.h)	TPR*
Doxorubicin (17.3)	2.4	414	173
4-demethoxy-4'-O-methyldoxorubicin (1.8)	0.3	105	350
4-deoxy-4'-iododoxorubicin (9.2)	5.1	335	66

TPR – tumour to plasma AUC ratio.

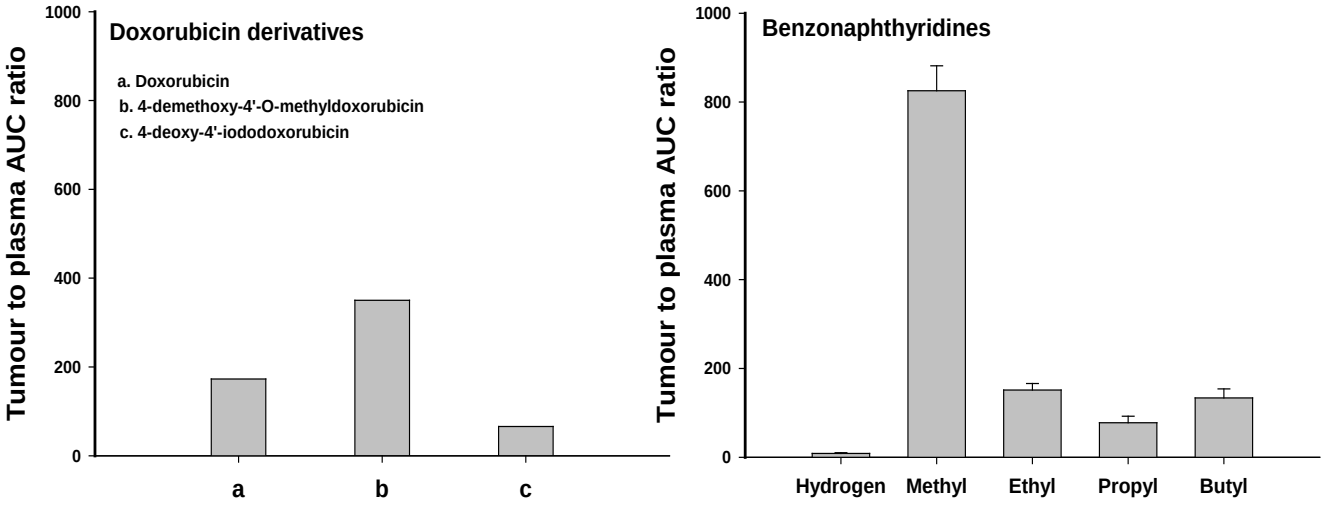

Figure 7.5 Tumour to plasma AUC ratios after i.v. or i.p. administration of doxorubicin or benzonaphthyridine derivatives to mice. Previously published data from doxorubicin analogues was summarised for comparison [154, 198].

7.4 *In vitro* pharmacology

A high-throughput 96-well equilibrium dialysis apparatus [139] was utilised to determine the plasma protein binding, microsomal and tumour binding of the benzonaphthyridine derivatives. While the traditional equilibrium dialysis [199-201] with 20-cell Dianorm Dialyser [202] is a well-established method, the volume of plasma or tissue homogenates needed are substantial (1 ml per cell) and the small number of dialysis cells limited the number of experiments possible. Longer equilibration times and associated volume shifts from the dialysate to the plasma side due to differences in osmotic pressure were major disadvantages. Another approach, ultrafiltration is a rapid way of estimating plasma protein binding with a potential disadvantage of non-specific binding of the drug to the filtration apparatus [203]. The volume of plasma or homogenates used in this high-throughput 96-well approach was reduced to 125 µl per sample providing a significant reduction in the costs as well as increasing the output per run.

The plasma protein binding for this benzonaphthyridine series correlated with Log D, but did not appear to have a major role in predicting the tumour pharmacokinetics *in vivo* [146]*.* Increasing lipophilicity typically results in increased protein binding as the hydrophobic forces drive interactions with plasma proteins. Basic compounds are known to have high affinity for alpha1-acid glycoprotein [204] due to their electrostatic interaction with acidic residues [205]. Elevated levels of alpha1-acid glycoprotein, which commonly occurs in cancer inflammatory diseases, may be partially responsible for the reduced V_{SS}/F observed in tumour-bearing mice [206, 207].

The *in vitro* microsomal stability was greatest for the methyl derivative, which had the longest $T_{½}$ (24 min) compared to the other derivatives in the series. The stability in liver microsomes was assessed by microsomal oxidation only, while other metabolic pathways such as glucuronidation may be involved. Further work needs to be done to determine the various metabolic pathways and excretory routes for the benzonaphthyridine derivatives and whether major differences exist between them. It could be speculated that the methyl derivative is less susceptible to metabolism within the tumour and the apparent increases metabolic stability may be partially responsible for its higher AUC and longer tumour retention *in vivo*. Little is known about the drug metabolising enzymes present or metabolic capacity of the Colon-38 tumour and this should be investigated further.

7.5 Pharmacokinetics in other tumour models

The pharmacokinetics of the methyl derivative in mice were evaluated in a s.c. Lewis Lung murine tumour as well as in human melanoma xenografts inoculated in mice. The tumour/plasma ratios in these tumours were lower than those for the Colon-38 tumour, while concentrations in the normal tissue such as kidney were greater in mice with melanoma xenografts than tumour. Comparing the tumour (LLTC) pharmacokinetics to previously published results of other DNA binding anti-cancer agents such as doxorubicin, daunorubicin, asulacrine and DACA. SN 28049's TPR was significantly higher ($P < 1 \times 10^{-3}$) than these other drugs (see Table 7-3). This may be anomalous to the *in vivo* activity (growth delay or increase in life span) of SN 28049 in this tumour model, as shown in Table 7-4, which was also observed with doxorubicin, which had an insignificant ILS % of 25 despite a high TPR of 26.1. On the contrary, asulacrine and DACA had high activity in mice with LLTC tumour and the yet the tumour exposures were only 2.2 and 18.5-fold greater than the corresponding plasma exposures, as compared to doxorubicin (26.1). Hence, higher AUCs in this tumour model may not necessarily translate to a superior anti-tumour activity as SN 28049 is only less active (growth delay – 9 days) and other underlying cellular mechanisms may play a role.

Differences in tumour vascularity are known to influence concentrations of the drug within a similar tumour type and may ultimately lead to a differential accumulation of the drug. This inter-tumour heterogeneity well known with human melanoma xenografts, may be attributed to tumour specific vascular networks [168, 208, 209]. These differences are most likely due to the differences in the production of angiogenic factors by the tumour cells, and/or in their ability to attract and stimulate normal cells to produce angiogenic factors [210]. It has also been shown that tumours derived from the same tumour when transplanted to different organs may develop highly different vascular networks [209, 211]. While there is no data supporting such differences in tumour vasculature among the various murine (Colon-38 and LLTC) and xenografted melanoma (NZM4, NZM10, NZM52 and LOX IMVI) tumours used in this study; it may be speculated that vascular casting techniques and window chamber preparations to identify the structural basis for such inhomogeneities [212-214] may aid in explaining the differential retention of SN 28049.

The highest tumour AUC was in the C57 mice with Colon-38 tumour (825-fold higher than plasma, Table 7-3) and was 5-fold greater than doxorubicin (438 µM.h). Comparing the *in vivo* activity, SN 28049 was curative after a single i.p. dose, while the other drugs tested

required repeated administration resulting in only a marginal to no activity (Table 7-4). The selective tumour uptake and longer retention of SN 28049 as determined by its pharmacokinetics may explain this correlation with its curative activity in this tumour model.

Table 7-3 Plasma and tumour AUC after administration of DNA binding agents to either Lewis Lung or Colon-38 tumour-bearing mice.

Lewis Lung Drug (μmol/kg)	Plasma AUC (μM.h)	Tumour AUC (μM.h)	TPR*	Data Source
Doxorubicin (17.3)	6.4	167	26.1	[196]
Daunorubicin (17.7)	28.1	62	2.2	[196]
Amsacrine (57.7)	6	37	6.0	[147]
Asulacrine (57.7)	31	68	2.2	[147]
DACA (410.0)	23.4	431	18.5	[120]
SN 28049 (25.0)	2.7	217	80.4	P. Lukka, unpublished data

Colon-38 Drug (μmol/kg)	Plasma AUC (μM.h)	Tumour AUC (μM.h)	TPR*	Data Source
Doxorubicin (17.3)	2.4	414	173	[154]
SN 28049 (25.0)	2.8	2334	833	[215]

TPR – tumour to plasma AUC ratio.

Table 7-4 *In vivo* activity data of DNA binding anti-cancer agents in mice with LLTC and Colon-38 tumours.

Lewis Lung, s.c. Drug (μmol/kg)	Growth delay (days)	Data Source
SN 28049 (26.3)[a]	9	B. Baguley, unpublished data

[a] mice were dosed i.p. on days 0 and 7.

Colon-38, s.c. Drug (μmol/kg)	Growth delay (days)	Data Source
Doxorubicin (12.3)[b]	8	[118]
Daunorubicin (7.2)[b]	inactive	[118]
Amsacrine (31.0)[b]	2	[113]
Asulacrine (33.8)[b]	8	[118]
DACA (547.0)[c]	19	[118]
SN 28049 (26.3)[d]	curative (>20)	[113]

[b] mice were dosed i.p. on days 0, 4 and 8.

[c] mice were given two doses (273.5 μmol/kg) 1 h apart.

[d] mice were dosed i.p., single dose.

Lewis Lung, i.v. Drug (μmol/kg)	ILS (%)	Data Source
Doxorubicin (4.7)[e]	25	[111]
Daunorubicin (7.4)[e]	12	[111]
Amsacrine (31.0)[e]	42	[111]
Asulacrine (33.8)[f]	curative	[111]
DACA (274.0)[f]	curative	[112]

[e] mice were dosed i.p. on days 5, 9 and 13.

[f] mice were dosed i.p. on days 1, 5 and 9.

7.6 Retention and antiproliferative activity in culture

Retention of the benzonaphthyridine derivatives in Colon-38 cultures following washes with drug-free medium was quite high with the methyl derivative showing lower drug loss compared to the hydrogen and other more lipophilic analogues in this series. Additionally, experiments with other cell cultures (LLTC, NZM4, NZM10 and NZM52) confirmed this longer retention of the methyl derivative within tumour cells.

Comparing the retention of the methyl derivative to DACA, a topoisomerase poison previously developed in the ACSRC, the uptake in LLTC cultures was rapid (20 sec) with more than 90 % of the drug washed out by the third wash [216]. It is inconclusive from these studies whether lipophilicity is responsible for this phenomenon as a more hydrophilic DACA derivative, 9-amino-5-methylsulfonyl DACA (Log P, 1.62) demonstrated a similar washout pattern from the cultures [217]. Another study with bis(carboxylato)dichlorido(ethane-1,2-diamine)platinum(IV) complexes (Figure 7.6) demonstrated that an increase in lipophilicity of the platinum compound increased their cellular accumulation (Figure 7.7, Table 7-5) [190].

In the benzonaphthyridine series, the IC_{50} values for Colon-38 cultures appeared to correlate in a non-linear fashion with lipophilicity, with the methyl derivative as the most potent. These results are not in agreement with a previous study with anthracycline analogues, where an inverse correlation between IC_{50} and lipophilicity was observed (i.e. more lipophilic analogues had lower IC_{50} values). Lipophilic analogues of doxorubicin and daunorubicin were also tested for their cytotoxicity in LoVo (doxorubicin sensitive) and Lovo/Dx (doxorubicin resistant) human colon adenocarcinoma cultures [86, 218]. Structural modifications were made either on: a) aglycone moiety; b) sugar moiety; or c) both sugar and aglycone moiety. Six analogues with varying lipophilicity (Figure 7.8) were chosen and their IC_{50} against LoVo cells determined as shown in Table 7-6. The increase in lipophilicity of the analogues decreased the IC_{50} values in the human colon adenocarcinoma (LoVo) cultures. The cellular uptake as measured by intracellular concentration was 10-times higher with the most lipophilic compound.

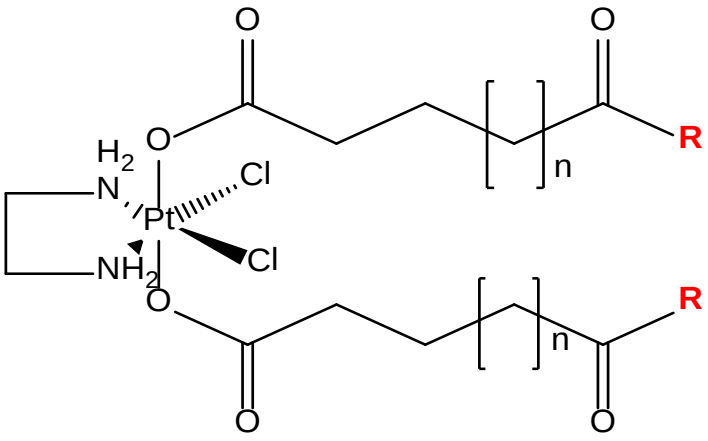

1 n = 0; R = OH
2 n = 0; R = OCH_3
3 n = 0; R = OC_2H_5
4 n = 0; R = OC_3H_7
5 n = 0; R = OC_4H_9

Figure 7.6 Chemical structure of platinum (IV) complexes.

Table 7-5 Antiproliferative activity (IC_{50}) and cellular accumulation of platinum (IV) complexes in human colon carcinoma (SW480) culture. Data summarised from Reithofer et al [190].

Compound	Log P	IC_{50} (μM)	Pt accumulation (fg/cell)
1	--	95.0	6.6
2	–0.8	16.0	19.7
3	–0.3	4.1	59.8
4	0.7	0.6	197.3
5	1.7	0.2	541.4

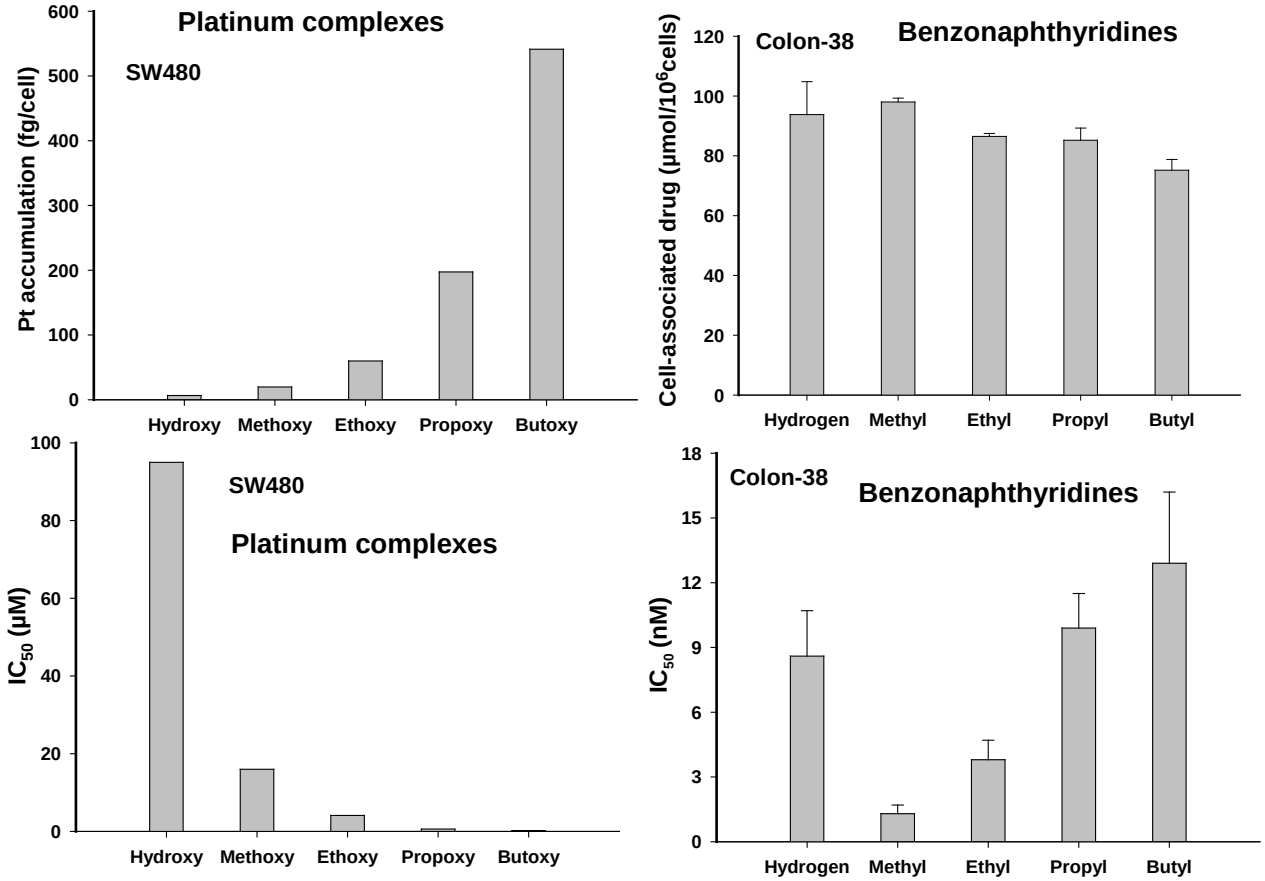

Figure 7.7 Cell-associated benzonaphthyridine (hydrogen – butyl) concentrations, IC_{50} values in Colon-38 culture, Pt accumulation and IC_{50} values of platinum (IV) complexes in human colon carcinoma (SW480) culture. Platinum complexes data from Reithofer et al [190].

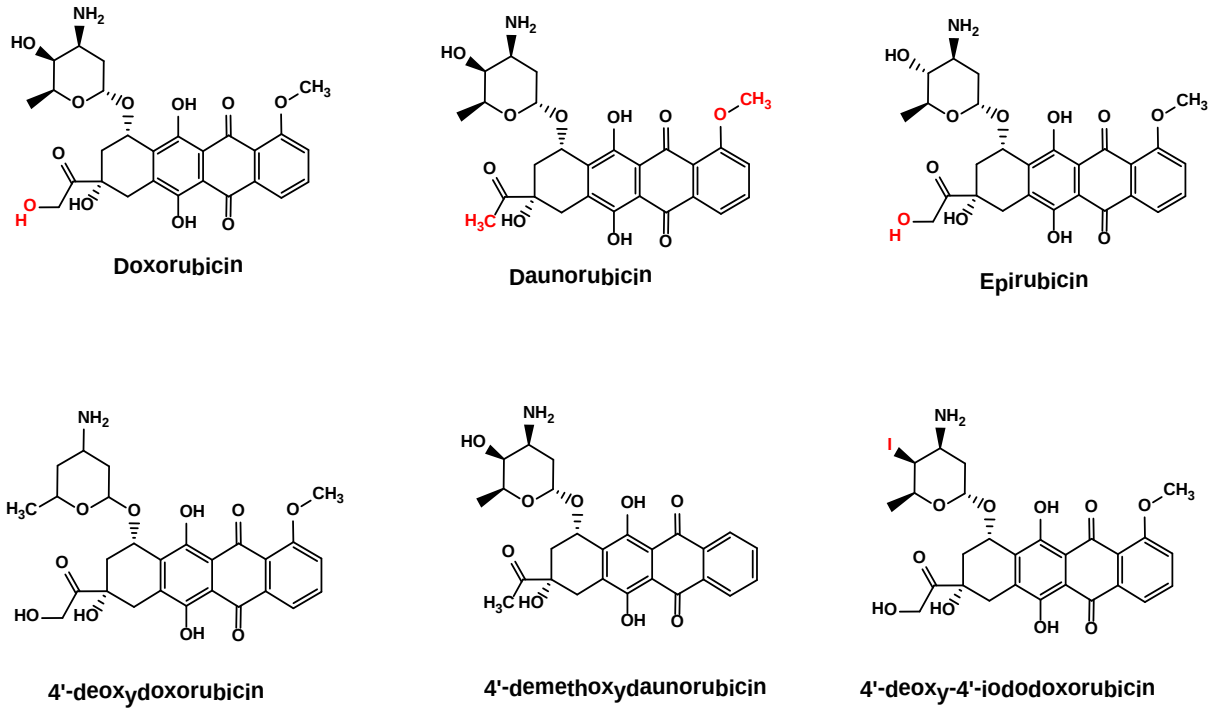

Figure 7.8 Chemical structures of anthracycline derivatives.

Table 7-6 Lipophilicity and IC_{50} values of doxorubicin analogues in human colon adenocarcinoma (LoVo) cell line. Data from Facchetti et al [86].

Compound	Log D	IC_{50} (LoVo)
Doxorubicin	–0.3	60.0 ± 12.0
Daunorubicin	0.2	42.0 ± 14.0
Epirubicin	0.05	61.0 ± 2.0
4'-deoxydoxorubicin	0.004	12.0 ± 0.7
4'-demethoxydaunorubicin	0.9	5.4 ± 3.0
4'-deoxy-4'-iododoxorubicin	1.5	6.0 ± 2.0

Increasing lipophilicity was also thought to be advantageous to overcome multi-drug resistance. In a study by Bennis et al, more lipophilic analogues of daunorubicin, 4'-demethoxydaunorubicin and pirarubicin were compared to doxorubicin [219] in doxorubicin resistant variants of MCF7, a human breast cancer cell line [220] and K562 leukaemia cultures [221]. In these cultures, (Table 7-7), pirarubicin and 4'-demethoxydaunorubicin were more potent than doxorubicin and had a much lower resistance factor.

Table 7-7 Resistance factors of doxorubicin, 4'-demethoxydaunorubicin and pirarubicin. [219].

Drug	Log D	Resistance factor (MCF7)	Resistance factor (K562)
Doxorubicin	–0.3	1225	15
4'-demethoxydaunorubicin	0.9	182	2.8
Pirarubicin	2.3	345	3.3

Table 7-8 Intracellular accumulation (nmol/10^6cells) of doxorubicin, 4'-demethoxydaunorubicin and pirarubicin in doxorubicin-resistant MCF7 and K562 cells after a 2 h exposure [219].

Drug	MCF7/doxR	K562/doxR
Doxorubicin	0.2	0.6
4'-demethoxydaunorubicin	2.9	3.0
Pirarubicin	9.7	19.1

Cellular accumulation of pirarubicin and 4'-demethoxydaunorubicin was rapid, with the maximum concentration being reached after 1 h (Table 7-8). The greatest accumulation was observed for pirarubicin than 4'-demethoxydaunorubicin and doxorubicin. On the contrary, with the benzonaphthyridine series, the accumulation and the retention in Colon-38 cultures did not correlate with lipophilicity. The methyl derivative (SN 28049) was observed to have unique properties (higher accumulation and longer retention) in culture, which supports the high exposure and retention observed in the tumours *in vivo*. While the mechanism for the unique uptake and retention of the methyl derivative is unkown, it can be speculated that greater sequestration into intracellular acidic vesicles or organelles compared to the other analogues, may be partially responsible. However this compartmentalisation of the compound within the cell may divert a drug from its intended target in the nucleous and thus reduce its activity. With the benzonaphthyridines, it is speculated that such sequestration may act as an intracellular pool for the active moiety, with a slow leaching out, or release of drug, prolonging its exposure to the nuclear taget and thus resulting in greater anti-tumour activity.

7.7 Future research

- Since tumour retention and selectivity of the methyl derivative were demonstrated with the Colon-38 tumours in mice, in addition to moderate selectivity for melanoma xenografts and Lewis Lung tumours. It would be of interest to analyse *in vivo* drug retention in tumours with other sites of origin, such as brain.
- Tumour concentrations measured *in vivo* represent an average measurement of the drug as the matrix was homogenised and it would be of interest to determine the tumour distribution of drug. Improved techniques utilising micro dialysis probes may allow sampling from different regions of tumour which may allow quantitating the diffusion efficiency of this drug more accurately.
- Results from the experiments assessing the cell-associated drug revealed that each of the benzonaphthyridine derivatives was retained in culture (chapter 6). The intracellular disposition of these derivatives should be studied by techniques, such as confocal microscopy, imaging mass spectrometry such as secondary ion mass spectrometry (SIMS) [222, 223] to determine their subcellular localisation and whether differences between the analogues or between different tumour types are observed.
- Tumour retention studies of the methyl derivative using cell lines may be extended to the primary cultures developed from tumour samples collected from cancer patients as well as in other colon cancer cell lines of both murine and human origin.
- A small but significant susceptibility of each of the derivatives to multi-drug resistance was observed utilising cultures of CCRF-CEM leukaemia cultures over-expressing MRP1 and P-gp. Further studies are required to complement the cell association studies (chapter 6) with retention/drug efflux studies.
- The routes of excretion, metabolic pathways, metabolism within tumour and tumour cultures are not yet fully understood for this series and require further study.

References

1. http://www.who.int/mediacentre/factsheets/fs297/en/index.html. 2011

2. Jemal A, Bray F, Center MM, Ferlay J, Ward E, Forman D. Global cancer statistics. *CA: A Cancer Journal for Clinicians*. 2011;61:69-90

3. Cancer New Registrations and Deaths. 2009

4. Pusey WA. Report of cases treated with Rontgen rays. *J Am Med Assoc*. 1902;XXXVIII:911-919

5. Beatson G. On the treatment of inoperable cases of carcinoma of the mamma: Suggestions for a new method of treatment, with illustrative cases.1. *The Lancet*. 1896;148:104-107

6. Lissauer. Zwei Falle von Leucaeme. *Berliner Klin. Wochnschr.* 1865;2:403-404

7. Krumbhaar EB, Krumbhaar HD. The Blood and Bone Marrow in Yelloe Cross Gas (Mustard Gas) Poisoning: Changes produced in the Bone Marrow of Fatal Cases. *J Med Res*. 1919;40:497-508 493

8. Berenblum I. The modifying influence of dichloro-ethyl sulphide on the induction of tumours in mice by tar. *J Pathol Bacteriol*. 1929;32:425-434

9. Berenblum I. Experimental inhibition of tumour induction by mustard gas and other compounds. *J Pathol Bacteriol*. 1935;40:549-558

10. Goodman LS, Wintrobe MM, Dameshek W, Goodman MJ, Gilman A, McLennan MT. Nitrogen mustard therapy: Use of Methyl-Bis(Beta-Chloroethyl)amine Hydrochloride and Tris(Beta-Chloroethyl)amine Hydrochloride for Hodgkin's Disease, Lymphosarcoma, Leukemia and Certain Allied and Miscellaneous Disorders. *J Am Med Assoc*. 1946;132:126-132

11. Gilman A. The initial clinical trial of nitrogen mustard. *Am J Surg*. 1963;105:574-578

12. Chabner BA, Roberts TG. Chemotherapy and the war on cancer. *Nat Rev Cancer*. 2005;5:65-72

13. DeVita VT, Chu E. A History of Cancer Chemotherapy. *Cancer Res*. 2008;68:8643-8653

14. Aznavoorian S, Stracke ML, Krutzsch H, Schiffmann E, Liotta LA. Signal transduction for chemotaxis and haptotaxis by matrix molecules in tumor cells. *J Cell Biol*. 1990;110:1427-1438

15. Ohtani H. Stromal reaction in cancer tissue: pathophysiologic significance of the expression of matrix-degrading enzymes in relation to matrix turnover and immune/inflammatory reactions. *Pathol Int*. 1998;48:1-9

16. Kinzler KW, Vogelstein B. Landscaping the Cancer Terrain. *Science*. 1998;280:1036-1037

17. Bissell MJ, Radisky D. Putting tumours in context. *Nat Rev Cancer*. 2001;1:46-54

18. Roskelley CD, Bissell MJ. The dominance of the microenvironment in breast and ovarian cancer. *Semin Cancer Biol*. 2002;12:97-104

19. Brekken C, Bruland OS, de Lange Davies C. Interstitial fluid pressure in human osteosarcoma xenografts: significance of implantation site and the response to intratumoral injection of hyaluronidase. *Anticancer Res*. 2000;20:3503-3512

20. Netti PA, Berk DA, Swartz MA, Grodzinsky AJ, Jain RK. Role of Extracellular Matrix Assembly in Interstitial Transport in Solid Tumors. *Cancer Res*. 2000;60:2497-2503

21. Minchinton AI, Tannock IF. Drug penetration in solid tumours. *Nat Rev Cancer*. 2006;6:583-592

22. Di Paolo A, Bocci G. Drug distribution in tumors: Mechanisms, role in drug resistance, and methods for modification. *Curr Oncol Rep*. 2007;9:109-114

23. Berk DA, Yuan F, Leunig M, Jain RK. Direct in vivo measurement of targeted binding in a human tumor xenograft. *Proc Natl Acad Sci U S A*. 1997;94:1785-1790

24. Coley HM, Amos WB, Twentyman PR, Workman P. Examination by laser scanning confocal fluorescence imaging microscopy of the subcellular localisation of anthracyclines in parent and multidrug resistant cell lines. *Br J Cancer*. 1993;67:1316-1323

25. Lee CM, Tannock IF. Inhibition of endosomal sequestration of basic anticancer drugs: influence on cytotoxicity and tissue penetration. *Br J Cancer*. 2006;94:863-869

26. Kerr DJ, Kaye SB. Aspects of cytotoxic drug penetration, with particular reference to anthracyclines. *Cancer Chemother Pharmacol*. 1987;19:1-5

27. Kyle AH, Huxham LA, Chiam ASJ, Sim DH, Minchinton AI. Direct Assessment of Drug Penetration into Tissue Using a Novel Application of Three-Dimensional Cell Culture. *Cancer Res*. 2004;64:6304-6309

28. Song CW, Lyon JC, Luo Y. Intra- and extracellular pH in solid tumors: influence on therapeutic response. In: Teicher B, ed. *Drug resistance in oncology*. New York: Marcel Dekker; 1993:25-51.

29. Song CW, Park HJ, Ross BD. Intra- and extracellular pH in solid tumor. In: Teicher B, ed. *Antiangiogenic agents in cancer therapy*. Totowa, NJ: Humana Press; 1998:51-64.

30. Webb SD, Sherratt JA, Fish RG. Mathematical Modelling of Tumor Acidity: Regulation of Intracellular pH. *J Theor Biol*. 1999;196:237-250

31. Švastová E, Hulíková A, Rafajová M, Zat'ovičová M, Gibadulinová A, Casini A, et al. Hypoxia activates the capacity of tumor-associated carbonic anhydrase IX to acidify extracellular pH. *FEBS Letters*. 2004;577:439-445

32. Song CW, Griffin R, Park HJ. Influence of Tumor pH on Therapeutic Response. In: Teicher B, ed. *Cancer Drug Discovery and Development: Cancer Drug Resistance*. Totowa, NJ: Humana Press Inc; 2006:21-42.

33. Gerweck LE, Rhee JG, Koutcher JA, Song CW, Urano M. Regulation of pH in murine tumor and muscle. *Radiat Res*. 1991;126:206-209

34. Ashby BS. pH studies in human malignant tumours. *Lancet*. 1966;2:312-315

35. Wike-Hooley JL, Haveman J, Reinhold HS. The relevance of tumour pH to the treatment of malignant disease. *Radiother Oncol*. 1984;2:343-366

36. Vaupel P, Kallinowski F, Okunieff P. Blood flow, oxygen and nutrient supply, and metabolic microenvironment of human tumors: a review. *Cancer Res*. 1989;49:6449-6465

37. Engin K, Leeper DB, Cater JR, Thistlethwaite AJ, Tupchong L, McFarlane JD. Extracellular pH distribution in human tumours. *Int J Hyperthermia*. 1995;11:211-216

38. Lin JC, Levitt SH, Song CW. Relationship between vascular thermotolerance and intratumor pH. *Int J Radiat Oncol Biol Phys*. 1992;22:123-129

39. Roos A, Boron WF. Intracellular pH. *Physiol Rev*. 1981;61:296-434

40. Madshus IH. Regulation of intracellular pH in eukaryotic cells. *Biochem. J.* 1988;250:1-8

41. Grinstein S, Rothstein A. Mechanisms of regulation of the Na+/H+ exchanger. *J Membr Biol*. 1986;90:1-12

42. Tannock IF, Rotin D. Acid pH in tumors and its potential for therapeutic exploitation. *Cancer Res*. 1989;49:4373-4384

43. Frelin C, Vigne P, Ladoux A, Lazdunski M. The regulation of the intracellular pH in cells from vertebrates. *Eur J Biochem*. 1988;174:3-14

44. Lyons JC, Kim GE, Song CW. Modification of Intracellular pH and Thermosensitivity. *Radiat Res*. 1992;129:79-87

45. Raghunand N, Mahoney BP, Gillies RJ. Tumor acidity, ion trapping and chemotherapeutics: II. pH-dependent partition coefficients predict importance of ion trapping on pharmacokinetics of weakly basic chemotherapeutic agents. *Biochem Pharmacol*. 2003;66:1219-1229

46. Mahoney BP, Raghunand N, Baggett B, Gillies RJ. Tumor acidity, ion trapping and chemotherapeutics: I. Acid pH affects the distribution of chemotherapeutic agents in vitro. *Biochem Pharmacol*. 2003;66:1207-1218

47. Ojugo AS, McSheehy PM, Stubbs M, Alder G, Bashford CL, Maxwell RJ, et al. Influence of pH on the uptake of 5-fluorouracil into isolated tumour cells. *Br J Cancer*. 1998;77:873-879

48. Reeves PR, Barnfield DJ, Longshaw S, McIntosh DA, Winrow MJ. Disposition and metabolism of atenolol in animals. *Xenobiotica*. 1978;8:305-311

49. Reeves PR, McAinsh J, McIntosh DA, Winrow MJ. Metabolism of atenolol in man. *Xenobiotica*. 1978;8:313-320

50. McAinsh J, Holmes BF. Pharmacokinetic studies with atenolol in the dog. *Biopharm Drug Dispos*. 1983;4:249-261

51. Marten TR, Bourne GR, Miles GS, Shuker B, Rankine HD, Dutka VN. The metabolism of ICI 118,587, a partial agonist of beta 1-adrenoceptors, in mice, rats, rabbits, dogs, and humans. *Drug Metab Dispos*. 1984;12:652-660

52. Bastain W, Boyce MJ, Stafford LE, Morton PB, Clarke DA, Marlow HF. Pharmacokinetics of xamoterol after intravenous and oral administration to volunteers. *Eur J Clin Pharmacol*. 1988;34:469-473

53. Gottesman MM, Pastan I. Biochemistry of multidrug resistance mediated by the multidrug transporter. *Annu Rev Biochem*. 1993;62:385-427

54. Georges E, Sharom FJ, Ling V. Multidrug Resistance and Chemosensitization: Therapeutic Implications for Cancer Chemotherapy. In: Tom August MWAFM, Alan N, eds. *Advances in Pharmacology*. Academic Press; 1990:185-220.

55. Priebe W, Perez-Soler R. Design and tumor targeting of anthracyclines able to overcome multidrug resistance: a double-advantage approach. *Pharmacol Ther*. 1993;60:215-234

56. Skovsgaard T, Nissen NI. Membrane transport of anthracyclines. *Pharmacol Ther*. 1982;18:293-311

57. Mankhetkorn S, Dubru F, Hesschenbrouck J, Fiallo M, Garnier-Suillerot A. Relation among the resistance factor, kinetics of uptake, and kinetics of the P-glycoprotein-mediated efflux of doxorubicin, daunorubicin, 8-(S)-fluoroidarubicin, and idarubicin in multidrug-resistant K562 cells. *Mol Pharmacol*. 1996;49:532-539

58. Smith DA, Jones BC, Walker DK. Design of drugs involving the concepts and theories of drug metabolism and pharmacokinetics. *Med Res Rev*. 1996;16:243-266

59. Pliška V, Testa B, van de Waterbeemd H. Lipophilicity: The Empirical Tool and the Fundamental Objective. An Introduction. *Lipophilicity in Drug Action and Toxicology*. Wiley-VCH Verlag GmbH; 2008:1-6.

60. Richet C. On the relationship between the toxicity and the physical properties of substances. *Compt Rendus Seances Soc Biol*. 1893;9:775-776

61. Mannhold R. The Impact of Lipophilicity in Drug Research: A Case Report on β-Blockers. *Mini Rev Med Chem*. 2005;5:197-205

62. Waring MJ. Lipophilicity in drug discovery. *Expert Opin Drug Discov*. 2010;5:235-248

63. Arnott JA, Planey SL. The influence of lipophilicity in drug discovery and design. *Expert Opin Drug Discov*. 2012;7:863-875

64. Testa B, Crivori P, Reist M, Carrupt P-A. The influence of lipophilicity on the pharmacokinetic behavior of drugs: Concepts and examples. *Perspectives in Drug Discovery and Design*. 2000;19:179-211

65. Avdeef A. pH-metric log P. II: Refinement of partition coefficients and Ionization constants of multiprotic substances. *J Pharm Sci*. 1993;82:183-190

66. Gocan S, Cimpan G, Comer J. Lipophilicity measurements by liquid chromatography. *Adv Chromatogr*. 2006;44:79-176

67. Scherrer RA, Donovan SF. Automated Potentiometric Titrations in KCl/Water-Saturated Octanol: Method for Quantifying Factors Influencing Ion-Pair Partitioning. *Anal Chem*. 2009;81:2768-2778

68. Sha'afi RI, Gary-Bobo CM, Solomon AK. Permeability of red cell membranes to small hydrophilic and lipophilic solutes. *J Gen Physiol*. 1971;58:238-258

69. Lipinski CA, Lombardo F, Dominy BW, Feeney PJ. Experimental and computational approaches to estimate solubility and permeability in drug discovery and development settings. *Adv Drug Del Rev*. 1997;23:3-25

70. Gleeson MP. Generation of a Set of Simple, Interpretable ADMET Rules of Thumb. *J Med Chem*. 2008;51:817-834

71. Dressman JB, Amidon GL, Reppas C, Shah VP. Dissolution Testing as a Prognostic Tool for Oral Drug Absorption: Immediate Release Dosage Forms. *Pharm Res*. 1998;15:11-22

72. Amidon GL, Lennernäs H, Shah VP, Crison JR. A Theoretical Basis for a Biopharmaceutic Drug Classification: The Correlation of in Vitro Drug Product Dissolution and in Vivo Bioavailability. *Pharm Res*. 1995;12:413-420

73. Kakemi K, Arita T, Hori R, Konishi R. Absorption and excretion of drugs. XXX. Absorption of barbituric acid derivatives from rat stomach. *Chem Pharma Bull (Tokyo)*. 1967;15:1534-1539

74. Lee AJ, King JR, Barrett DA. Percutaneous absorption: a multiple pathway model. *J Controlled Release*. 1997;45:141-151

75. Garrigues TM, Pérez-Varona AT, Climent E, Bermejo MV, Martín-Villodre A, Plá-Delfina JM. Gastric absorption of acidic xenobiotics in the rat: Biophysical interpretation of an apparently atypical behaviour. *Int J Pharm*. 1990;64:127-138

76. Wagner JG, Sedman AJ. Quantitaton of rate of gastrointestinal and buccal absorption of acidic and basic drugs based on extraction theory. *J Pharmacokinet and Pharmacodyn*. 1973;1:23-50

77. Camenisch G, Alsenz J, van de Waterbeemd H, Folkers G. Estimation of permeability by passive diffusion through Caco-2 cell monolayers using the drugs' lipophilicity and molecular weight. *Eur J Pharm Sci*. 1998;6:313-319

78. Adson A, Burton PS, Raub TJ, Barsuhn CL, Audus KL, Ho NFH. Passive diffusion of weak organic electrolytes across Caco-2 cell monolayers: Uncoupling the contributions of hydrodynamic, transcellular, and paracellular barriers. *J Pharm Sci*. 1995;84:1197-1204

79. Kubinyi H. Quantitative structure-activity relationships. IV. Non-linear dependence of biological activity on hydrophobic character: a new model. *Arzneimittelforschung*. 1976;26:1991-1997

80. Klippert P, Borm P, Noordhoek J. Prediction of intestinal first-pass effect of phenacetin in the rat from enzyme kinetic data — correlation with in in vivo data using mucosal blood flow. *Biochem Pharmacol*. 1982;31:2545-2548

81. Øie S, Tozer TN. Effect of altered plasma protein binding on apparent volume of distribution. *J Pharm Sci*. 1979;68:1203-1205

82. Kearns EH, Di L. *Drug-like properties: concepts, structure design and methods*. Elsevier; 2008.

83. Summerfield SG, Read K, Begley DJ, Obradovic T, Hidalgo IJ, Coggon S, et al. Central Nervous System Drug Disposition: The Relationship between in Situ Brain Permeability and Brain Free Fraction. *J Pharmacol Exp Ther*. 2007;322:205-213

84. Valko K, Nunhuck S, Bevan C, Abraham MH, Reynolds DP. Fast gradient HPLC method to determine compounds binding to human serum albumin. Relationships with octanol/water and immobilized artificial membrane lipophilicity. *J Pharm Sci*. 2003;92:2236-2248

85. Arcamone F, Casazza AM, Cassinelli G, Di Marco A, Penco S. *Doxorubicin and related compounds. II. Structure-activity considerations.* The Hague: M. Nijhoff Publishers; 1982.

86. Facchetti I, Grandi M, Cucchi P, Geroni C, Penco S, Vigevani A. Influence of lipophilicity on cytotoxicity of anthracyclines in LoVo and LoVo/Dx human cell lines. *Anticancer Drug Des*. 1991;6:385-397

87. Hofsli E, Nissen-Meyer J. Reversal of multidrug resistance by lipophilic drugs. *Cancer Res*. 1990;50:3997

88. Genka S, Deutsch J, Shetty UH, Stahle PL, John V, Lieberburg IM, et al. Development of lipophilic anticancer agents for the treatment of brain tumors by the esterification of water-soluble chlorambucil. *Clin Exp Metastasis*. 1993;11:131-140

89. Gedda L, Ghaneolhosseini H, Nilsson P, Nyholm K, Pettersson J, Sj, et al. The influence of lipophilicity on binding of boronated DNA-intercalating compounds in human glioma spheroids. *Anticancer Drug Des*. 2000;15:277-286

90. Pratesi G, Beretta GL, Zunino F. Gimatecan, a novel camptothecin with a promising preclinical profile. *Anticancer Drugs*. 2004;15:545-552

91. Liu W-P, Ye Q-S, Yu Y, Chen X-Z, Hou S-Q, Lou L-G, et al. Novel Lipophilic Platinum(II) Compounds of Salicylate Derivatives. *Platin Met Rev*. 2008;52:163-171

92. Pommier Y. DNA topoisomerase I and II in cancer chemotherapy: update and perspectives. *Cancer Chemother Pharmacol*. 1993;32:103-108

93. Wang JC. DNA Topoisomerases. *Annu Rev Biochem*. 1996;65:635-692

94. Denny WA. Dual topoisomerase I/II poisons as anticancer drugs. *Expert Opin Investig Drugs*. 1997;6:1845-1851

95. Leppard JB, Champoux JJ. Human DNA topoisomerase I: relaxation, roles, and damage control. *Chromosoma*. 2005;114:75-85

96. Wall ME, Wani M. Camptothecin. Discovery to clinic. *Ann N Y Acad Sci*. 1996;803:1-12

97. Strumberg D, Pilon AA, Smith M, Hickey R, Malkas L, Pommier Y. Conversion of Topoisomerase I Cleavage Complexes on the Leading Strand of Ribosomal DNA into 5'-Phosphorylated DNA Double-Strand Breaks by Replication Runoff. *Mol Cell Biol*. 2000;20:3977-3987

98. Baldwin EL, Berger AC, Corbett AH, Osheroff N. Mms22p protects Saccharomyces cerevisiae from DNA damage induced by topoisomerase II. *Nucleic Acids Res*. 2005;33:1021-1030

99. Tewey KM, Rowe TC, Yang L, Halligan BD, Liu LF. Adriamycin-induced DNA damage mediated by mammalian DNA topoisomerase II. *Science*. 1984;226:466-468

100. Rowe TC, Chen GL, Hsiang Y-H, Liu LF. DNA Damage by Antitumour Acridines Mediated by Mammalian DNA Topoisomerase II. *Cancer Res*. 1986;46:2021-2026

101. Pommier Y, Minford JK, Schwartz RE, Zwelling LA, Kohn KW. Effects of the DNA intercalators 4'-(9-acridinylamino)methanesulfon-m-anisidide and 2-methyl-9-hydroxyellipticinium on topoisomerase II mediated DNA strand cleavage and strand passage. *Biochemistry*. 1985;24:6410-6416

102. Pommier Y, Schwartz RE, Zwelling LA, Kohn KW. Effects of DNA intercalating agents on topoisomerase II induced DNA strand cleavage in isolated mammalian cell nuclei. *Biochemistry*. 1985;24:6406-6410

103. Morris SK, Lindsley JE. Yeast Topoisomerase II Is Inhibited by Etoposide After Hydrolyzing the First ATP and Before Releasing the Second ADP. *J Biol Chem*. 1999;274:30690-30696

104. Froelich-Ammon SJ, Osheroff N. Topoisomerase Poisons: Harnessing the Dark Side of Enzyme Mechanism. *J Biol Chem*. 1995;270:21429-21432

105. Cline SD, Macdonald TL, Osheroff N. Azatoxin Is a Mechanistic Hybrid of the Topoisomerase II-Targeted Anticancer Drugs Etoposide and Ellipticine. *Biochemistry*. 1997;36:13095-13101

106. Berger JM. Type II DNA topoisomerases. *Curr Opin Struct Biol*. 1998;8:26-32

107. Snyder RD. Assessment of atypical DNA intercalating agents in biological and in silico systems. *Mutat Res*. 2007;623:72-82

108. Cordonnier DMH, Hildebrand M-P, Baldeyrou B, Lansiaux A, Keuser C, Benzschawel K, et al. Design, synthesis and biological evaluation of new oligopyrrole carboxamides linked with tricyclic DNA-intercalators as potential DNA ligands or topoisomerase inhibitors. *Eur J Med Chem*. 2007;42:752-771

109. Berger JM. Structure of DNA topoisomerases. *Biochim Biophys Acta*. 1998;1400:3-18

110. Cain BF, Atwell GJ, Denny WA. Potential antitumour agents. 16. 4'-(Acridin-9-ylamino)methanesulfonanilides. *J Med Chem*. 1975;18:1110-1117

111. Baguley BC, Denny WA, Atwell GJ, Finlay GJ, Rewcastle GW, Twigden SJ, et al. Synthesis, Antitumour Activity, and DNA Binding Properties of a New Derivative of Amsacrine, N-5-Dimethyl-9-[(2-methoxy-4-methylsulfonylamino)phenylamino]-4-acridinecarboxamide. *Cancer Res*. 1984;44:3245-3251

112. Atwell GJ, Rewcastle GW, Baguley BC, Denny WA. Potential antitumour agents. 50. In vivo solid-tumor activity of derivatives of N-[2-(dimethylamino)ethyl]acridine-4-carboxamide. *J Med Chem*. 1987;30:664-669

113. Deady LW, Rodemann T, Zhuang L, Baguley BC, Denny WA. Synthesis and Cytotoxic Activity of Carboxamide Derivatives of Benzo[b] [1,6]naphthyridines. *J Med Chem*. 2003;46:1049-1054

114. Cain BF, Atwell GJ. The experimental antitumour properties of three congeners of the acridylmethanesulphonanilide (AMSA) series. *Eur J Cancer*. 1974;10:539-549

115. Baguley BC, Kernohan AR, Wilson WR. Divergent activity of derivatives of amsacrine (m-AMSA) towards Lewis lung carcinoma and P388 leukaemia in mice. *Eur J Cancer Clin Oncol*. 1983;19:1607-1613

116. Denny WA, Atwell GJ, Baguley BC. Potential antitumour agents. 40. Orally active 4,5-disubstituted derivatives of amsacrine. *J Med Chem*. 1984;27:363-367

117. Baguley BC, Falkenhaug E-M. The interaction of ethidium with synthetic double-stranded polynucleotides at low ionic strength. *Nucleic Acids Res*. 1978;5:161-171

118. Baguley BC, Zhuang L, Marshall ES. Experimental solid tumour activity of N-[2-(dimethylamino)ethyl]-acridine-4-carboxamide. *Cancer Chemother Pharmacol*. 1995;36:244-248

119. Paxton JW, Young D, Evans SMH, Kestell P, Robertson IGC, Cornford EM. Pharmacokinetics and toxicity of the antitumour agentN-[2-(dimethylamino)ethyl]acridine-4-carboxamide after i.v. administration in the mouse. *Cancer Chemother Pharmacol*. 1992;29:379-384

120. Paxton JW, Young D, Evans SMH, Robertson IGC, Kestell P. Tumour profile of N -[2-(dimethylamino)ethyl]acridine-4-carboxamide after intraperitoneal administration in the mouse. *Cancer Chemother Pharmacol*. 1993;32:320-322

121. Twelves CJ, Gardner C, Flavin A, Sludden J, Dennis I, de Bono J, et al. Phase I and pharmacokinetic study of DACA (XR5000): a novel inhibitor of topoisomerase I and II. CRC Phase I/II Committee. *Br J Cancer*. 1999;80:1786-1791

122. Dittrich C, Coudert B, Paz-Ares L, Caponigro F, Salzberg M, Gamucci T, et al. Phase II study of XR 5000 (DACA), an inhibitor of topoisomerase I and II, administered as a 120-h infusion in patients with non-small cell lung cancer. *Eur J Cancer*. 2003;39:330-334

123. Spicer JA, Gamage SA, Atwell GJ, Finlay GJ, Baguley BC, Denny WA. Structure−Activity Relationships for Acridine-Substituted Analogues of the Mixed Topoisomerase I/II Inhibitor N-[2-(Dimethylamino)ethyl]acridine-4-carboxamide. *J Med Chem*. 1997;40:1919-1929

124. Gamage SA, Spicer JA, Atwell GJ, Finlay GJ, Baguley BC, Denny WA. Structure−Activity Relationships for Substituted Bis(acridine-4-carboxamides): A New Class of Anticancer Agents. *J Med Chem*. 1999;42:2383-2393

125. Spicer JA, Gamage SA, Rewcastle GW, Finlay GJ, Bridewell DJA, Baguley BC, et al. Bis(phenazine-1-carboxamides): Structure−Activity Relationships for a New Class of Dual Topoisomerase I/II-Directed Anticancer Drugs. *J Med Chem*. 2000;43:1350-1358

126. De Jonge MJ, Kaye S, Verweij J, Brock C, Reade S, Scurr M, et al. Phase I and pharmacokinetic study of XR11576, an oral topoisomerase I and II inhibitor, administered on days 1-5 of a 3-weekly cycle in patients with advanced solid tumours. *Br J Cancer*. 2004;91:1459-1465

127. Mistry P, Stewart AJ, Dangerfield W, Baker M, Liddle C, Bootle D, et al. In vitro and in vivo characterization of XR11576, a novel, orally active, dual inhibitor of topoisomerase I and II. *Anticancer Drugs*. 2002;13:15-28

128. Deady LW, Rogers ML, Zhuang L, Baguley BC, Denny WA. Synthesis and cytotoxic activity of carboxamide derivatives of benzo[b][1,6]naphthyridin-(5H)ones. *Bioorg Med Chem*. 2005;13:1341-1355

129. Bridewell DJ, Porter A, Finlay GJ, Baguley BC. The role of topoisomerases and RNA transcription in the action of the antitumour benzonaphthyridine derivative SN 28049. *Cancer Chemother Pharmacol*. 2008;62:753-762

130. Lukka PB, Paxton JW, Kestell P, Baguley BC. Pharmacokinetics and distribution of SN 28049, a novel DNA binding anticancer agent, in mice. *Cancer Chemother Pharmacol*. 2010;65:1145-1152

131. Lukka PB. Pharmacokinetics and metabolism of SN 28049 in mice. *The University of Auckland*. 2007

132. Lukka PB, Kestell P, Paxton JW, Baguley BC. Development and validation of a liquid chromatography-mass spectrometry (LC-MS) assay for the determination of the anti-cancer agent N-[2-(dimethylamino)ethyl]-2,6-dimethyl-1-oxo-1,2-dihydrobenzo[b]-1,6-naph thyridine-4-carboxamide (SN 28049). *J Chromatogr B Analyt Technol Biomed Life Sci*. 2008;875:368-372

133. Rane A, Wilkinson GR, Shand DG. Prediction of hepatic extraction ratio from in vitro measurement of intrinsic clearance. *J Pharmacol Exp Ther*. 1977;200:420-424

134. Gillette JR. Factors affecting drug metabolsim. *Ann N Y Acad Sci*. 1971;179:43-66

135. Houston JB. Relevance of in vitro kinetic parameters to in vivo metabolism of xenobiotics. *Toxicology In Vitro*. 1994;8:507-512

136. Bachmann KA, Ghosh R. The use of in vitro methods to predict in vivo pharmacokinetics and drug interactions. *Curr Drug Metab*. 2001;2:299-314

137. Smith PK, Krohn RI, Hermanson GT, Mallia AK, Gartner FH, Provenzano MD, et al. Measurement of protein using bicinchoninic acid. *Anal Biochem*. 1985;150:76-85

138. Boudinot FD, Jusko WJ. Fluid shifts and other factors affecting plasma protein binding of prednisolone by equilibrium dialysis. *J Pharm Sci*. 1984;73:774-780

139. Banker MJ, Clark TH, Williams JA. Development and validation of a 96-well equilibrium dialysis apparatus for measuring plasma protein binding. *J Pharm Sci*. 2003;92:967-974

140. Mannhold R, Rekker R. The hydrophobic fragmental constant approach forcalculating log P in octanol/water and aliphatic hydrocarbon/water systems. *Perspect Drug Discovery Des*. 2000;18:1-18

141. Siim BG, Hicks KO, Pullen SM, van Zijl PL, Denny WA, Wilson WR. Comparison of aromatic and tertiary amine N-oxides of acridine DNA intercalators as bioreductive drugs: Cytotoxicity, DNA binding, cellular uptake, and metabolism. *Biochem Pharmacol*. 2000;60:969-978

142. Jagow R, Kampffmeyer H, Kinese M. The preparation of microsomes. *Naunyn Schmiedebergs Arch Pharmacol*. 1965;251:73-87

143. Barter ZE, Bayliss MK, Beaune PH, Boobis AR, Carlile DJ, Edwards RJ, et al. Scaling Factors for the Extrapolation of In Vivo Metabolic Drug Clearance From *In Vitro* Data: Reaching a Consensus on Values of Human Micro-somal Protein and Hepatocellularity Per Gram of Liver. *Curr Drug Metabol*. 2007;8:33-45

144. Davies B, Morris T. Physiological Parameters in Laboratory Animals and Humans. *Pharm Res*. 1993;10:1093-1095

145. Obach RS, Baxter JG, Liston TE, Silber BM, Jones BC, Macintyre F, et al. The Prediction of Human Pharmacokinetic Parameters from Preclinical and In Vitro Metabolism Data. *J Pharmacol Exp Ther*. 1997;283:46-58

146. Colmenarejo G, Alvarez-Pedraglio A, Lavandera J-L. Cheminformatic Models To Predict Binding Affinities to Human Serum Albumin. *J Med Chem*. 2001;44:4370-4378

147. Kestell P, Paxton JW, Evans PC, Young D, Jurlina JL, Robertson IGC, et al. Disposition of Amsacrine and Its Analogue 9-({2-Methoxy-4-[(methylsulfonyl)-amino]phenyl}amino)-N,5-dimethyl-4-acridinecarboxamide (CI-921) in Plasma, Liver, and Lewis Lung Tumors in Mice. *Cancer Res*. 1989;50:503-508

148. Paxton JW, Jurlina JL, Foote SE. The binding of amsacrine to human plasma proteins. *J Pharm Pharmacol*. 1986;38:432-438

149. Andress LD, Whitfield LR, Chang T. Characterisation of CI-921, the amsacrine analog, binding to human plasma and plasma proteins. *Proc. Am. Assoc. Pharm. Sci.* 1988:1460

150. Hartmann G, Vassileva V, Piquette-Miller M. Impact of endotoxin-induced changes in p-glycoprotein expression on disposition of doxorubicin in mice. *Drug Metab Dispos*. 2005;33:820-828

151. Eksborg S, Ehrsson H, Ekqvist B. Protein binding of anthraquinone glycosides, with special reference to adriamycin. *Cancer Chemother Pharmacol*. 1982;10:7-10

152. Evans SM, Robertson IG, Paxton JW. Plasma protein binding of the experimental antitumour agent acridine-4-carboxamide in man, dog, rat and rabbit. *J Pharm Pharmacol*. 1994;46:63-67

153. Obach RS. Prediction of Human Clearance of Twenty-Nine Drugs from Hepatic Microsomal Intrinsic Clearance Data: An Examination of In Vitro Half-Life Approach and Nonspecific Binding to Microsomes. *Drug Metabol Dispos*. 1999;27:1350-1359

154. Formelli F, Carsana R, Pollini C. Comparative pharmacokinetics and metabolism of doxorubicin and 4-demethoxy-4′-O-methyldoxorubicin in tumor-bearing mice. *Cancer Chemother Pharmacol*. 1986;16:15-21

155. Liptrott NJ, Owen A. The role of cytokines in the regulation of drug disposition: extended functional pleiotropism? *Expert Opin Drug Metab Toxicol*. 2011;7:341-352

156. Morgan ET, Goralski KB, Piquette-Miller M, Renton KW, Robertson GR, Chaluvadi MR, et al. Regulation of Drug-Metabolizing Enzymes and Transporters in Infection, Inflammation, and Cancer. *Drug Metab Dispos*. 2008;36:205-216

157. Slaviero KA, Clarke SJ, Rivory LP. Inflammatory response: an unrecognised source of variability in the pharmacokinetics and pharmacodynamics of cancer chemotherapy. *Lancet Oncol*. 2003;4:224-232

158. Saleem A, Price PM. Early tumor drug pharmacokinetics is influenced by tumor perfusion but not plasma drug exposure. *Clin Cancer Res*. 2008;14:8184-8190

159. Rygaard J, Poulsen CO. Heterotransplantation Of A Human Malignant Tumour to “Nude” Mice. *Acta Pathol Microbiol Scand*. 1969;77:758-760

160. Giovanella BC, Yim SO, Stehlin JS, Williams LJ. Development of Invasive Tumors in the “Nude” Mouse After Injection of Cultured Human Melanoma Cells. *J Natl Cancer Inst*. 1972;48:1531-1533

161. Slee J. The morphology and development of ‘ragged’— a mutant affecting the skin and hair of the house mouse I. Adult morphology. *Journal of Genetics*. 1957;55:100-121

162. Flanagan S. 'Nude', a new hairless gene with pleiotropic effects in the mouse. *Genet Res*. 1966;8:295-309

163. Wilkoff LJ, Dulmadge EA, Chopra DP. Viability of cultured Lewis lung cell populations exposed to beta-retinoic acid. *Proc Soc Exp Biol Med*. 1980;163:233-236

164. Baguley BC, Marshall ES, Holdaway KM, Rewcastle GW, Denny WA. Inhibition of growth of primary human tumour cell cultures by a 4-anilinoquinazoline inhibitor of the epidermal growth factor receptor family of tyrosine kinases. *Eur J Cancer*. 1998;34:1086-1090

165. Leopold WR, 3rd, Corbett TH, Griswold DP, Jr., Plowman J, Baguley BC. Experimental antitumor activity of the amsacrine analogue CI-921. *J Natl Cancer Inst*. 1987;79:343-349

166. Harirforoosh S, Jamali F. Effect of inflammation on kidney function and pharmacokinetics of COX-2 selective nonsteroidal anti-inflammatory drugs rofecoxib and meloxicam. *J Appl Toxicol*. 2008;28:829-838

167. Brown JM. Tumor microenvironment and the response to anticancer therapy. *Cancer Biol Ther*. 2002;1:453-458

168. Konerding MA, Malkusch W, Klapthor B, van Ackern C, Fait E, Hill SA, et al. Evidence for characteristic vascular patterns in solid tumours: quantitative studies using corrosion casts. *Br J Cancer*. 1999;80:724-732

169. Tannock IF, Rotin D. Acid pH in Tumors and Its Potential for Therapeutic Exploitation. *Cancer Res*. 1989;49:4373-4384

170. Lu P, Weaver VM, Werb Z. The extracellular matrix: A dynamic niche in cancer progression. *J Cell Biol*. 2012;196:395-406

171. Gottesman MM, Fojo T, Bates SE. Multidrug resistance in cancer: role of ATP-dependent transporters. *Nat Rev Cancer*. 2002;2:48-58

172. Gillet J-P, Gottesman M. Mechanisms of Multidrug Resistance in Cancer. In: Zhou J, ed. *Multi-Drug Resistance in Cancer*. Humana Press; 2010:47-76.

173. Krishna R, Mayer LD. Multidrug resistance (MDR) in cancer: Mechanisms, reversal using modulators of MDR and the role of MDR modulators in influencing the pharmacokinetics of anticancer drugs. *Eur J Pharm Sci*. 2000;11:265-283

174. Baguley BC. Multiple Drug Resistance Mechanisms in Cancer. *Mol Biotechnol*. 2010

175. Szakacs G, Paterson JK, Ludwig JA, Booth-Genthe C, Gottesman MM. Targeting multidrug resistance in cancer. *Nat Rev Drug Discov*. 2006;5:219-234

176. Teodori E, Dei S, Martelli C, Scapecchi S, Gualtieri F. The functions and structure of ABC transporters: implications for the design of new inhibitors of Pgp and MRP1 to control multidrug resistance (MDR). *Curr Drug Targets*. 2006;7:893-909

177. Juranka PF, Zastawny RL, Ling V. P-glycoprotein: multidrug-resistance and a superfamily of membrane-associated transport proteins. *FASEB J*. 1989;3:2583-2592

178. Mori M, Mimori K, Shiraishi T, Haraguchi M, Ueo H, Barnard GF, et al. Motility related protein 1 (MRP1/CD9) expression in colon cancer. *Clin Cancer Res*. 1998;4:1507-1510

179. Foley GE, Lazarus H, Farber S, Uzman BG, Boone BA, McCarthy RE. Continuous culture of human lymphoblasts from peripheral blood of a child with acute leukemia. *Cancer*. 1965;18:522-529

180. Beck WT, Mueller TJ, Tanzer LR. Altered Surface Membrane Glycoproteins in Vinca Alkaloid-resistant Human Leukemic Lymphoblasts. *Cancer Res*. 1979;39:2070-2076

181. Davey RA, Longhurst TJ, Davey MW, Belov L, Harvie RM, Hancox D, et al. Drug resistance mechanisms and MRP expression in response to epirubicin treatment in a human leukaemia cell line. *Leuk Res*. 1995;19:275-282

182. Corbett TH, Griswold DP, Roberts BJ, Peckham JC, Schabel FM. Tumor Induction Relationships in Development of Transplantable Cancers of the Colon in Mice for Chemotherapy Assays, with a Note on Carcinogen Structure. *Cancer Res*. 1975;35:2434-2439

183. Tanigawa N, Kern DH, Hikasa Y, Morton DL. Rapid Assay for Evaluating the Chemosensitivity of Human Tumors in Soft Agar Culture. *Cancer Res*. 1982;42:2159-2164

184. Sondak VK, Bertelsen CA, Tanigawa N, Hildebrand-Zanki SU, Morton DL, Korn EL, et al. Clinical Correlations with Chemosensitivities Measured in a Rapid Thymidine Incorporation Assay. *Cancer Res*. 1984;44:1725-1728

185. Pruijn FB, van Daalen M, Holford NHG, Wilson WR. Mechanisms of enhancement of the antitumour activity of melphalan by the tumour-blood-flow inhibitor 5,6-dimethylxanthenone-4-acetic acid. *Cancer Chemother Pharmacol*. 1997;39:541-546

186. Doyle LA, Yang W, Abruzzo LV, Krogmann T, Gao Y, Rishi AK, et al. A multidrug resistance transporter from human MCF-7 breast cancer cells. *Proc Natl Acad Sci U S A*. 1998;95:15665-15670

187. Kool M, de Haas M, Scheffer GL, Scheper RJ, van Eijk MJT, Juijn JA, et al. Analysis of Expression of cMOAT (MRP2), MRP3, MRP4, and MRP5, Homologues of the Multidrug Resistance-associated Protein Gene (MRP1), in Human Cancer Cell Lines. *Cancer Res*. 1997;57:3537-3547

188. Roth M, Obaidat A, Hagenbuch B. OATPs, OATs and OCTs: the organic anion and cation transporters of the SLCO and SLC22A gene superfamilies. *Br J Pharmacol*. 2012;165:1260-1287

189. Davey RA, Su GM, Hargrave RM, Harvie RM, Baguley BC, Davey MW. The potential of N-[2-(dimethylamino)ethyl]acridine-4-carboxamide] to circumvent three multidrug-resistance phenotypes *in vitro*. *Cancer Chemother Pharmacol*. 1997;39:424-430

190. Reithofer MR, Bytzek AK, Valiahdi SM, Kowol CR, Groessl M, Hartinger CG, et al. Tuning of lipophilicity and cytotoxic potency by structural variation of anticancer platinum(IV) complexes. *J Inorg Biochem*. 2011;105:46-51

191. Obach RS, Lombardo F, Waters NJ. Trend Analysis of a Database of Intravenous Pharmacokinetic Parameters in Humans for 670 Drug Compounds. *Drug Metabol Dispos*. 2008;36:1385-1405

192. Agarwal S, Uchida Y, Mittapalli RK, Sane R, Terasaki T, Elmquist WF. Quantitative Proteomics of Transporter Expression in Brain Capillary Endothelial Cells Isolated from P-Glycoprotein (P-gp), Breast Cancer Resistance Protein (Bcrp), and P-gp/Bcrp Knockout Mice. *Drug Metabol Dispos*. 2012;40:1164-1169

193. Carter SK, Bakowski MT, Hellmann K. *Chemotherapy of Cancer*. New York: Wiley Medical; 1987.

194. Krogsgaard-Larsen P, Christensen A. GABA agonists. Synthesis and structure-activity studies on analogues of isoguvacine and THIP. *Eur J Med Chem*. 1979;14:157-164

195. Sinkula A, Yalkowsky S. Rationale for design of biologically reversible drug derivatives: prodrugs. *J Pharm Sci*. 1975;64:181-210

196. Martini A, Donelli NG, Mantovani A, Pacciarini MA, Fogar-Ottaviano EF, Morasca L, et al. Antineoplastic activity and pharmacokinetics of adriamycin and daunomycin in tumor bearing mice. *Oncology*. 1977;34:173-178

197. Bertazzoli C, Bellini O, Magrini U, Tosana MG. Quantitative experimental evaluation of adriamycin cardiotoxicity in the mouse. *Cancer Treat Rep*. 1979;63:1877-1883

198. Formelli F, Carsana R, Pollini C. Pharmacokinetics of 4'-Deoxy-4'-iodo-doxorubicin in Plasma and Tissues of Tumor-bearing Mice Compared with Doxorubicin. *Cancer Res*. 1987;47:5401-5406

199. Osborne WA. Intracellular colloidal salts. *J Physiol*. 1906;34:84-92

200. Northrop JH, Kunitz M. The Combination of Salts and Proteins : Ii. A Method for the Determination of the Concentration of Combined Ions from Membrane Potential Measurements. *J Gen Physiol*. 1926;9:351-360

201. Klotz IM, Walker FM, Pivan RB. The Binding of Organic Ions by Proteins. *J Am Chem Soc*. 1946;68:1486-1490

202. Furlong CE, Morris RG, Kandrach M, Rosen BP. A multichamber equilibrium dialysis apparatus. *Anal Biochem*. 1972;47:514-526

203. Pacifici GM, Viani A. Methods of determining plasma and tissue binding of drugs. Pharmacokinetic consequences. *Clin Pharmacokinet*. 1992;23:449-468

204. Schmid K. Preparation and Properties of Serum and Plasma Proteins. XXIX. Separation from Human Plasma of Polysaccharides, Peptides and Proteins of Low Molecular Weight. Crystallization of an Acid Glycoprotein1a,b,c. *J Am Chem Soc*. 1953;75:60-68

205. Kremer JM, Wilting J, Janssen LH. Drug binding to human alpha-1-acid glycoprotein in health and disease. *Pharmacol Rev*. 1988;40:1-47

206. Paxton JW. Alpha 1 -acid glycoprotein and binding of basic drugs. *Methods Find Exp Clin Pharmacol*. 1983;5:635-648

207. Jackson PR, Tucker GT, Woods HF. Altered plasma drug binding in cancer: role of alpha 1-acid glycoprotein and albumin. *Clin Pharmacol Ther*. 1982;32:295-302

208. Solesvik OV, Rofstad EK, Brustad T. Vascular structure of five human malignant melanomas grown in athymic nude mice. *Br J Cancer*. 1982;46:557-567

209. Bernsen HJ, Rijken PF, Oostendorp T, van der Kogel AJ. Vascularity and perfusion of human gliomas xenografted in the athymic nude mouse. *Br J Cancer*. 1995;71:721-726

210. Carmeliet P, Jain RK. Angiogenesis in cancer and other diseases. *Nature*. 2000;407:249-257

211. Gulliksrud K, Mathiesen B, Galappathi K, Rofstad EK. Quantitative assessment of hypoxia in melanoma xenografts by dynamic contrast-enhanced magnetic resonance imaging: intradermal versus intramuscular tumors. *Radiother Oncol*. 2010;97:233-238

212. Grunt TW, Lametschwandtner A, Staindl O. The vascular pattern of basal cell tumors: Light microscopy and scanning electron microscopic study on vascular corrosion casts. *Microvasc Res*. 1985;29:371-386

213. Dewhirst MW, Tso CY, Oliver R, Gustafson CS, Secomb TW, Gross JF. Morphologic and hemodynamic comparison of tumor and healing normal tissue microvasculature. *Int J Radiat Oncol Biol Phys*. 1989;17:91-99

214. Shah-Yukich AA, Nelson AC. Characterization of solid tumor microvasculature: a three-dimensional analysis using the polymer casting technique. *Lab Invest*. 1988;58:236-244

215. Lukka PB, Paxton JW, Kestell P, Baguley BC. Comparison of a homologous series of benzonaphthyridine anti-cancer agents in mice: divergence between tumour and plasma pharmacokinetics. *Cancer Chemother Pharmacol*. 2012;70:151-160

216. Haldane A, Finlay GJ, Hay MP, Denny WA, Baguley BC. Cellular uptake of N-[2-(dimethylamino)ethyl]acridine-4-carboxamide (DACA). *Anticancer Drug Des*. 1999;14:275-280

217. Denny WA, Atwell GJ, Rewcastle GW, Baguley BC. Potential antitumor agents. 49. 5-Substituted derivatives of N-[2-(dimethylamino)ethyl]-9-aminoacridine-4-carboxamide with in vivo solid-tumor activity. *J Med Chem*. 1987;30:658-663

218. Grandi M, Geroni C, Giuliani FC. Isolation and characterization of a human colon adenocarcinoma cell line resistant to doxorubicin. *Br J Cancer*. 1986;54:515-518

219. Bennis S, Faure P, Chapey C, Hu Y-P, Fourche J, Yamani JE, et al. Cellular pharmacology of lipophilic anthracyclines in human tumor cells in culture selected for resistance to doxorubicin. *Anticancer Drugs*. 1997;8:610-617

220. Soule HD, Vazguez J, Long A, Albert S, Brennan M. A human cell line from a pleural effusion derived from a breast carcinoma. *J Natl Cancer Inst*. 1973;51:1409-1416

221. Batist G, Tulpule A, Sinha BK, Katki AG, Myers CE, Cowan KH. Overexpression of a novel anionic glutathione transferase in multidrug-resistant human breast cancer cells. *J Biol Chem*. 1986;261:15544-15549

222. Trim PJ, Francese S, Clench MR. Imaging mass spectrometry for the assessment of drugs and metabolites in tissue. *Bioanalysis*. 2009;1:309-319

223. Boxer SG, Kraft ML, Weber PK. Advances in imaging secondary ion mass spectrometry for biological samples. *Annu Rev Biophys*. 2009;38:53-74